NASA TECHNICAL TRANSLATION

NASA TT F-535

NASA TT F-535

c.1

LOAN COPY: RETU
AFWL (WLIL
KIRTLAND AFB, I

0068974

TECH LIBRARY KAFB, NM

SOME PROBLEMS OF THE PHYSICS OF HIGH ENERGIES AND COSMIC RAYS

S. A. Azimov, Editor

Institute of Nuclear Physics, Academy of Sciences, Uzbek SSR

"Fan" Press, Tashkent, 1967

NATIONAL AERONAUTICS AND SPACE ADMINISTRATION • WASHINGTON, D. C. • APRIL 1969

TECH LIBRARY KAFB, NM
0068974

SOME PROBLEMS OF THE PHYSICS OF HIGH ENERGIES AND COSMIC RAYS

S. A. Azimov, Editor

Translation of "Nekotoryye Voprosy Fiziki Vysokikh Energiy i Kosmicheskikh Luchey," "Fan" Press, Tashkent, 1967

NATIONAL AERONAUTICS AND SPACE ADMINISTRATION

For sale by the Clearinghouse for Federal Scientific and Technical Information
Springfield, Virginia 22151 – CFSTI price $3.00

TABLE OF CONTENTS

Annotation iv

Abstracts iv

G. G. Arushanov. Elastic Scattering of Strongly-Interacting Particles at High Energies 1

S. A. Azimov, G. G. Arushanov, U. G. Gulyamov, and A. A. Yuldashev. Elastic πp^-, pp^-, $p\bar{p}^-$, and Kp-Interactions at High Energies 43

S. A. Azimov, M. S. Rasulkulov and V. M. Chudakov. Azimuthal Angular Distribution of Shower Particles and Gray Tracks Formed by Particles of Cosmic Radiation in a Photoemulsion 51

Sh. Abduzhamilov, S. A. Azimov, L. P. Chernova, G. M. Chernov and V. M. Chudakov. On Inelastic Coherent Interactions of High-Energy Protons with Complex Nuclei 56

S. A. Azimov, B. K. Nikishin, I. V. Rechitskiy, and V. M. Chudakov. Study of Inelastic $\pi^- p$-Collisions with a Slow Recoil Proton at an Energy of 17 GeV 65

S. A. Azimov, Ye. V. Beter, U. G. Gulyamov, N. B. Eroshkina, and A. Ya. Levin. Study of Coherent Inelastic Interactions of Pions with an Energy of 17.2 BeV with Heavy Nuclei of a Photoemulsion 77

S. A. Azimov and R. Karimova. Study of Angular Correlations of Particles in Nuclear Disintegrations with Fragments 97

S. A. Azimov, E. S. Bakhromi, Yu. D. Bogachkin, Kh. Zaynutdinov, and R. Karimov. Gas-Discharge Tubes with a Large Effective Area 111

S. A. Azimov and Yu. V. Polyak. Energy Transfer to an Electron-Photon Component During the Interaction of Particles with Graphite Nuclei . 122

SOME PROBLEMS OF THE PHYSICS OF HIGH ENERGIES AND COSMIC RAYS

ACADEMICIAN S. A. AZIMOV, EDITOR
INSTITUTE OF NUCLEAR PHYSICS, ACADEMY OF SCIENCES UZBEK SSR

ANNOTATION: This collection presents results of studies which revealed the diffraction dissociation of protons on complex nuclei of a photoemulsion at an energy of 24 BeV, as well as a detailed analysis of the coherent interactions of π-mesons with an energy of 17 BeV. An analysis of the experimental data is made by means of original methods which are based on the utilization of mathematical statistics and relativistic kinematics. Inelastic proton-nucleon collisions are examined for a wide range of energies.
This document is intended for specialists engaged in research on cosmic rays, physics of elementary particles and nuclear physics, as well as for a broad group of scientific workers, instructors, and students interested in these problems.

Elastic Scattering of Strongly-Interacting Particles at High Energies

G. G. Arushanov

ABSTRACT: The extensive experimental data on the elastic $\pi^{\pm}$ p-, pp-, $K^{\pm}$p-interactions at high energies (E > 5 GeV) are processed by means of phase analysis in an optical model of the interaction of the particles. The optical model is described and it is shown that it is intermediate between the model of the potential (actual) well and the model of the compound nucleus. A number of optical potentials are examined and their applicability is discussed. In the summation of the Faxen-Holtsmark series, some general results are obtained without specifying the type of $a_l(k)$ and without the limitation to small angles. The imaginary part of the scattering amplitude in the nonphysical region of $t > 0$ is examined and similarly in the physical region for $t = -4k^2$. Some relationships which stem from the unitarity are defined, and the extremal value of the differential cross section of elastic scattering is obtained for a random angle at any energies. Some inequalities are obtained for the cross section of the elastic scattering, in particular the upper bounds for the scattering cross section in the region of the front diffraction peak. Most of the results have been obtained by the Legendre binomila expansion of the amplitude scattering, but a more convenient integral expression is derived for (1) very small angles and high energies, and (2) for any angles and any energies.

Elastic πp^-, pp^-, $p\bar{p}^-$, and Kp^-Interactions at High Energies
S. A. Azimov, G. G. Arushanov, U. G. Gulyamov, and A. A. Yuldashev

ABSTRACT: The theoretical differential cross section of elastic scattering in the front hemisphere ($0° \leq \theta \leq 90°$) is compared with existing experimental results of the scattering of pions, protons, antiprotons, and kaons on protons at high energies. The theoretical results obtained (1) for elastic scattering of particles in the vicinity of zero, and (2) scattering at angles of $0° < \theta \leq 90°$ are compared with the experimental data on p^-, pp^-, pp^-, Kp^-scatterings. Agreement between theory and experiment is satisfactory.

Azimuthal Angular Distribution of Shower Particles and Gray Tracks Formed by Particles of Cosmic Radiation in a Photoemulsion
S. A. Azimov, M. S. Rasulkulov and V. M. Chudakov

ABSTRACT: A description is given of the azimuthal angular distribution of gray tracks (grain density greater than 1.4 g_0) in 33 showers. The distribution of angles ϕ for the 33 showers is not in agreement with the isotropic distribution. In at least a portion of the showers, there is a tendency to emit shower particles and gray tracks in opposite directions. The observed effects can be explained on the basis of concepts of the development of an intranuclear cascade.

On Inelastic Coherent Interactions of High-Energy Protons With Complex Nuclei
Sh. Abduzhamilov, S. A. Azimov, L. P. Chernova, G. M. Chernov and V. M. Chudakov

ABSTRACT: A method is described which makes it possible to register with high effectiveness the degree of nonuniformity in the angular distributions in a laboratory system and the differences between the angular distributions of secondary particles detected with its aid in showers which are taken as pp- and pn-collisions. The method involves a study of m showers with the same energy of primary particles and the same number n of secondary charged particles. The values of F (angular nonhomogeneity of showers) are greater for n = 3 and 5 than for n = 2, 4, and 6. The nonmonotonic dependence of F on n makes it possible to conclude that for an even number of particles n, pp-collisions have been primarily selected, while for n = 3 and 5, besides pn-collisions, there are showers of another nature with a substantially different angular distribution in the laboratory system.

Study of Inelastic π^-p-Collisions With a Slow Recoil Proton at an Energy of 17 GeV

S. A. Azimov, B. K. Nikishin, I. V. Rechitskiy, and V. M. Chudakov

ABSTRACT: Inelastic π^-p-interactions with free and quasifree protons of a photoemulsion are described. The results of the determinations of the angle of departure of the secondary particle with the Z axis in the XYZ system, because of the ultrarelativistic approach, are to be regarded as auxiliary. The angular correlations and the distribution of the residual effective masses indicate the possible existence of a resonance with a mass of 3.2 GeV, but such a conclusion can be made only on the basis of more extensive experimental data which are not available at present.

Study of Coherent Inelastic Interactions of Pions With an Energy of 17.2 BeV With Heavy Nuclei of a Photoemulsion

S. A. Azimov, Ye. V. Beter, U. G. Gulyamov, N. B. Eroshkina, and A. Ya. Levin

ABSTRACT: The photoemulsion procedure was used to study coherent interactions, using a pile of an Ilford G = 5 photoemulsion (600 microns thick) of 16 plates, irradiated with π^--mesons with a pulse of 17.2 ± 0.2 BeV/c. An analysis of the distribution with respect to q_1 confirms the dominant role of processes on heavy nuclei. The form of the summary theoretical distributions depends on the diffraction characteristics of the nuclei which participate in the process, the law of increase in the cross section with increasing atomic weight, and the background of the noncoherent interactions. The Coulomb variant of the process plays an insignificant role.

Study of Angular Correlations of Particles in Nuclear Disintegrations With Fragments

S. A. Azimov and R. Karimova

ABSTRACT: The angular correlations and their possible dependence on the energy and number of fragments in splitting was studied with a nuclear photoemulsion having an average proton sensitivity of 30-40 MeV and irradiated with protons of 660 MeV. There was no angular correlation between the light particles and the fragment in the center-of-mass system. This indicates that the emission of light particles and emission of fragments are not simultaneous. The emission of fragments from the nucleus precedes the evaporation of light particles.

Gas-Discharge Tubes With a Large Effective Area
S. A. Azimov, E. S. Bakhromi, Yu. D. Bogachkin, Kh. Zaynutdinov, and R. Karimov

ABSTRACT: Methods are described for making gas-discharge tubes and their characteristics are given. In order to reduce the cost, technical neon, instead of spectrally pure, was used. The tubes were filled to a pressure not exceeding atmospheric. A generator was developed which produces single rectangular pulses with an amplitude of 5-25 kv. The tubes were made of ZS-5 type glass, 80 cm long, outside diameter 1.8 cm, and wall thickness 1.2 mm. The tubes are light-sensitive and should be insulated. For a pulse duration greater than 3 microsec, the effectiveness of the tubes is practically independent of the pulse duration; for less than 3 microsec, the effectiveness drops.

Energy Transfer to an Electron-Photon Component During the Interaction of Particles With Graphite Nuclei
S. A. Azimov and Yu. V. Polyak

ABSTRACT: The energy transferred by primary nuclear-active particles and nuclear-active particles of second generation to the electron-photon component was measured from the maximum cascade which developed in lead. During the interaction of nuclear-active particles, a considerable portion of the energy of the primary particles is transferred to the electron-photon component.

ELASTIC SCATTERING OF STRONGLY-INTERACTING PARTICLES AT HIGH ENERGIES[1]

G. G. Arushanov

At the present, there is much experimental data on the elastic $\pi^{\pm}$ p-, $p\bar{p}$-, $K^{\pm}$p-interaction at high energies (E > 5 GeV). The last three or four years have been particularly fruitful in this respect. The theoretical interpretation of the results is available in many references. The approach based on the use of an optical model for the interaction of high-energy particles is both conventional and simple. The turning point in the physics of elementary particles was the dual spectral representations for the elastic-scattering amplitude discussed by Mandel'shtam (1958), the use of the analytic properties of the component amplitudes as functions of two complex variables, energy and orbital moment (Regge, 1959), and finally, the comment by Mandel'shtam (1960) made at the Berkely Conference, as a result of which it became possible to utilize Regge's ideas (which are clearly valid in the nonrelativistic quantum theory) in high-energy physics applications. On the basis of this theory, a number of relations were obtained and then checked experimentally. The main achievement of the theory was the prediction of the contraction of the diffraction pattern with rising energy, which was not observed in the experiments on pp-scattering. However, with the accumulation of experimental facts, it became clear that this theory cannot satisfactorily describe the experimental data, at least in its simplest form, in particular the absence of contraction in the πp-scattering and its simultaneous presence in pp-scattering. /3*

In connection with the previous comments, different phenomenological theories and models are of interest. In this context, it is possible to obtain many useful results which facilitate an analysis of the experimental data. In studying the scattering amplitude, it is convenient to expand it into a series of Legendre polynomials /4

$$f(x) = \frac{1}{2k} \sum_{l=0}^{\infty} (2l+1)\, a_l(k)\, P_l(x), \qquad (1)$$

[1]See also [1-6].

*Numbers in the margin indicate pagination in the foreign text.

where $a_l = 1 - S_l = 1 - \eta_l e^{2i\alpha_l}$; S_l is the scattering matrix; η_l and α_l are real numbers; $-\pi/2 \leqslant \alpha_l \leqslant \pi/2$ and due to the unitary nature of the scattering matrix $0 \leqslant \eta_l \leqslant 1$, x = cos θ (θ is the scattering angle). The series (1) is sometimes called the Faxen-Holtsmark series. The magnitude η_l characterizes the inelastic processes. For small energies, when the inelastic channels are closed, all the η_l are equal to unity. The differential cross section of the elastic scattering $\frac{d\sigma}{d\Omega}$ and the complete cross sections of the elastic σ_{el} and inelastic σ_{in} interactions, as well as the interaction σ_t, are expressed by the corresponding partial parameters:

$$\frac{d\sigma}{d\Omega} = \sigma(x) = |f(x)|^2 = \frac{1}{4k^2}\left|\sum_{l=0}^{\infty}(2l+1)\,a_l P_l(x)\right|^2, \tag{2}$$

$$\sigma_{el} = \frac{\pi}{k^2}\sum_{l=0}^{\infty}(2l+1)\left|1-\eta_l e^{2i\alpha_l}\right|^2 =$$

$$= \frac{\pi}{k^2}\sum_{l=0}^{\infty}(2l+1)\left(1-2\eta_l\cos 2\alpha_l+\eta_l^2\right), \tag{3}$$

$$\sigma_{in} = \frac{\pi}{k^2}\sum_{l=0}^{\infty}(2l+1)\left(1-\eta_l^2\right), \tag{4}$$

$$\sigma_t = \frac{2\pi}{k^2} \sum_{l=0}^{\infty} (2l+1)\,(1-\eta_l \cos 2\alpha_l) = \frac{4\pi}{k}\, Im\, f(1) \qquad (5)$$

Equation (3) can be thus rewritten as /5

$$\sigma_{el} = \frac{\pi}{k^2}\left(\sum_{l=0}^{\infty} (2l+1)\,(1-\eta_l)^2 + \sum_{l=0}^{\infty} (2l+1)\, 4\eta_l \sin^2 \alpha_l \right). \qquad (3')$$

The elastic scattering which is governed by the presence of inelastic channels is diffractional and specified by the first term of Equation (3').

The component amplitude $a_l(k)$ depends on the orbital number l and the energy k. If we knew this dependence, then the problem of elastic scattering could be solved because according to Equations (1) - (5) we could calculate any value that characterizes the elastic interaction. Since the $a_l(k)$ are unknown in the strong interactions of interest, one often proceeds in the opposite direction. From known experimental data on the angular distribution and total cross sections, one finds $a_l(k)$ i.e., phase analysis, more correctly, component analysis, is accomplished. The processing of experimental data by means of phase analysis is one of the most important problems in the scattering theory because the phases can be related with parameters that characterize the internal structure of the particles. This is achieved in an optical model for the interaction of particles, a brief description of which is given in Section 1.

§ 1. Optical Model for Interaction at High-Energies.

The first model of nuclear reactions was proposed by Bethe and Fermi. According to this model, the action of the nucleus on the incident particle was replaced by the action of a simple, real, potential well. However, the discovery of resonances during the scattering of neutrons of small energies contradicted the conclusions derived from this simple model. The results of experiments have led Niels Bohr to the conclusion that the interaction of an incident particle with the nucleus should bear the nature of a strong interaction and, therefore, the incident particles should be immediately captured by the nucleus, which results in the formation of a compound nucleus with subsequent decomposition that does not depend on the method of formation. In spite of the success of this model in the interpretation of nuclear reactions,

it has some disadvantages, as any model would. The main disadvantage is that this model can only describe nuclear reactions at small energies when the formation of a compound nucleus is possible. For large energies, the average length of the free run of an incident particle becomes comparable in magnitude with the radius of the nucleus. In this case, the nucleus is no longer an absolutely black target which absorbs all particles that fall on it. The nucleus becomes partly transparent, i.e., the incident particle can pass through it without, in general, being subjected to collisions. /6

The fact that the nucleus should be transparent at high energies was first observed in 1949 by Fernbach, Serber, and Taylor. In the optical model they proposed, the scattering element (nuclear substance) is regarded as a refracting and absorbing medium in complete analogy with geometric optics. In accordance with this model, a complex refractive index is introduced, i.e., a complex potential well. Thus, the optical model is an intermediate step between the model of the (real) potential well and the model of the compound nucleus. The optical model was applied for the first time by the authors to an analysis of neutron-nucleus scattering with an energy of 90 Mev. This application has led to good agreement of the experimental data with the phenomenological optical model. Later, geometrical optics representations have been applied with success to the analysis of the experimental data on πp- and pp-scattering at high energies.

Let us examine a number of optical potentials and discuss the validity of the geometrical optics approximation.

Specific Potentials. In the quasiclassical approximation (WKB approximation), we have for large energies:

$$a_l = 1 - \exp\left(2i\delta_l(k)\right),$$

$$\delta_l(k) = \alpha_l(k) + i\beta_l(k) = \delta(\rho) = -\int_\rho^\infty \frac{V(r)\,r}{(r^2-\rho^2)^{1/2}}\,dr, \tag{6}$$

where $\rho = (l + 1/2)\lambda$ is the impact parameter and V(r) is the complex optical potential.

The elastic scattering amplitude in the geometrical optics approximation has the form

$$f = ik\int_0^\infty a(\rho)\,J_0(k\theta\rho)\,\rho d\rho, \tag{7}$$

where $\mathbf{a}(\rho)$ is determined by Equation (6). We will assume that the optical potential is purely imaginary: $\alpha_\eta = 0$, i.e., the scattering is purely diffractional. The total cross sections in the approximation under consideration are given by

$$\sigma_{el} = 2\pi \int_0^\infty \rho \left(1 - \exp\left(-2\beta(\rho)\right)\right)^2 d\rho$$
$$\sigma_t = 4\pi \int_0^\infty \rho \left(1 - \exp\left(-2\beta(\rho)\right)\right)^2 d\rho \qquad (8)$$

/7

Let us examine several specific potentials.

1. Rectangular potential well:

$$V(r) = \begin{cases} -iV_0 & r \leqslant R \\ 0 & , r > R. \end{cases} \qquad (9)$$

In this case, we get

$$\beta(\rho) = \begin{cases} V_0 (R^2 - \rho^2)^{1/2}, & \rho \leqslant R \\ 0, & \rho > R, \end{cases} \qquad (10)$$

$$f = ikR^2 \left[\frac{J_1(k\theta R)}{k\theta R} - \sum_{n=0}^{\infty} \frac{(-1)^n}{(n!)^2} \left(\frac{k\theta R}{2} \right)^{2n} a_n \right], \qquad (11)$$

where

$$a_n = \int_0^1 \exp(-ax) (1 - x^2)^n x dx,$$
$$\sigma_{el} = \pi R^2 \left[1 - \frac{7}{2a^2} + 4e^{-a} \left(\frac{1}{a} + \frac{1}{a^2} \right) - e^{-2a} \left(\frac{1}{a} + \frac{1}{2a^2} \right) \right], \qquad (12)$$

$$\sigma_t = 2\pi R^2 \left[1 - \frac{2}{a^2} + 2e^{-a}\left(\frac{1}{a} + \frac{1}{a^2}\right)\right], \qquad a = 2V_0 R. \tag{13}$$

2. Gauss potential

$$V(r) = -iV\exp(-\alpha^2 r^2). \tag{14}$$

In this case, we get

$$\beta(\rho) = \frac{V}{2\alpha}\sqrt{\pi}\exp(-\alpha^2\rho^2), \tag{15}$$

$$f = \frac{ik}{2\alpha^2}\sum_{n=1}^{\infty}\frac{(-a_1)^{n+1}}{nn!}\exp\left(-\frac{k^2\theta^2}{4\alpha^2 n}\right), \tag{16}$$

$$\sigma_{el} = \sigma_t - \frac{\pi}{\alpha^2}\left[C + \ln(2a_1) - E_i(-2a_1)\right], \tag{17}$$

/8

$$\sigma_t = \frac{2\pi}{\alpha^2}\left[C + \ln a_1 - E_i(-a_1)\right], \qquad a_1 = \frac{V}{\alpha}\sqrt{\pi} \tag{18}$$

Here $E_i(x)$ is the integral exponential function, and C - Euler constant.

3. Yukawa potential

$$V(r) = -ige^{-\alpha r}/r. \tag{19}$$

In this case

$$\beta(\rho) = gK_0(\alpha\rho), \tag{20}$$

so that for large ρ

$$\beta(\rho) \simeq g\sqrt{\frac{\pi}{2\alpha\rho}}\, e^{-\alpha\rho}. \tag{21}$$

4. Let us also examine a potential of the type

$$V(r) = -iVe^{-\alpha^2 r^2}/r^2. \tag{22}$$

In this case,

$$\beta(\rho) = V\frac{e^{-\alpha^2\rho^2}}{\rho}\int_0^\infty \frac{\exp(-\alpha^2\rho^2x^2)}{1+x^2}\,dx. \tag{23}$$

For very small and very large ρ, we get

$$\begin{aligned}\beta(\rho) &\cong \frac{\pi}{2}V\frac{e^{-\alpha^2\rho^2}}{\rho}, \quad \rho \ll \alpha^{-1}\\ \beta(\rho) &\cong \frac{\sqrt{\pi}}{2\alpha}V\frac{e^{-\alpha^2\rho^2}}{\rho^2}, \quad \rho \gg \alpha^{-1}\end{aligned} \tag{23'}$$

As illustrated by analysis of the existing experimental data for high energies (E > 5 BeV) and small pulse transfers $\left((t) < 0.5\ (\text{BeV/c})^2\right)$, all the models examined above yield satisfactory results. For example, experiments on pp-scattering yield the following values for the parameters of the optical model:

$V_0R = 0.5$: $R^2 = 13.5$ mbn (rectangular well) /9

$\frac{V}{\alpha}\sqrt{\pi} = 2.0$; $\alpha^2 = 0.22$ mbn^{-1} (Gauss potential)

$g = 2.5$; $\alpha^2 = 0.83$ mbn^{-1} (Yukawa potential)

Comments on the Applicability. It was assumed above that the optical potential exists. However, this circumstance is not at all obvious. In order to substantiate the optical model of the nucleus, much work has been done by D. I. Blokhintsev who showed that in general there does not exist a complex optical potential that could be interpreted as an optical index of refraction and absorption of the waves within the scattering element. However, in the case where the geometrical optics are applicable, such a potential does exist. We shall not examine here this problem. We only wish to make the following observation. If we write the integral expression for the Legendre polynomials

$$P_l(\cos\theta) = \frac{1}{l!}\int_0^\infty e^{-x\cos\theta} J_0(x\sin\theta)\, x^l dx, \quad 0 \leqslant \theta < \frac{\pi}{2}, \tag{24}$$

and substitute in (1), then we get an exact representation for the amplitude scattering:

$$f = \frac{i}{2k}\int_0^\infty J_0(y\sin\theta) e^{-y\cos\theta} A(k, y)\, dy, \quad 0 \leqslant \theta < \frac{\pi}{2}, \tag{25}$$

where

$$A(k, y) = \sum_{n=0}^{\infty} (2n+1)\, a_n(k)\, \frac{y^n}{n!} \tag{26}$$

By comparing this expression with formula (7), we see that the latter is obtained from the exact formula (25) by the substitution

$$\sum_{n=0}^{\infty}(2n+1)\frac{y^n}{n!}a_n(k) \to e^{y\cos\theta}(2y+1)\,a\left(\frac{y}{k}\right). \qquad [27]$$

On the other hand, we observe that

$$\sum_{n=0}^{\infty}(2n+1)\frac{y^n}{n!} = (2y+1)\,e^y. \qquad [28]$$

Consequently, it can be said that the geometrical optics approximation assumes that: (1) small angles exist ($\theta \simeq 0$); (2) a certain average /10

$\overline{a}_n(k) = a\left(\frac{y}{k}\right)$ is placed outside the sign of the sum in Equation (27).

§ 2. Summation of the Faxen-Holtsmark Series.

In Section 1, the component amplitude was set as the function of the impact parameter, and the differential and total interaction cross sections were determined by means of Equations (7) and (8). We examined four types of optical potentials and we showed that for small momentum transfers, in which only Equation (7) can be valid, their results match the experiment satisfactorily. The specific type of potential does not play a large role. In this section, we get certain general results without specifying the $a_l(k)$. Also in this section, unlike the preceding one, we are not limited to small angles. The result (7) is actually obtained from the general expression (1) by the replacement of the summation by integration. As observed at the end of section 1, this operation is valid only for very small scattering angles ($\theta \simeq 0$), while for angles that differ notably from zero it is necessary to use a more accurate expression. We shall make use of the well-known Euler-Maclaurin formula:

$$\sum_{l=l_0}^{l_1} f(l) = \int_{l_0}^{l_1} f(l)\,dl + \frac{1}{2}[f(l_0)+f(l_1)] + \\ + \sum_{k=1}^{n}\frac{B_{2k}}{(2k)!}\left[f^{(2k-1)}(l_1) - f^{(2k-1)}(l_0)\right] + R_n. \qquad (29)$$

With respect to the $a_l(k)$, the following is assumed: these amplitudes and their derivatives, examined as functions of an orbital moment, approach zero at a rate faster than the exponent at infinity. This assumption means

physically that the interactions under consideration have a short-acting nature.

Back-Scattering in the Vicinity of 180°. By substituting $P_l(-1) = (-1)^l$ in the general expression (1), we rewrite it in the form

$$2ikf(-1) = \sum_{n=0}^{\infty} (4n+3)(a_{2n+1} - a_{2n}) + 2\sum_{n=0}^{\infty} a_{2n}. \tag{30}$$ /11

The difference that appears in the parentheses can be expressed in terms of the derivatives by the relation

$$a_{l+1} - a_l \equiv \Delta a_l = \sum_{k=1}^{\infty} \frac{1}{k!} a_l^{(k)}. \tag{31}$$

By means of the Euler-Maclaurin formula, we get

$$\left.\begin{aligned} 2\sum_{n=1}^{\infty} a_{2n} &\simeq 2\sum_{n=0}^{n_0-1} a_{2n} + \int_{l_0}^{\infty} a_l dl + a_{l_0} - \frac{1}{3} a'_{l_0} \\ \sum_{n=0}^{\infty} (4n+3)(a_{2n+1} - a_{2n}) &\simeq \sum_{n=0}^{n_0-1} (4n+3)(a_{2n+1} - a_{2n}) - \\ &- \int_{l_0}^{\infty} a_l dl - (l_0+1) a_{l_0} + a_{l_0}\left(\frac{l_0}{2} + \frac{7}{12}\right) - \\ &- \frac{1}{8} a'_{l_0} (l_0 = 2n_0) \end{aligned}\right\} \tag{32}$$

with an accuracy up to the second derivative inclusively.

Consequently, the back-scattering amplitude is equal to

$$2ikf(-1) \simeq 2\sum_{n=0}^{n_0-1} a_{2n} + \sum_{n=0}^{n_0-1} (4n+3)(a_{2n+1} - a_{2n}) - \\ -l_0 a_{l_0} + a'_{l_0}\left(\frac{l_0}{2} + \frac{1}{4}\right) - \frac{1}{8} a''_{l_0}. \tag{33}$$

with an accuracy up to the second derivative.

If it is assumed that $n_0 = 1$, i.e., $l_0 = 2$, then we get

$$2ikf(-1) \simeq -a'_0 + \frac{5}{4} a'_2 - \frac{5}{2} a''_0 - \frac{1}{8} a''_2 \simeq \\ \simeq \frac{1}{4}\left(a'_0 - \frac{1}{2} a''_0\right). \tag{34}$$

Thus, the back-scattering amplitude is determined not by the a_{l_0} but by their derivatives. /12

Now let us examine the scattering in the vicinity of 180°, i.e., let $\theta = \pi - \alpha$, where $\alpha \ll \pi$. In this case, we get

$$f\left(-1 + \frac{\alpha^2}{2}\right) \simeq f(-1) + \\ + \frac{l}{2k} \frac{1}{2} \sum_{l=0}^{\infty} (2l+1) l (l+1) (-1)^{l+1} a_l \frac{\alpha^2}{2}. \tag{35}$$

In calculating finally the sum which appears here, we have the following expressions for the scattering amplitude and cross section near 180°:

$$f\left(-1 + \frac{\alpha^2}{2}\right) \simeq f(-1) + \frac{i a_0 \alpha^2}{4k}, \\ \sigma\left(-1 + \frac{\alpha^2}{2}\right) = \sigma(-1) - \frac{\alpha^2}{2k} (\mathrm{Re} f(-1)\, \mathrm{Im}\, a_0 - \tag{36}$$

$$- \mathrm{Im} f(-1)\, \mathrm{Re}\, a_0). \tag{36'}$$

Scattering at 90° and in the Vicinity of 90° Let us derive an approximate formula for the scattering amplitude at 90°. A more accurate result suitable not only in the case of 90° scattering, but also for any fixed angle different from zero, will be obtained in the next paragraph.

The 90° scattering amplitude can be written in the form

$$2ikf(0) \simeq \sum_{n=0}^{\infty} \sqrt{8n+5}\,(a_{4n+2} - a_{4n}) + \\ + \sum_{n=0}^{\infty} \sqrt{8n+5} - (\sqrt{8n+1})\, a_{4n}. \tag{37}$$

With an accuracy up to the second derivative inclusively, we have

$$\sum_{n=n_0}^{\infty} \sqrt{8n+5}\,(a_{4n+2} - a_{4n}) \simeq \frac{1}{4} \int_{l_0}^{\infty} \sqrt{2l+5}\,\Delta a_l\, dl + \\ + \sqrt{2l_0+5}\left(a'_{l_0} + \frac{1}{3} a'_{l_0}\right), \tag{38}$$

$$\sum_{n=n_0}^{\infty} (\sqrt{8n+5} - \sqrt{8n+1})\, a_{4n} \simeq \\ \simeq \frac{1}{4} \int_{l_0}^{\infty} (\sqrt{2l+5} - \sqrt{2l+1})\, a_l\, dl + \tag{39}$$

/13

$$+ (\sqrt{2l_0+5} - \sqrt{2l_0+1}) \left(\frac{a_{l_0}}{2} - \frac{1}{3} a'_{l_0}\right),$$

where $l_0 = 4\,n_0$, and it is assumed that $l_0 \neq 0$. The integral that appears in Equation (38) has the form

$$\int_{l_0}^{\infty} (2l+5)^{1/3}\, \Delta a_l\, dl = \sum_{k=1}^{\infty} \frac{2^k}{k!} \int_{l_0}^{\infty} (2l+5)^{1/3}\, a_l^{(k)}\, dl, \tag{40}$$

where

$$\int_{l_0}^{\infty}(2l+5)^{1/3}a_l^{(k)}dl = -(2l_0+5)^{1/3}a_{l_0}^{(k-1)} + \cdot$$
$$+(2l_0+5)^{-1/3}a_{l_0}^{(k-2)} + 1\,(2l_0+5)^{-3/3}a_{l_0}^{(k-3)} +$$
$$+1\cdot3\,(2l_0+5)^{-5/3}a_{l_0}^{(k-4)} + 1\cdot3\cdot5\,(2l_0+5)^{-7/3}a_{l_0}^{(k-5)} +$$
$$+\cdots+1\cdot3\cdot5\ldots(2k-5)\,(2l_0+5)^{-\frac{2k-3}{2}}a_{l_0} -$$
$$-1\cdot3\cdot5\ldots(2k-3)\int_{l_0}^{\infty}(2l+5)^{-\frac{2k-1}{2}}a_l\,dl. \qquad [41]$$

As can be seen from the last two formulas, the series (40) converges very rapidly. Assuming that $n_0 = 1$, i.e., $l_0 = 4$, we get the following expression for the 90° scattering amplitude:

$$2ikf(0) \simeq (-0{,}26+\beta(k))a_4 - 0{,}5\,a_0' + 1{,}5a_4' - 5{,}5\,a_0, \qquad (42)$$

where

$$0 < \beta(k) < 0{,}5. \qquad (43)$$

Now, let us examine the scattering in the 90° region, i.e., let $\theta = \frac{\pi}{2} \pm \alpha$, where $\alpha \ll \pi/2$. Calculation gives

$$2ikf(\pm\alpha) \simeq 2ikf(0) + 4a_4\alpha^2. \qquad (44)$$

It is seen from this expression that the scattering cross section in the region of angles close to 90° should be symmetric with respect to $\pi/2$. If $\beta(k) > 0.26$, then the 90° scattering cross section has a minimum; however, if $\beta(k) < 0.26$, then there is a maximum at 90°. The first case is apparently realized, as shown by experiments. /14

Scattering at angles different from 0 and π. Let us write the scattering amplitude in the form of the sum of two terms:

$$f(x)=\frac{i}{2k}\left(\sum_{l=0}^{l_0-1}(2l+1)\,a_l P_l(x)+\sum_{l_0}^{\infty}(2l+1)\,a_l P_l(x)\right), \tag{45}$$

where l_0 is a certain fixed integer number. For a finite l_0, in order to evaluate the first sum, one can as a first approximation assume that $a_l \simeq a_{l_0}(l<l_0)$ for sufficiently high energies, and consequently:

$$\sum_{l=0}^{l_0-1}(2l+1)\,a_l P_l(x)\simeq a_{l_0}\,l_0\frac{P_{l_0-1}(x)-P_{l_0}(x)}{1-x}. \tag{46}$$

In order to calculate the second sum when $\theta\neq 0,\ \pi$, we shall utilize the well-known asymptotic formula for the Legendre polynomials

$$P_l(\cos\theta)\cong\sqrt{\frac{1}{\pi l\sin\theta}}\cos\varphi(\theta,l), \tag{47}$$

where

$$\varphi(\theta,l)=(l+1/2)\theta-\frac{\pi}{4}. \tag{48}$$

Thus, the problem reduces to the calculation of the sum

$$\sum_{l=l_0}^{\infty}l^{1/2}a_l\cos\varphi(\theta,l). \tag{49}$$

Summation by means of the Euler-Maclaurin formula leads to the following result for the scattering amplitude (with an accuracy up to a_{l_0}):

$$f(x)=\frac{i}{2k}\left\{\sum_{l=0}^{l_0-1}(2l+1)a_lP_l(x)+2\sqrt{\frac{2}{\pi\sin\theta}}\times\right.$$

$$\times\left[\left[-\theta^{-1}\,l_0^{1/2}a_{l_0}\sin\varphi(\theta,l_0)-\theta^{-2}\left(\frac{1}{2}\,l_0^{-1/2}a_{l_0}+\right.\right.\right.$$

$$+l_0^{1/2}a'_{l_0}\Big)\cos\varphi(\theta,l_0)+\theta^{-3}\left(\frac{1}{2}\left(-\frac{1}{2}\right)l_0^{-3/2}a_{l_0}+\right.$$

$$+l_0^{-1/2}a'_{l_0}\Big)\sin\varphi(\theta,l_0)+\theta^{-4}\left(\frac{1}{2}\left(-\frac{1}{2}\right)\left(-\frac{3}{2}\right)l_0^{-5/2}a_{l_0}-\right. \qquad (50)\quad /15$$

$$\left.-\frac{3}{4}\,l_0^{-3/2}a'_{l_0}\Big)\cos\varphi(\theta,l_0)+\cdots\right]+\left[\frac{1}{2}\,l_0^{1/2}a_{l_0}\cos\varphi(\theta,l_0)-\right.$$

$$-\frac{1}{12}\left(\frac{1}{2}\,l_0^{-1/2}a_{l_0}\cos\varphi(\theta,l_0)-l_0^{1/2}a_{l_0}\theta\sin\varphi(\theta,l_0)+\right.$$

$$\left.\left.+l_0^{1/2}a'_{l_0}\cos\varphi(\theta,l_0)+\cdots\right]\right].$$

In selecting a sufficiently large l_0, Equation (50) can be used to calculate the scattering cross section for any fixed angle that differs from zero and 180°. If one could disregard terms of the order of a'_{l_0} and higher derivatives, then the result (50) would assume the form

$$f(x)\,\frac{i}{2k}\left\{\sum_{l=0}^{l_0-1}(2l+1)\,a_lP_l(x)+a_{l_0}(k)\,C(\theta,l_0)\right\}, \qquad (51)$$

where

$$C(\theta,l_0)=2\sqrt{\frac{2}{\pi\sin\theta}}\left[\sin\varphi(\theta,l_0)\left(-\theta^{-1}\,l_0^{1/2}-\right.\right.$$

$$\left.-\theta^{-3}\frac{1}{4}\,l_0^{-3/2}+\frac{\theta}{12}\,l_0^{1/2}\right)+\cos\varphi(\theta,l_0)\left(-\frac{1}{2}\theta^{-2}\,l_0^{-1/2}+\right. \qquad (52)$$

$$\left.\left.+\frac{3}{8}\theta^{-4}\,l_0^{-5/2}+\frac{1}{2}\,l_0^{1/2}-\frac{1}{24}\,l_0^{-1/2}\right)\right].$$

It follows from Equations (51) and (34) that, if the absorption is very great such that the parameters a_l are real when $l \ll l_0$, then the scattering amplitude is purely imaginary for all the angles that differ from zero. Also, it follows from these results that the scattering cross section at fixed angles that differ from zero should satisfy the inequality

$$\sigma(\theta) \leqslant \lambda^2, \quad \theta \neq 0, \quad \lambda \to 0. \tag{53}$$

Relationship of the Back-Scattering Amplitude with the Partial Amplitude and Total Cross Section. For the acceleration energy presently attainable, the experiments on the elastic πp- and Kp-interaction indicate that the /16

parameter $X \equiv \sigma(\theta) / \left(\frac{k\sigma_t}{4\pi}\right)^2$, which is frequently used in the analysis of experimental data, depends only on the transferred 4-momentum and does not depend (or depends very weakly) on the energy. Let us assume that the parameter X, specified by Equation (54), ceases to depend on the energy when the latter approaches infinity. Then, the following correlation between the back-scattering amplitude, the total interaction cross section σ_t, and the partial s-amplitude a_0 takes place:

$$f(180^\circ) = \frac{i\sigma_t(k)}{4} \frac{d}{dk}\left(\frac{a_0(k)}{\sigma_t(k)}\right). \tag{55}$$

Actually, the partial s-amplitude is equal to

$$\begin{aligned} a_0(k) &= -ik\int_{-1}^{1} f(x)\,dx = -ik\frac{ik\sigma_t}{4\pi}\int_{-1}^{1}\frac{f(x)}{\frac{ik\sigma_t}{4\pi}}dx = \\ &= \frac{ik_t}{8\pi}\int_{0}^{-4k^2} X_1(t)\,dt, \end{aligned} \tag{56}$$

where

$$X_1(t) \equiv \frac{f(x)}{\frac{ik\sigma_t}{4\pi}}$$

by assumption depends only on t and not on k. Dividing (56) by σ_t and taking the derivative with respect to k, we get the result (55). Thus, if the derivative which appears in (55) is known, one could calculate the scattering cross section for any transferred momenta that differ from zero.

Let us compare the result (55) with Equation (34). In order to facilitate this comparison, let us assume that it is possible to use quasi-classical principles. Let us assume that $a_l(k)$ depends on l and k through the combination $\rho = (l + 1/2)\lambda$, which can be called an impact parameter in the quasi-classical sense. Equating (34) and (55), we have /17

$$-a_0' + \frac{5}{2} a_0^* = 2ka_0 \left(\frac{1}{a_0} \frac{da_0}{dk} - \frac{1}{\sigma_t} \frac{d\sigma_t}{dk} \right). \tag{57}$$

Substituting in here the derivatives, we get

$$\frac{5}{2} a^* \left(\frac{1}{2k} \right) = - \frac{2a\left(\frac{1}{2k} \right)}{\sigma_t} k^2 \frac{d\sigma_t}{dk}. \tag{58}$$

If $a^* \left(\frac{1}{2k} \right) \underset{k \to \infty}{\to} 0$, then

$$k^2 \frac{d\sigma_t}{dk} \underset{k \to \infty}{\to} 0. \tag{59}$$

We wish to observe that Equation (55) can also be written in the form

$$f(-1) = \frac{1}{4} \left[\int_{-1}^{1} f(k, x)\, dx + k \int_{-1}^{1} \frac{\partial f(x, k)}{\partial k} dx - \right.$$
$$\left. - \frac{k}{\sigma_t} \frac{d\sigma_t}{dk} \int_{-1}^{1} f(k, x)\, dx \right] \tag{60}$$

Scattering with Very Small Momentum Transfers. In this and in the subsequent paragraphs, some results will be obtained by using the mean-value theorem in order to calculate a definite integral. Unlike the preceding study, we shall partition the series at the L-th member, where L is the minimum number of waves that participate in the scattering. According to Grishin and Ogievetskiy,

$$(L+1)^2=\frac{k^2\sigma_t^2}{4\pi\sigma_{el}}(1+\delta^2),\ \delta=\frac{\operatorname{Re}f(0)}{\operatorname{Im}f(0)}\ . \tag{61}$$

It will also be assumed that the scattering amplitude is imaginary.

For small angles we have

$$P_l(\cos\theta)\simeq 1-l(l+1)\frac{\theta^2}{4}. \tag{62}$$

Substituting this expression in (1), we get /18

$$f(x)=f(1)\left[1-\frac{\theta^2}{4}\frac{\sum_{l=0}^{L}(2l+1)l(l+1)a_l}{\sum_{l=0}^{L}(2l+1)a_l}\right]. \tag{63}$$

In passing from the summation to integration, and utilizing the mean-value theorem, we get

$$f(x)=f(1)\left(1-\frac{\theta^2}{4}\bar{l}(\bar{l}+1)\right), \tag{64}$$

where $\bar{l}$ is a certain number contained between 0 and L:

$$\bar{l}=\alpha(k)L,\quad 0<\alpha(k)<1, \tag{65}$$

Also, generally speaking, $\alpha(k)$ can depend on the energy. In order to evaluate this factor in (65), we wish to observe that for high energies the scattering takes place essentially at small angles; and on this basis (64) can be rewritten as

$$f(x) \simeq f(1) \exp\left(-\frac{\theta^2}{4}\bar{l}(\bar{l}+1)\right) \tag{64'}$$

and we get

$$\sigma_{el} = 2\pi\left(\frac{k\sigma_t}{4\pi}\right)^2 (1+\delta^2)\int_0^{\infty} e^{-\frac{\theta^2}{2}\bar{l}(\bar{l}+1)}\theta d\theta = \frac{\sigma_{el}}{2\alpha^2(k)}, \tag{66}$$

i.e.,

$$\alpha^2(k) = {}^1/_2.$$

Thus, for small angles,

$$\frac{\sigma(\theta)}{\sigma(0)} = 1 - \frac{\sigma_t^2}{16\pi\sigma_{el}}k^2\theta^2 = 1 + \frac{\sigma_t^2}{16\pi\sigma_{el}}t, \tag{67}$$

where

$$|t| \ll \frac{16\pi\sigma_{el}}{\sigma_t^2}.$$

The t-coefficient in (67) is inversely proportional to the width of the diffraction peak

$$\Gamma \sim \frac{\sigma_{el}}{\sigma_t^2}. \tag{68}$$

Hence, it is seen that for these energies, there is contraction of the diffraction cone when the ratio σ_{el}/σ_t^2 decreases with increasing energy (for example, in the case of pp-scattering); however, if this ratio increases, then the diffraction cone should display an expansion (for example, in the case of $\bar{p}p$-scattering). It is pertinent to obtain also the lower bound for the parameter $X(s, t)$. When t is close to zero, we have /19

$$X_1(s, t) = 1 + at, \tag{69}$$

where

$$a \equiv \frac{\pi}{2k^4\sigma_t} \sum_{l=0}^{L} (2l+1)\, l\,(l+1)\, a_l(k).$$

On the basis of the Cauchy inequality, we get

$$\sum_{l=0}^{L} (2l+1)\, l\,(l+1)\, \gamma_l(k) \leqslant \left(\sum_{l=0}^{L} (2l+1)\, l^2\,(l+1)^2 \right)^{4/3} \times$$

$$\times \left(\sum_{l=0}^{L} (2l+1)\, \gamma_l^2\,(k) \right)^{1/3} \simeq \frac{L^3 k \sqrt{\sigma_{el}}}{\sqrt{3\pi}}$$

and consequently,

$$X(s, t) \geqslant 1 + \frac{\sigma_t^2}{16\sqrt{3}\,\pi\sigma_{el}}\, t. \tag{70}$$

We wish to observe that (70) does not contradict (67).

In accordance with (67), for small scattering angles,

$$f(\theta) \simeq f(0) \exp\left[-\frac{k^2\sigma_t^2}{16\pi\sigma_{el}} (1 - \cos\theta) \right],$$

where, in accordance with the optical theorem,

$$f(0) = \frac{ik\sigma_t}{4\pi}.$$

For the component amplitude, we get

$$\gamma_l \equiv 1 - \eta_l = -ik \int_{-1}^{1} f(\theta) P_l(\cos\theta) d\cos\theta = \frac{k^2 \sigma_t}{4\pi} e^{-a} A_l,$$

where /20

$$a \equiv \frac{k^2 \sigma_t^2}{16\pi\sigma_{el}}, \quad A_l \equiv \int_{-1}^{1} e^{ax} P_l(x)\, dx.$$

We wish to observe that γ_l, as well as A_l, satisfies the recurrence relationship

$$\gamma_{l+1} = \gamma_{l-1} - (2l+1)\gamma_l a^{-1}, \quad l = 1, 2\ldots \qquad \text{(a)}$$

By substituting the Rodrigues formula for the Lengendre polynomials in the integral expression for A_l and integrating l times by parts, we get

$$2^l l!\, A_l = e^{ax} \sum_{k=0}^{l-1} (-1)^k a^k \frac{d^{l-k-1}}{dx^{l-k-1}} (x^2-1)^l \Big|_{-1}^{1} +$$

$$+ (-1)^l a^l \int_{-1}^{1} e^{ax} (x^2-1)^l dx = (-1)^l a^l \int_{-1}^{1} e^{ax} (x^2-1)^l\, dx.$$

The last integral is equal to

$$\int_{-1}^{1} e^{ax} (x^2-1)^l dx = -i\sqrt{\pi}\, l! \left(\frac{2}{a}\right)^{l+1/2} I_{l+1/2}(-a).$$

Thus, the formula for the component amplitude will have the form

$$\gamma_l = i(-1)^{l+1} \frac{k^2\sigma_t}{4\sqrt{\pi}} e^{-a} \sqrt{\frac{2}{a}} I_{l+1/2}(-a). \tag{71}$$

It is possible to obtain a simpler expression when $l \ll L$ and $l \gg 1$. Actually, in the integral which expresses γ_l through $f(\theta)$, the main role is played by the small angles, for which

$$P_l(\cos\theta) \simeq 1 - \frac{l(l+1)}{2}(1-\cos\theta) \simeq \exp\left[-\frac{l(l+1)}{2}(1-x)\right]$$
$$\left(l \ll L, \theta \sim \frac{1}{L}\right).$$

For this reason,

$$\gamma_l \simeq \frac{k^2\sigma_t}{4\pi} \frac{1}{a + \frac{l(l+1)}{2}}$$

or, since $l \ll L \left(a \simeq \frac{(L+1)^2}{4}\right)$, /21

$$\gamma_l \underset{l<L}{\simeq} \frac{4\sigma_{el}}{\sigma_t} \exp\left[-\frac{l(l+1)}{k^2\sigma_t^2} 8\pi\sigma_{el}\right]. \tag{72}$$

In the case of $l \gg 1$, the recurrence relationship for γ_l can be rewritten in the form of the differential equation

$$\frac{d\gamma_l}{dl} \simeq -\frac{(2l+1)}{2a}\gamma_l,$$

which gives

$$\gamma_l \underset{l>1}{\simeq} Ce^{-\frac{l(l+1)}{2a}}.$$

In order to find the factor C, which does not depend on l, we shall make use of the fact that for small angles and $l \gg 1$,

$$P_l(\cos\theta) \approx J_0\left((l+1/2)\,\theta\right).$$

Then,

$$\gamma_l \underset{l>1}{\approx} \frac{k^2\sigma_t}{4\pi}\int_0^\infty e^{-a\frac{\theta^2}{2}} J_0\left((l+1/2)\,\theta\right)\theta d\theta = \frac{k^2\sigma_t}{4\pi}\,a^{-1}\,e^{-\frac{(l+1/2)^2}{2a}}.$$

Thus, for large l, we get the result (72):

$$\gamma_l \underset{l>1}{\approx} \frac{4\sigma_{el}}{\sigma_t}\exp\left[-\frac{(l+1/2)^2}{k^2}\frac{8\pi\sigma_{el}}{\sigma_t^2}\right] = \frac{4\sigma_{el}}{\sigma_t}\exp\left[-\frac{8\pi\sigma_{el}}{\sigma_t^2}\,\rho^2\right],$$

where $\rho = (l+1/2)\,k^{-1}$ is the collision parameter.

Since when $k \to \infty$ $L \to \infty$, the result (72) can be considered valid for all l.

Let us now examine the limitations imposed on the cross sections by the recurrence relationship (a) for γ_l.

By utilizing (a) we get for the scattering amplitude:

$$f(\theta) = \frac{i}{2k}\left(a\sum_{l=1}^{\infty}(\gamma_{l-1}-\gamma_{l+1})P_l(\cos\theta)+\gamma_0\right) = \tag{A}$$
$$= \frac{i}{2k}\left[a(\gamma_0 P_1+\gamma_1 P_2)+a\sum_{l=2}^{\infty}\gamma_l(P_{l+1}-P_{l-1})+\gamma_0\right]$$

In case of forward scattering, $(a \gg 1,\ \gamma_0 \simeq \gamma_1)$, we have

$$f(0) = \frac{i}{k}a\gamma_0 = i\frac{k\sigma_t}{4\pi}\frac{\sigma_t}{4\sigma_{el}}\gamma_0, \qquad /22$$

i.e.,

$$\gamma_0 \simeq \frac{4\sigma_{el}}{\sigma_t}.$$

In case of back scattering,

$$f(180°) = \frac{i}{2k}\left[-a(\gamma_0 - \gamma_1) + \gamma_0\right].$$

Substituting (72) here, we get

$$f(180°) \simeq i\frac{16\pi\sigma_{el}^2}{k^3\,\sigma_t^3}.$$

Assuming that for large energies γ_l decreases monotonically with increasing l, we get from (A), when $\theta \neq 0, 180°$,

$$|f(\theta)| \leqslant \frac{1}{2k}\left(a|\gamma_0 P_1 + \gamma_1 P_2| + \gamma_0 + a\gamma_2|P_1 + P_2|\right).$$

For the total cross sections, we get with the aid of (a):

$$\sigma_t = \frac{2\pi}{k^2}\left(a\sum_{l=1}^{\infty}(\gamma_{l-1} - \gamma_{l+1}) + \gamma_0\right) = \frac{2\pi}{k^2}\left(a(\gamma_0 + \gamma_1) + \gamma_0\right),$$

$$\sigma_t \simeq \frac{\sigma_t^2}{4\sigma_{el}}\gamma_0,$$

i.e.,

$$\sigma_{el} = \frac{\pi}{k^2}\left(a\sum_{l=1}^{\infty}\gamma_l(\gamma_{l-1} - \gamma_{l+2}) + \gamma_0\right) \simeq$$

$$\simeq -\frac{\pi}{k^2}a\int_0^{\infty} 2\gamma_l\,\gamma_l\,dl = \frac{\pi}{k^2}a\gamma_0^2 = \frac{\sigma_t^2}{16\sigma_{el}}\gamma_0^2,$$

i.e.

$$\gamma_0 \simeq \frac{4\sigma_{el}}{\sigma_t}.$$

The Ratio σ_{el}/σ_t. By utilizing the mean-value theorem, we get

$$\frac{\sigma_{el}}{\sigma_t} = \frac{\int_0^\infty (2l+1)\,\gamma_l^2 dl}{2\int_0^\infty (2l+1)\,\gamma_l dl} = \frac{\bar{\gamma}_l}{2}, \tag{73}$$

where $\bar{\gamma}_l$ is contained between 0 and γ_0. From (73), it follows that

$$\frac{\sigma_{el}}{\sigma_t} < \frac{\gamma_0}{2}.$$

If one selects for $\bar{\gamma}_l$ the natural value $\gamma_0/2$, then

$$\frac{\sigma_{el}}{\sigma_t} \simeq \frac{\gamma_0}{4}. \tag{74}$$

The relationship (74) also follows from the more general and strict result (72) when $l = 0$.

§ 3. Real Part of the Forward- and Back-Scattering Amplitude.

1. Let us examine the imaginary part of the scattering amplitude in the non-physical region $t > 0$, i.e., $\cos\theta \equiv z > 1$:

$$\operatorname{Im} f(z) = \frac{1}{2k}\sum_{l=0}^{\infty}(2l+1)\,a_l P_l(z), \tag{75}$$

where, due to the unitary condition,

$$0 \leqslant \frac{a_l}{2} \leqslant 1. \tag{76}$$

Let us find the extremum of the expression (75) for the fixed, total interaction σ_t and elastic scattering σ_{el} cross sections. By utilizing the Lagrange method for finding the conditional extremum, it is easy to show that the extremum is reached when

$$a_l = \alpha - \beta P_l(z). \tag{77}$$

Since z > 1, this expression, starting from a certain l_0, becomes negative; and on this basis we assume that

$$a_l = \begin{cases} \alpha - \beta P_l(z), & 0 \leqslant l \leqslant l_0 \\ 0, & l > l_0, \end{cases} \tag{77'}$$

where l_0 is determined from the condition

$$\alpha - \beta P_{l_0}(z) = 0. \tag{78}$$

For α and β we get /24

$$\left.\begin{aligned} \alpha &= \frac{2k \operatorname{Im} f(1)}{a_0}\left(1 + A\sqrt{a_1^2}\right) \\ \beta &= 2k \operatorname{Im} \dot{f}(1)\, A \end{aligned}\right\}, \tag{79}$$

where

$$\left.\begin{aligned} A &\equiv \left[\frac{\dfrac{a_0 \sigma_{el}}{4\pi \operatorname{Im}^2 f(1)} - 1}{a_0 a_2 - a_1^2}\right]^{1/2} \\ a_n &\equiv \sum_{l=0}^{l_0} (2l+1)\, P_l^n(z) \\ & \qquad n = 0, 1, 2, \end{aligned}\right\}. \tag{80}$$

From the condition of positiveness of the expression in the rectangular brackets, we have the lower boundary

$$(l_0 + 1)^2 \geqslant \frac{k^2 \sigma_t^2}{4\pi \sigma_{el}}.$$

Substituting (79) in (76), we get the equation for the determination of l_0:

$$\frac{a_2 - 2a_1 P_{l_0} + a_0 P_{l_0}^2}{(a_0 P_{l_0} - a_1)^2} = \frac{\sigma_{el}}{4\pi \operatorname{Im}^2 f(1)}. \tag{81}$$

A study of the left-hand side of (81) makes it possible to find the upper boundary

$$(l_0+1)\leqslant \frac{4}{3}\frac{k^2\sigma_t^2}{4\pi\sigma_{el}}.$$

For the extremum value of the imaginary part of the scattering amplitude in the non-physical region, we get the following expression:

$$\frac{\operatorname{Im} f(z)}{\operatorname{Im} f(1)}=\frac{1}{a_0}\left[a_1+\frac{a_0a_2-a_1^2}{a_0P_{l_0}-a_1}\right]. \tag{82}$$

2. Now let us examine a similar problem in the physical region for t = $-4k^2$, i.e., in the case of back-scattering. For α and β we get the expressions

$$\alpha=\frac{2\operatorname{Im} f(1)\,4\pi\sigma_{el}}{k\sigma_t^2(1+\Delta^2)}-(-)^L\sqrt{\frac{4\pi\sigma_{el}}{1+\Delta^2}}\frac{\varphi(k)}{\sigma_t}, \tag{83}$$

$$\beta=-k\varphi(k), \tag{84}$$

where /25

$$\varphi(k)\equiv(-)^L\left[\frac{\frac{\sigma_{el}}{\pi}-\frac{4\operatorname{Im}^2 f(1)}{(L+1)^2}}{(L+1)^2-1}\right]^{1/2}, \tag{85}$$

and where L is the effective number of waves that participate in the scattering and that can be written in the form

$$(L+1)^2=\frac{k^2\sigma_t^2}{4\pi\sigma_{el}}(1+\Delta^2),\ \Delta^2\geqslant\delta^2\geqslant 0 \tag{86}$$

(δ is the ratio of the real part of the forward scattering amplitude to its imaginary part). By means of (86), Equation (85) is rewritten as

$$\varphi(k) \equiv (-)^L \left[\frac{\Delta^2}{(1+\Delta^2)\left(\frac{k^2 \sigma_t^2}{4\sigma_{el}^2}(1+\Delta^2) - \frac{\pi}{\sigma_{el}} \right)} \right]^{1/2}. \tag{85'}$$

The extremum of the imaginary part of the back-scattering amplitude now has the form

$$2 \operatorname{Im} f(-1) = (-)^L \sqrt{\frac{\sigma_{el}}{\pi(1+\Delta^2)}} - \varphi(k) \left(1 + \frac{k^2 \sigma_t^2}{4\pi\sigma_{el}}(1+\Delta^2) \right). \tag{87}$$

The requirement of convergence of this expression to zero when $k \to \infty$ leads to the following result:

$$\delta^2 \leqslant \Delta^2 \underset{k \to \infty}{\longrightarrow} \frac{4\pi\sigma_{el}}{k^2 \sigma_t^2}. \tag{88}$$

This does not contradict the experiment.

§ 4. Certain Relationships Derived From the Unitary Condition.

The exact unitary condition for the elastic scattering amplitude T(t) has the form

$$\operatorname{Im} T(t) = \frac{1}{8\pi^{3/2}} \left\{ \int_{t_1=-4k^2}^{0} \int_{\varphi=0}^{2\pi} T^*(t_2) T(t_1) \, dt_1 d\varphi + 2\pi G(t) \right\}, \tag{89}$$

where t is the square of the transferred 4-momentum;

$$t_2 = -2k^2 \left\{ 1 - \left(1 + \frac{t}{2k^2} \right) \left(1 + \frac{t_1}{2k^2} \right) - \right.$$

$$- \sqrt{\left[\left(\frac{t}{2k^2}\right)^2 + 2\frac{t_1}{2k^2}\right]\left[\left(\frac{t_1}{2k^2}\right) + 2\frac{t}{2k^2}\right]\cos\varphi}\Bigg\};$$

$$G(t) = \frac{\pi}{k^2}\sum_{l=0}^{\infty}(2l+1)\left(1-\eta_l^2\right)P_l\left(1+\frac{t_1}{2k^2}\right),\ G(0) = \sigma_{in}. \qquad \text{/26}$$

The scattering amplitude is normalized such that the optical theorem has the form

$$\operatorname{Im} T(0) \equiv T_I(0) = \frac{\sigma_t}{4\sqrt{\pi}}.$$

Expanding the left-hand and right-hand sides of (89) into a series in powers of t, and equating the coefficients of the first power, we get

$$4\sqrt{\pi}\,T_I'(0) = J_1 + J_2 + A,$$

where

$$T_I'(0) = \frac{\sqrt{\pi}}{4k^4}\sum_{l=0}^{\infty}(2l+1)(1-\eta_l\cos 2\alpha_l)\frac{l(l+1)}{2},$$

$$A \equiv \frac{\pi}{2k^4}\sum_{l=0}^{\infty}(2l+1)\left(1-\eta_l^2\right)\frac{l(l+1)}{2},$$

$$J_1 = \int_{-4k^4}^{0}\left[T_I(t_1)\,T_I'(t_1) + T_R(t_1)\,T_R'(t_1)\right]\left(1+\frac{t_1}{2k^2}\right)dt_1 =$$

$$= \frac{1}{2}\left(\frac{d\sigma}{dt}\Big|_0 + \frac{d\sigma}{dt}\Big|_{-4k^4}\right) - \frac{\sigma_{el}}{4k^2},$$

$$J_2(k) = \int_{-4k^4}^{0}\left(T_I(t_1)\,T_I^*(t_1) + T_R(t_1)\,T_R^*(t_1)\right)\left(\frac{t_1^2}{4k^4} + t_1\right)dt_1,$$

i.e.,

$$\frac{1}{2}\left(\frac{d\sigma}{dt}\Big|_0 + \frac{d\sigma}{dt}\Big|_{-4k^4}\right) = \frac{dE(t)}{dt}\Big|_0 + \frac{E(0)}{4k^2} - J_2(k), \qquad (90)$$

where

$$E(t) \equiv \frac{\pi}{k^2} \sum_{l=0}^{\infty} (2l+1)\left(1 - 2\eta_l \cos 2\alpha_l + \eta_l^2\right) P_l\left(1 + \frac{t}{2k^2}\right),$$
$$E(0) = \sigma_{el},\ E(t) + G(t) = 4\sqrt{\pi}\, T_l(t).$$

Equation (90) is exact. Equation (90) is given in [3] without consideration of J_2. If the energies are so small that only the s- and p-waves play a role in the scattering, then $J_2 = 0$ and the formula given in [3] will be valid. /27
However, in the general case, it is necessary to use the result (90). When $k \to \infty$

$$J_2(k) = \sigma_t a - \sigma_{in} b - \frac{\sigma_t^2}{32\pi},$$

where

$$a = \frac{4\sqrt{\pi}}{\sigma_t} \frac{dT_l}{dt}\bigg|_0 = \frac{\sigma_t^2}{32\pi\sigma_{el}},\ b = \frac{1}{\sigma_{in}} \frac{dG}{dt}\bigg|_0.$$

In the Van Hove model, a ≈ 0.89b and we thus have in this model:

$$J_2(k) \simeq a\left(\sigma_t - \frac{\sigma_{in}}{0{,}89}\right) - \frac{\sigma_t^2}{32\pi} \simeq -0{,}12\, \frac{\sigma_t^2 \sigma_{in}}{32\pi\sigma_{el}} < 0.$$

Hence, for high energies, the basic formula in [3] should have the form

$$\frac{1}{2}\left(\frac{d\sigma}{dl}\bigg|_0 + \frac{d\sigma}{dt}\bigg|_{-4k^2}\right) \geqslant \frac{dE}{dt}\bigg|_0 + \frac{E(0)}{4k^2}. \tag{90'}$$

2. If it is assumed that the real part of the amplitude is equal to zero when $k \to \infty$, then the unitary condition is written as

$$\varphi(x) = \frac{k}{4\pi}\left[\int_{y=-1}^{1} \int_{\varphi=0}^{2\pi} \varphi\left(\widehat{xy}\right) \varphi(y)\, dy d\varphi + G(x)\right], \tag{89'}$$

where

$$\varphi(x) = -if(x) = \mathrm{Im} f(x),\ \widehat{xy} = xy - \sqrt{(1-x^2)(1-y^2)}\cos\varphi$$

Writing

$$\frac{k}{4\pi} G(x) = \frac{k}{4\pi}\frac{\pi}{k^2}\sum_{l=0}^{\infty}(2l+1)\left(1-\eta_l^2\right) = \alpha(x)\varphi(x),$$

where

$$\alpha(x) = \frac{\sum_{l=0}^{\infty}(2l+1)\left(1-\eta_l^2\right)P_l(x)}{2\sum_{l=0}^{\infty}(2l+1)\left(1-\eta_l\right)P_l(x)},\ \alpha(t) = 1 - \frac{\sigma_{el}}{\sigma_t},$$

we represent Equation (89') in the form

$$\left(1-\alpha(x)\right)\varphi(x) = \frac{k}{4\pi}\int_{y=-1}^{1}\int_{\varphi=0}^{2\pi}\varphi\left(\widehat{xy}\right)\varphi(y)\,dy\,d\varphi. \qquad (89'')$$

Hence, we conclude that /28

$$\int_0^{2\pi}\varphi\left(\widehat{xy}\right)d\varphi = \frac{8\pi}{k}\left(1-\alpha(x)\right)\delta(x-y).$$

When y = 1 and x ≃ 1, we get

$$\varphi(x) = \frac{4\sigma_{el}}{k\sigma_t}\delta(1-x),\ x\simeq 1,\ k\to\infty, \qquad (91)$$

which corresponds to

$$1-\eta_l = \frac{2\sigma_{el}}{\sigma_t}.$$

If $G(x)$ is known, then (89') can be regarded as an integral equation with respect to $\phi(x)$. In the Van Hove model, when $x \simeq 1$,

$$G(x) = \sigma_{in}(1 + b(1 - x)).$$

When $x \simeq 1$, substituting

$$\varphi(x) = \frac{k\sigma_t}{4\pi}(1 + a(1 - x))$$

in (89'), we have

$$a = \frac{1}{\sigma t}\left[\pi \int_{-1}^{1} \varphi(y)\varphi''(y)(1 - y^2)\,dy + b\sigma_{in}\right].$$

§ 5. Extremum Value of the Differential Cross Section of Elastic Scattering.

In this section, we obtain the extremum value of the differential cross section of a random-angle elastic scattering for any energies when the forward-scattering amplitude and the total cross section of elastic scattering σ_{el} are given. The case of high energies is examined in greater detail. From the general formula, in particular, it follows that when $k \to \infty$ (k is the wave number in the center-of-inertia system), then the ratio of the extremum value of the 90° scattering cross section to the 180° value approaches zero as k^{-1}.

In order to derive our results, we are searching for an extremum of the differential cross section of elastic scattering for fixed values (given experimentally) of the imaginary and real parts of the forward-scattering amplitude and σ_{el}. Let us assume that in the sums which express the cross sections and amplitudes through component amplitudes, we can limit ourselves to a finite number of component waves L. Then the Lagrange method leads to the following /29
system of linear algebraic equations for the determination of the component amplitudes f_l which achieve the extremum of the differential cross section.

$$\left.\begin{aligned} \mathrm{Re} f_l &= \alpha\,\mathrm{Re} f(x) P_l(x) + \beta_1 \\ \mathrm{Im} f_l &= \alpha\,\mathrm{Im} f(x) P_l(x) + \beta_2 \end{aligned}\right\}, \qquad (92)$$

where α, β_1, β_2, are Lagrange multipliers, while

$$f(x) = \sum_{l=0}^{L} (2l+1) f_l P_l(x), \quad x = \cos\theta$$

is the scattering amplitude; and also, due to the unitary condition,

$$0 \leqslant k|f_l| \leqslant 1.$$

From (92) we have

$$\mathrm{Re}\, f(x) = \frac{a_1}{1-\alpha a_2}\beta_1, \quad \mathrm{Im}\, f(x) = \frac{a_1}{1-\alpha a_2}\beta_2.$$

i.e.

$$\sigma(x) = \frac{a_1^2}{(1-\alpha a_2)^2}\left(\beta_1^2 + \beta_2^2\right), \tag{93}$$

where the following notation has been introduced:

$$a_n = \sum_{l=0}^{L} (2l+1) P_l^n(x), \quad n = 0, 1, 2.$$

From the conditions specified by the relations σ_{el}, $\mathrm{Re}\, f(1)$ and $\mathrm{Im}\, f(1)$ with f_l we find the Lagrange factors:

$$\left.\begin{aligned} \alpha &= \frac{\left(a_0 \frac{\sigma_{el}}{4\pi} - \sigma(1)\right) \pm \sqrt{a_1^2\left(\frac{\sigma_{el}}{4} a_0 - \sigma(1)\right) \frac{\sigma(1)}{a_0 a_2 - a_1^2}}}{\frac{\sigma_{el}}{4\pi}\left(a_0 a_2 - a_1^2\right) - a_2\, \sigma(1)} \\ \beta_1 &= \frac{1-\alpha a_2}{a_0 - \alpha\left(a_0 a_2 - a_1^2\right)} \mathrm{Re}\, f(1), \\ \beta_2 &= \frac{1-\alpha a_2}{a_0 - \alpha\left(a_0 a_2 - a_1^2\right)} \mathrm{Im}\, f(1) \end{aligned}\right\}. \tag{94}$$

The extremum value of the differential cross section of elastic scattering is then equal to

$$X(x)=\frac{\sigma(x)}{\sigma(1)}=\frac{a_1^2\left[\frac{\sigma_{el}}{4\pi}\left(a_0a_2-a_1^2-a_2\,\sigma(1)\right]^2\right.}{\left[a_1^2\sigma(1)\pm\sqrt{a_1^2\,\sigma(1)\left(\frac{k\sigma_t}{4\pi}\right)^2\left(\Delta^2-\delta^2\right)\left(a_0a_2-a_1^2\right]^2}\right.}, \tag{95}$$

/30

where δ is the ratio of the real part of the forward-scattering amplitude to its imaginary part, while Δ^2 is related to L by means of the formula

$$(L+1)^2=\frac{k^2\sigma_t^2}{4\pi\sigma_{el}}(1+\Delta^2),\ \Delta^2\geqslant\delta^2.$$

The result (95) is valid for any energies and any scattering angle. Let us examine certain specific cases of (95) at high energies.

Region of diffraction peak. When $\theta<<L^{-1}$

$$X(\theta)\simeq 1+\frac{\sigma_t^2}{16\pi\sigma_{el}}k^2\theta^2+\frac{5}{12}\left(\frac{\sigma_t^2}{16\pi\sigma_{el}}\right)^2k^4\theta^4+\ldots \tag{96}$$

Back-Scattering. In this case, from the general formula (95), we have

$$X(180^\circ)=\frac{(1+\Delta^2)\frac{k^2\sigma_t^2}{4\pi\sigma_{el}}\left[\Delta^2-\delta^2-\frac{4\pi\sigma_{el}}{k^2\sigma_t^2}\right]^2}{(1+\delta^2)\left[\sqrt{1+\delta^2}\pm\sqrt{(\Delta^2-\delta^2)\left[\frac{k^2\sigma_t^2}{4\pi\sigma_{el}}(1+\Delta^2)-1\right]}\right]^2}. \tag{97}$$

We shall require that the back-scattering cross section should disappear when the energy approaches infinity. Then, it follows from (97) that it is necessary to select a plus sign before the radical and to require that the relation (98) should be satisfied when $\kappa \to \infty$.

$$\Delta^2 - \delta^2 \underset{k\to\infty}{\longrightarrow} \frac{4\pi\sigma_{el}}{k^2\sigma_t^2}. \tag{98}$$

Let, asymptotically,

$$\delta^2(k) \underset{k\to\infty}{\simeq} \frac{a_1}{k^{n_1}} + O\left(\frac{1}{k^{n_1+\varepsilon_1}}\right),$$

$$\Delta^2(k) \underset{k\to\infty}{\simeq} \frac{a_2}{k^{n_2}} + O\left(\frac{1}{k^{n_2+\varepsilon_2}}\right), \quad \varepsilon_1, \varepsilon_2 > 0,$$

where $a_1 > 0$, and $a_2 > 0$. Let us assume that the equalities $a_1 = a_2$, and $n_1 = n_2$. cannot be satisfied simultaneously. Then, it follows from (98) that /31

$$\delta^2 \underset{k\to\infty}{\lesssim} \frac{1}{k^2}, \quad \Delta^2 \underset{k\to\infty}{\sim} \frac{1}{k^2}. \tag{99}$$

90° Scattering. In this case

$$|\sqrt{a_2}| = a_1 = \begin{cases} (-1)^{\frac{L}{2}}(L+1)\dfrac{(L-1)!!}{L!!}, & L \text{ is even} \\ (-1)^{\frac{L+3}{2}} L \dfrac{(L-2)!!}{(L-1)!!}, & L \text{ is odd} \end{cases}$$

Then, considering

$$\lim_{L\to\infty} \frac{(L-1)!!}{L!!} = \left(\frac{2}{\pi L}\right)^{1/2},$$

for the ratio of the extremum value of the back-scattering cross section to the 90° cross section, we get

$$\frac{\sigma(-1)}{\sigma(0)} \underset{k\to\infty}{\simeq} \frac{k\sigma_t}{4\pi}\left(\frac{\pi^3}{\sigma_{el}}\right)^{1/2}. \tag{100}$$

§ 6. Some Inequalities for the Cross Section of Elastic Scattering.

1. The known limitations imposed on the cross section of elastic scattering are based on the unitary and analytic conditions, and also on a moderate increase with respect to energy of the scattering amplitude. However, the derivation of these limitations involves a number of mathematical difficulties and, besides, the results thus obtained contain an indefinite constant. In [6], a constraint was obtained for the magnitude of the elastic scattering amplitude in the region of the diffraction peak, without the presence of any unknown constants. At the same time, use was made of the unitary condition and it was assumed that the real part of the amplitude is less than that of the imaginary part; we also used the fact that in the region of the peak, the cross section decreases with increasing scattering angle.

In this section, we obtain certain inequalities for the cross section of elastic scattering, in particular the upper bounds for the scattering cross section in the region of the forward diffraction peak. These results are stronger than the corresponding ones in [6]. Also, our results have been obtained for less strict conditions than in [6].

2. In this paragraph, we shall obtain the upper bound for the cross section of elastic scattering in the region of the diffraction peak. /32

A. In the region of the diffraction peak, we have

$$\sigma^{1/2}(x) \leqslant \frac{1}{1-x}\int_x^1 \sigma^{1/2}(x)\,dx, \quad x \equiv \cos\theta. \tag{101}$$

Substituting in the right-hand side of this inequality

$$\sigma^{1/2}(x) = \frac{1}{2k}\left|\sum_{l=0}^{\infty}(2l+1)\,a_l(k)\,P_l(x)\right| \tag{102}$$

and considering that the basic role in the sum is played by the orbital moments $l < k$, for small angles $(\theta \ll k^{-1})$ we get, after integration:

$$\sigma^{1/2}(x) \leqslant \frac{k}{|t|} \sum_{l=0}^{\infty} |a_l| (P_{l-1}(x) - P_{l+1}(x)). \tag{103}$$

Let us assume that $|a_0| \geqslant |a_1| \geqslant |a_2| \geqslant \ldots \geqslant 0$; and also $|a_0| \leqslant 1$ to the unitary condition. Then, by means of the Abel inequality, we finally get the following upper bound for the differential cross section of elastic scattering in the region of the diffraction peak:

$$\sigma(x) \leqslant \frac{4k^2 |a_0|^2}{t^2} \leqslant \frac{4k^2}{t^2}. \tag{104}$$

Equation (104) gives the same dependence on the energy and on the transferred momentum as the result obtained by Malkov (see formula (20) in [6]). However, the result (104) is stronger than formula (20) in [6] since the number 538 is used there rather than the factor 4, i.e., the upper bound, as given by (104), is 135 times less than the corresponding result in [6]. It is also important to note that (104) has been obtained without the additional assumption that the real scattering amplitude does not exceed the imaginary amplitude in magnitude.

B. In the region of the diffraction peak, we have

$$\sigma(x) \leqslant \frac{1}{1-x} \int_x^1 \sigma(x)\, dx. \tag{105}$$

From this follows the obvious restriction /33

$$\sigma(x) < \frac{\sigma_{el}}{\pi} \frac{k^2}{|t|}. \tag{106}$$

The inequality (106) is general. In the course of its derivation, use was made only of the fact that the scattering cross section in the region of the diffraction peak decreases with increasing angle. Other assumptions, such as $|\mathrm{Ref}| \leqslant |\mathrm{Imf}|$ and $|a_l| \leqslant 1$, which were present in [6], were not made. In formula (106), the dependence on the energy is the same as in [6], but the dependence on the transferred momentum is here $|t|^{-1}$, while in [6] it is t^{-2}. For this reason, for small transferred momenta $(|t| \ll k^2)$ the result (106) is stronger than the result in [6].

3. In this paragraph we shall obtain the lower boundary for the cross section of elastic scattering averaged over the interval $[x_1, x_2]$. We have

$$\overline{\sigma^{1/2}}(x_1, x_2) = \frac{1}{x_2 - x_1} \int_{x_1}^{x_2} \sigma^{1/2}(x)\, dx =$$

$$= \frac{1}{2k(x_2 - x_1)} \int_{x_1}^{x_2} \left| \sum_{l=0}^{\infty} (2l+1)\, a_l P_l(x) \right| dx \geqslant \tag{107}$$

$$\geqslant \frac{1}{2k(x_2 - x_1)} \left| \int_{x_1}^{x_2} \sum_{l=0}^{\infty} (2l+1)\, a_l P_l(x)\, dx \right|$$

By changing the order of summation and integration, we obtain after integration,

$$\overline{\sigma^{1/2}}(x_2, x_1) \geqslant \frac{1}{2k(x_2 - x_1)} \left| \sum_{l=1}^{\infty} (a_{l-1} - a_{l+1}) \left(P_l(x_2) - P_l(x_1) \right) \right|. \tag{108}$$

Hence, when $x_2 \to x_1 = x$, we get the following formula:

$$\overline{\sigma^{1/2}}(x) \geqslant \frac{1}{2k} \left| \sum_{l=1}^{\infty} (a_{l-1} - a_{l+1}) \frac{dP_l(x)}{dx} \right|. \tag{109}$$

Let us examine two specific cases of the formula (108):

a) let $x_2 = 1$, $x_1 = x$, then

$$\overline{\sigma^{1/2}}(1, x) \geqslant \frac{1}{2k(1-x)} \left| \sum_{l=0}^{\infty} a_l (P_{l-1} - P_{l+1}) \right| = \tag{110}$$

$$= \frac{1}{2k(1-x)} \left| \sum_{l=1}^{\infty} (a_{l-1} - a_{l+1}) P_l - a_0 - a_1 \right|;$$

/34

b) let $x_2 = x$, $x_1 = -1$, then,

$$\overline{\sigma^{1/2}}(x-1) \geqslant \frac{1}{2k(1+x)}\left|2a_0 - \sum_{l=0}^{\infty} a_l(P_{l-1}(x) - P_{l+1}(x))\right| = \frac{1}{2k(1+x)}\left|a_0 - a_1 + \sum_{l=1}^{\infty}(a_{l-1} - a_{l+1})P_l(x)\right|. \quad (111)$$

The series (108) - (111) converge rapidly. However, during their calculation, it is necessary to observe great accuracy because their sum is, with respect to the modulus, much smaller than the very members of the series (this pertains particularly to large angles). For this reason, for evaluations of (108) - (111), it is necessary to possess accurate values of a_l. For evaluations in the case of angles that are not too large, we shall make use of the result in section 2 where, by using the quasi-classical approximation for $a_l(k)$ at high energies, the following result was obtained:

$$a_l(k) \simeq \frac{4\sigma_{el}}{\sigma_t}\exp\left[-\frac{2\pi\sigma_{el}}{k^2\sigma_t^2}(2l+1)^2\right]. \quad (112)$$

By selecting at 3.6 BeV/c σ_t = 31.5 mbn and σ_{el} = 6 mbn for $\bar{\pi}$p-scattering when x = 0.90, we get from (109): $\overline{\sigma}$ (0.90) $\geq$ 2 mbn, which agrees with the experimental value.

§ 7. Integral Expressions for the Scattering Amplitude.

All our results in sections 1-6 were obtained from the expansion of the scattering amplitude in a series of Legendre polynomials. However, in a number of cases, particularly for very high energies, it is more convenient to utilize the integral expressions for the scattering amplitude. Such a representation was given at the end of section 1. In this paragraph, we shall examine this problem in greater detail. /35

Case of Very Small Angles and Large Energies. In this case, it is possible in the basic formula (1) to replace the summation sign by the integration sign and the Legendre polynomials by the Bessel function of the zero order:

$$\sum \to \int, \; P_l(\cos\theta) \to J_0\left(\left(l + {}^1/_2\right)\theta\right). \tag{113}$$

Then, for the scattering amplitude, we obtain the following approximate integral expression:

$$f(\theta) \underset{k\to\infty}{\simeq} ik \int_0^\infty a(\rho) J_0(k\theta\rho)\, \rho \; d\rho, \; \rho \simeq \frac{l}{k}, \tag{114}$$

which becomes more accurate as the energy of the colliding particles increases. Equation (114) corresponds to the so-called eikonal approximation. Some authors generalize this approximation for the region outside the diffraction peak, replacing the expression (114) by

$$f(\theta) \underset{k\to\infty}{\simeq} ik \int_0^\infty a(\rho) J_0\left(2k\rho \sin\frac{\theta}{2}\right)\rho d\rho. \tag{115}$$

However, in our view, as we have already seen in section 2 during the summation of the Faxen-Holtsmark series (1) with the aid of the Euler-Maclaurin formula, the result (115) is doubtful for large scattering angles. Actually, (115) is only one integral member in the Euler-Maclaurin formula and the remaining members of this formula give a contribution of the same magnitude as (115).

We wish to observe also that (115), unlike (114), is an exact integral Bessel transform. For this reason, the relationship (115) would be exact if instead of $a(\rho)$ one would take a certain other function $b(\rho)$, which corresponds to the true amplitude:

$$f(\theta) = ik \int_0^\infty b(\rho) J_0\left(2k\rho \sin\frac{\theta}{2}\right)\rho d\rho. \tag{116}$$

The total cross sections corresponding to (116) are equal to

$$\sigma_t = 4\pi \int_0^\infty \mathrm{Re}\, b(\rho)\, \rho d\rho, \tag{117}$$

$$q_{el} = 2\pi \int_0^\infty \left| b(\rho) \right|^2 \rho d\rho. \tag{118}$$ /36

Case of Angles $0 \leqslant \theta < \frac{\pi}{2}$ and Any Energies. The Legendre polynomials are related to the Bessel functions of zero order by means of the Hobson formula:

$$P_l(\cos\theta) = \frac{1}{l!} \int_0^\infty l^{-y\cos\theta} J_0(y\sin\theta)\, y^l dy, \quad 0 \leqslant \theta < \frac{\pi}{2}. \tag{119}$$

Substituting this formula in (1), we obtain the following exact integral expression in the region of angles $0 \leqslant \theta < \frac{\pi}{2}$ and for any energies:

$$f(\theta) = \frac{i}{2k} \int_0^\infty J_0(y\sin\theta)\, e^{-y\cos\theta} A(y)\, dy, \tag{120}$$

$$A(y) \equiv \sum_{n=0}^{\infty} (2n+1)\, a_n \frac{y^n}{n!}, \quad 0 \leqslant \theta < \frac{\pi}{2}$$

Due to the unitary condition $0 \leqslant |a_n| \leqslant 2$

$$0 \leqslant A(y) < 2(2y+1)\, e^y; \tag{121}$$

$$\sigma_t = \frac{2\pi}{k^2} \int_0^\infty e^{-y} \mathrm{Re}\, A(y)\, dy. \tag{122}$$

Case of Any Angles and Any Energies. In order to obtain an integral expression of the amplitude in the general case, we wish to observe that the following relationship holds:

$$P_l(\cos\theta) = \int_0^\infty J_0\left(x\sin\frac{\theta}{2}\right) J_{2l+1}(x)\, dx, \quad 0 \leqslant \theta \leqslant \pi. \tag{123}$$

Substitution in formula (1) gives

$$f(\theta) = i\int_0^\infty A(\rho) J_0\left(2k\rho \sin\frac{\theta}{2}\right) d\rho. \tag{124}$$

$$A(\rho) \equiv \sum_{n=0}^{\infty} (2n+1) a_n J_{2n+1}(2k\rho), \quad 0 \leqslant \theta \leqslant \pi. \tag{125}$$ /37

Formula (124) agrees with (116) if we set in the latter:

$$k\rho\, b(\rho) = A(\rho). \tag{126}$$

REFERENCES

1. Azimov, S. A. and G. G. Arushanov, "Some Relations for the Elastic Scattering of Particles at High Energies," *Izv. AN Uzbek SSR*, No. 2, p. 71, 1964.
2. Arushanov, G. G., "The Lower Bound for the Back-Scattering Cross Section," *Yadernaya fizika*, No. 11, p. 938, 1965.
3. Arushanov, G. G., "Unitary Conditions and the Relationship Between the Forward- and Back-Scattering Cross Sections and the Total Cross Sections," *DAN Uzbek SSR*, No. 9, p. 21, 1965.
4. Azimov, S. A., G. G. Arushanov, U. G. Gulyamov and A. A. Yuldashev, "Elastic πp, pp, $\bar{p}p$, Kp- Interactions at High Energies," (published in this volume).
5. Arushanov, G. G., "Phenomenological Study of the Elastic Interaction of Photons, Pions, and Nucleons at High Energies," Author's abstract of Candidate Dissertation, Tashkent, 1964.
6. Malkov, Ye. I., "Limitations Imposed on the Cross Section of Elastic Forward Scattering in the Region of the Diffraction Peak," *ZhETF*, No. 11, p. 1558, 1965.

ELASTIC πp-, pp-, pp-, and Kp-INTERACTIONS AT HIGH ENERGIES

S. A. Azimov, G. G. Arushanov,
U. G. Gulyamov, and A. A. Yuldashev

During recent years, much experimental work has been conducted on the elastic interaction of pions, protons [1], antiprotons, and kaons with protons at accelerating energies of $E \leqslant 30$ BeV. Measurements were made of the angular distributions in a broad range of angles $(0^\circ \leqslant \theta < 180^\circ)$; the total elastic interaction cross sections σ_t were composed of the total cross section of elastic scattering σ_{el} and the total cross section of inelastic interaction σ_{in}: $\sigma_t = \sigma_{el} + \sigma_{in}$. For sufficiently high energies, these characteristics of the elastic interaction are subject to simple laws. /38

As shown by the experiment, the elastic scattering essentially takes place at small angles $\left(\theta \lesssim \frac{1}{k}\right)$. The real part of the amplitude is much smaller than the imaginary part; thus, for πp- and pp-interactions in the energy range of 5-15 BeV, the ratio of the real part of the forward-scattering amplitude to its imaginary part amounts to approximately 20% [1]. The total cross sections apparently approach constant values, which are, respectively,

$$\sigma_{el}(\pi p) \simeq 5 \text{ mbn}\,;\ \sigma_{el}(pp) \simeq 10 \text{ mbn}\,,\ \sigma_t(\pi p) \simeq 25 \text{ mbn}\,,$$
$$\sigma_t(pp) \simeq 40 \text{ mbn}.$$

Along with the experimental work, many theoretical studies were conducted in order to obtain a detailed understanding and interpretation of the established correlations. Unfortunately, up to date, there does not exist a fundamental microscopic theory of the interaction of strongly-interacting elementary particles (adrons). The basic methods of theoretical physics usually employed for the clarification of the phenomena that take place during collisions of particles are the quantum theory of fields and the dispersion relations. We feel, just as Van Hove [2] does, that progress in the theoretical understanding of the phenomena taking place at high energies cannot be achieved without a rational combination of the different phenomenological methods and models with the general theoretical principles (for example, the condition of a unitary collision operator $S{:}SS^+ = 1$). /39

The optical theorem which relates the imaginary part of the forward-scattering amplitude, or the forward-scattering cross section in the case of a sufficiently high energy where one disregards the real part of the amplitude in comparison with its imaginary part, to the total interaction cross section is the result of the unitary nature of the scattering matrix. This theorem is

very useful in the interpretation of the experimental data, as well as the general strict results of the theory. Due to the unitary nature of the scattering matrix, it is possible to obtain strict results in which the back-scattering cross section appears, and to use these results to evaluate the back-scattering cross section of the particles [3, 4].

In [5], we find various characteristics of the elastic interaction of adrons at high energies, and some relationships between them are calculated. The main assumption used in this case is the brief-acting nature of the forces between the adrons. From the results, in particular those of [5], it follows that the scattering cross section near 90° should be symmetric with respect to 90° and that the back-scattering cross section (at 180°) is characterized by a maximum. Neither of these conclusions contradicts the results of the experiments. The angular distribution in the elastic scattering of the adrons at high energies is also calculated in [5].

The main purpose of this paper is to compare the theoretical differential elastic-scattering cross section in the forward hemisphere ($0 \leqslant \theta \leqslant 90°$) with existing experimental results of the scattering of pions, protons, antiprotons, and kaons by high-energy protons.

Elastic scattering of particles in the vicinity of zero. Let us examine the normalized scattering amplitude

$$\varphi(t) \equiv \frac{f(t)}{i\frac{k\sigma_t}{4\pi}} = \frac{2\pi}{k^2\sigma_t}\sum_{l=0}^{\infty}(2l+1)\,a_l(k)\,P_l\left(1+\frac{t}{2k^2}\right), \tag{1}$$

where x = cos θ; θ is the scattering angle; k is the wave number; $t = 2k^2(1-x)$ is the invariant square of the transferred 4-momentum. /40

From formula (1) we first find the lower bound for the scattering cross section for very small momentum transfers. For small $|t|$, the Legendre polynomials are approximated by the expression

$$P_l\left(1+\frac{t}{2k^2}\right) \simeq 1 + \frac{1}{2k^2}\frac{l(l+1)}{2}t. \tag{2}$$

Substituting (2) in Equation (1) and utilizing the Cauchy inequality, we have

$$X(t) \equiv \frac{d\sigma}{dt}\Big/\left(\frac{d\sigma}{dt}\right)_{t=0} \geqslant 1 + \frac{\sigma_t^2}{8\sqrt{3\pi\sigma_{el}}}\cdot t. \tag{3}$$

Let us assume that at high energies the scattering amplitude is purely imaginary. With the aid of the mean-value theorem, the amplitude can be written in the form

$$f(x) = f(1)\left(1 - \overline{l}^2 \frac{\theta^2}{4}\right), \tag{4}$$

where $\overline{l}^2$ is some number between 0 and L^2;

$$L^2 = \frac{k^2\sigma_t^2}{4\pi\sigma_{el}}(1+\delta^2), \tag{5}$$

and where δ is the ratio of the real part of the forward-scattering amplitude to its imaginary part.

We write

$$\begin{gathered}\overline{l}^2 = \alpha(k)L^2 \\ (0 < \alpha(k) < 1),\end{gathered} \tag{6}$$

where $\alpha(k)$ can depend on the energy. In order to evaluate this factor, we take into account in (6) that the scattering takes place essentially at small angles for high energies. Then Equation (4) is rewritten in the form

$$f(x) = f(1)\, e^{-\overline{l}^2 \cdot \frac{\theta^2}{4}}. \tag{4'}$$

We have

$$\sigma_{el} = 2\pi\left(\frac{k\sigma_t}{4\pi}\right)^2 \int_0^\infty \rho\, e^{-\overline{l}^2 \frac{\theta^2}{2}} \theta d\theta = \frac{\sigma_{el}}{2\alpha(k)}.$$

Thus, for small angles $\left(\theta \ll L^{-1}\right)$, we get for the differential scattering cross section [5],

$$X(t) = 1 + \frac{\sigma_t^2}{16\pi\sigma_{el}} t \simeq \exp\left[\frac{\sigma_t^2}{16\pi\sigma_{el}} t\right] \tag{7}$$

or, in a form convenient for calculations:

$$X(t) \simeq \exp\left(\frac{2{,}5\ \sigma_t^2}{16\pi\sigma_{el}} \cdot t\right), \tag{7'}$$

where the cross sections are expressed in millibarns, while the momentum transfer is expressed in $(\text{BeV}/c)^2$ units.

We wish to observe that equation (7) was obtained earlier [6] in a somewhat different way, and also that the results of (3) and (7) do not contradict one another. Moreover, it follows from a comparison of Equations (3) and (7) that the sign of the inequality in (3) is close to equality.

Equation (7) is the basic result for scattering near zero. For a purely imaginary amplitude, the magnitude $\sigma_t^2 / 4\pi\sigma_{el}$ can be regarded as the square of the interaction radius

$$R^2(k) \simeq \frac{\sigma_t^2}{4\pi\sigma_{el}}. \tag{8}$$

It is obvious that the inverse of R^2 is proportional to the width of the diffraction peak:

$$\Gamma \sim R^{-2} \simeq \frac{4\pi\sigma_{el}}{\sigma_t^2}. \tag{9}$$

Hence, it follows that if the ratio σ_{el}/σ_t^2 decreases with increasing energy, then the diffraction pattern should narrow (possible, for example, in pp- and Kp-scatterings). However, if the indicated ratio increases with increasing energy, then a widening of the diffraction cone should be observed (possible, for example, in $p\bar{p}$-scattering); and, finally, if the ratio in question does not depend on the energy, then the diffraction cone also does not depend on the energy either, which is observed in πN-scattering.

At present, many researchers acknowledge that when $E \to \infty$, the total cross sections approach constant values and, consequently, there should be no narrowing in the aymptotes, i.e., the form of the diffraction cone ceases to depend on the energy. This experimental fact sharply contradicts the Regge conditions. This is the reason why most physicists now hold the opinion /42 that the Regge conditions are not capable of describing the phenomena during the collision of particles at high energies. The notion of the stability of the diffraction peak with rising energy was advanced by Nambu and Sugawara [7].

Scattering at angles of $0° < \theta < 90°$. The partial s-amplitude is

$$a_0(k) = ik\int_{-1}^{1} f(x)\,dx = -ik\frac{ik\sigma_t}{4\pi}\int_{-1}^{1}\frac{f(x)}{\frac{ik\sigma_t}{4\pi}}\,dx = \frac{k\sigma_t}{8\pi}\int_{0}^{-4k^2} X_1(t)\,dt, \tag{10}$$

where

$$X_1(t) = \frac{f(x)}{i\frac{k\sigma_t}{4\pi}},$$

and, by assumption, it does not depend on the energy. By dividing (10) by σ_t and taking the derivative with respect to k, we get

$$f(180°) = \frac{i\sigma_t}{4} \cdot \frac{d}{dk}\left(\frac{a_0(k)}{\sigma_t(k)}\right). \tag{11}$$

On the assumption of a purely imaginary amplitude, the following expression was obtained in [5] for the partial amplitude $a_l(k)$ at small orbital moments $(l \ll L)$:

$$a_l(k) = \frac{4\sigma_{el}}{\sigma_t} \exp\left[-\frac{8\pi\sigma_{el}}{\sigma_t}\rho^2\right], \tag{12}$$

where $\rho = \left(l + \frac{1}{2}\right)\lambda$ is the impact parameter. Substituting this parameter in (11), we find:

$$f(180°) = \frac{i \cdot \sigma_{el}}{\sigma_t} \frac{4\pi\sigma_{el}}{\sigma_t^2} k^{-3}. \tag{13}$$

In deriving expression (13), we disregarded the energy function of the ratio σ_{el}/σ_t^2. Using formula (13) in that region of transferred momenta where the value of X depends not on the energy but on the transferred momentum, when $t \neq 0$ we get for X(t):

$$X(t) \simeq (256)^3 10^{-2} \left(\frac{\sigma_{el}}{\sigma_t^2}\right)^4 t^{-4}, \tag{14}$$

where the cross section is measured in millibarns and the momentum transfer t is expressed in $(\text{BeV/c})^2$ units. If the statistics are taken into account, then (14) takes the form

$$X(t) \simeq (256)^3 10^{-2} \left(\frac{\sigma_{el}}{\sigma_t^2}\right) t^{-4} \left[1 + \frac{t^4}{(t+4p^2)^4} - \frac{t^2}{(t+4p^2)^2}\right] \qquad (15)$$

for pp-scattering. The factor in the brackets is less than unity for $t > -2p^2$ and greater than unity for $t < -2p^2$.

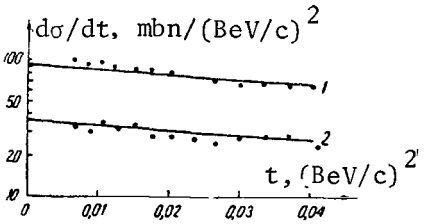

Figure 1. Comparison of the Theory with the Experiment for Small Momentum Transfers for pp-scattering with a momentum of 7.92 BeV/c (1) and for π^-p-scattering with a momentum of 9.89 BeV/c (2).

The t^{-4} law, obtained in [5] is close to the Serber result [8] calculated on the basis of the purely imaginary Yukawa potential. However, formula (14) derived by us is more general and rigorous, and it did not utilize any specific type of potential. Besides, as noted in [5], the operation of replacing the sign of summation for large scattering angles is not correct.

Equation (7) which is suitable for describing the scattering near zero, along with Equation (14) which should describe the scattering momentum transfers that differ from zero, express the differential scattering cross sections through total cross sections, namely through the ratio σ_t^2/σ_{el}, which is interpreted as the square of the interaction radius. If it is assumed that the interaction radius does not depend on the energy and type of scattering adrons when $E \to \infty$ [6], then the results of (7) and (14) can be regarded as universal and also as a generalization of the optical theorem at angles other than zero.

Comparison with the experiment. Let us compare the theoretical results of (7) and (14) with the available experimental data on πp-, pp-, $p\bar{p}$, and Kp-scatterings. The results of a comparison for small momentum transfers are shown in Figure 1, and a comparison of the t^{-4} law with the experiment [1, 12] is shown in Figure 2. The theoretical curves were plotted for the following values of the ratio σ_{el}/σ_t^2 : /44

$$\sigma_{el}/\sigma_t^2 = \left\{ \begin{array}{l} 0.88 \cdot 10^{-2}\ \text{mbn}^{-1} \text{ for } \pi p \\ 0.63 \cdot 10^{-2}\ \text{mbn}^{-1} \text{ for } pp \\ 0.53 \cdot 10^{-2}\ \text{mbn}^{-1} \text{ for } p\bar{p} \\ 1.1 \cdot 10^{-2}\ \text{mbn}^{-1} \text{ for } Kp \end{array} \right\}, \qquad (16)$$

which do not contradict the existing experimental data on total cross sections.

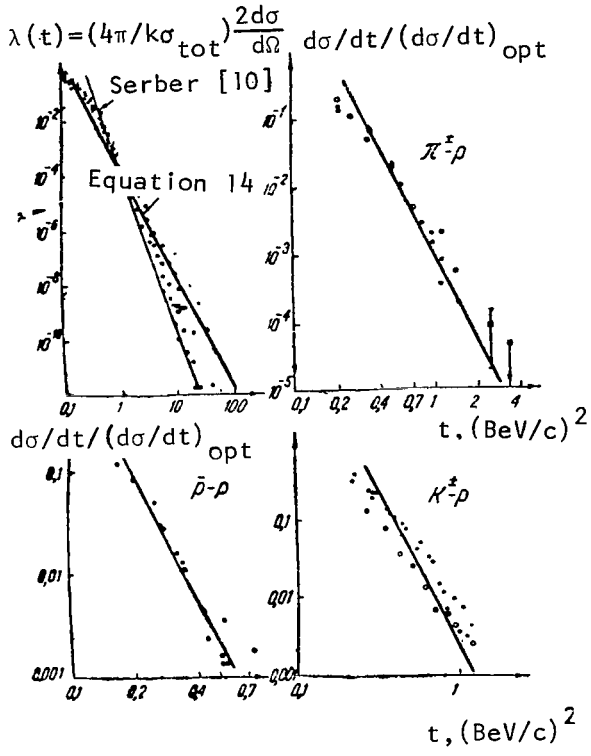

Figure 2. Comparison of Theoretical Curves with Experimental Curves for Large Momentum Transfers.

As can be seen from the figures, the agreement between theory and experiment is satisfactory. At the same time, for both small as well as large momentum transfers, scattering is described in terms of the same parameter (16) measured experimentally. /45

In conclusion, we wish to observe that Equation (7) agrees with the results of other theories for the description of small-angle scatterings. For example, if it is assumed that $\sigma_t \to$ const, $\sigma_{el} \to \frac{1}{\ln E}$, when $E \to \infty$, then (7) gives a Regge-type result. Equation (14), which describes scattering for large momentum transfers, is not in agreement with the predictions of other theories. In order to describe the large-angle scatterings, many researchers are utilizing a statistical model [9, 11] which leads to an exponential decrease of the large-angle scattering. At the same time, it is believed that a very rapid decrease in the large-angle pp-scattering cross section with increasing energy favors the statistical model. However, the considerations discussed by the authors in [11] deny the possibility of the indicated model in the case described.

REFERENCES

1. Lindenbaum, S. J., Preprint, Joint Institute of Nuclear Research, E-1802, 1964.
2. Van Hove, L., *Rev. Mod. Phys.*, Vol. 36, p. 655, 1964.
3. Arushanov, G. G., "Unitary Conditions and the Relations Between the Forward and Back-Scattering Cross Sections," *DAN Uzbek SSR*, No. 9, p. 21, 1965.
4. Arushanov, G. G., "The Lower Bound for Back-Scattering Cross Section. *Yadernaya fizika*, No. 11, p. 938, 1965.
5. Azimov, S. A. and G. G. Arushanov, "Some Relations for the Elastic Scattering of High-Energy Particles," *Izv. AN Uzbek SSR*, No. 2, p. 71, 1964.

6. Azimov, S. A. and G. G. Arushanov, "Elastic Interaction of High-Energy Particles," *DAN Uzbek SSR*, No. 12, 1963.
7. Nambu, Y. and M. Sugawara, *Phys. Rev. Lett.*, Vol. 10, p. 304, 1963.
8. Serber, R., *Phys. Rev. Lett.*, Vol. 10, p. 357, 1963; *Rev. Mod. Phys.*, Vol. 36, p. 649, 1964.
9. Fast, G., R. Hagedorn, *Nuovo Cim.*, Vol. 27, p. 208, 1963; *Nuovo Cim.*, Vol. 27, p. 856, 1963.
10. Jones, L. W., *Phys. Lett.*, Vol. 8, p. 287, 1964.
11. Ching-Hung, Woo., *Phys. Rev.*, Vol. 137, B-448, 1965.
12. Foley, K., et al., *Phys. Rev. Lett.*, Vol. 11, p. 503, 1963.

AZIMUTHAL ANGULAR DISTRIBUTION OF SHOWER PARTICLES AND GRAY TRACKS FORMED BY PARTICLES OF COSMIC RADIATION IN A PHOTOEMULSION

S. A. Azimov, M. S. Rasulkulov, and V. M. Chudakov

The study of azimuthal angular distribution of secondary particles is of interest in clarifying the mechanism of interaction of fast particles with nucleons and nuclei. /46

A procedure has already been developed for detecting different correlations in azimuthal angular distribution [1]. The introduced random values

$$\beta_k = \frac{\sum_{i \neq j} \cos(k\varepsilon_{ij})}{\sqrt{n(n-1)}} = \frac{\left[\sum_{i=1}^{n} \cos(k\varphi_i)\right]^2 + \left[\sum_{i=1}^{n} \sin(k\varphi_i)\right]^2 - n}{\sqrt{n(n-1)}}, \quad k = 1, 2 \tag{1}$$

(n is the number of secondary particles, ϕ_i is the azimuth angle of the i-th particle, and ε_{ij} is the angle between the projections of the tracks of two particles) have a mathematical expectation and a variance that are, respectively,

$$\left.\begin{aligned} \nu(\beta_k) &= 0 \\ \sigma^2(\beta_k) &= 1 \end{aligned}\right\}, \tag{2}$$

assuming azimuthal isotropy and independence of n angles ϕ_i. By means of the proposed procedure, the azimuthal asymmetry of shower particles was discovered in stars, which were formed by single-charge particles and which satisfy the criteria of selection.

$$\left.\begin{aligned} n_h + n_g &> 15 \\ n_s &\geqslant 10 \end{aligned}\right\}, \tag{3}$$

where $n_g + n_h$ is the number of strongly ionizing particles and n_s is the number of shower particles. In this paper, we shall describe the study of the azimuthal angular distribution of gray tracks in these same showers. We call gray tracks those tracks with a grain density greater than 1.4 g_0 (g_0 is the grain density on the tracks of fast electrons) and a run greater than 2.8 mm, which corresponds to a proton kinetic energy not less than 25 MeV. /47

In order to study the azimuthal angular distribution of gray tracks from 50 showers, which satisfy the criteria of selection (3) and those studied in [1], 33 showers whose peaks were more than 2.8 mm distant from each edge of our part of the pile were selected. The average energy of the primary particles can be evaluated by means of the Castangoli formula. In showers formed by protons with an energy of 24 GeV and having a number of particles, $n_h + n_g > 8$, $n_s \geqslant 8$. The Castangoli formula decreases the magnitude of the energy four-fold, on the average [2]. When this correction is taken into account for the test showers, the average energy amounts to ~ 50 GeV.

In each shower, we calculated the values of β_k for the shower particles and gray tracks separately, and we determined the average values of $\overline{\beta}_k = \frac{1}{N}\sum_{i=1}^{N}\beta_{ki}$ (N is the number of showers). The results of the data processing are shown below:

Type of particles *	$\overline{\beta}_1$	$\overline{\beta}_2$	a
Shower particles	$+0,78$ $(4,5)$	$-0,04$ $(0,21)$	$0,39^{+0,07}_{-0,06}$
Gray tracks	$+0,45$ $(2,6)$	$+0,28$ $(1,6)$	$0,44\pm0,11$

The parentheses show the difference $|\overline{\beta}_k| \cdot \sqrt{N}$ of the value $\overline{\beta}_k$ from its mathematical expectation in units of standard deviation; $\overline{n}_s = 21$, $\overline{n}_g = 9$, $\overline{\gamma}_c = 2.7$ are the median values of the 33 showers. Figure 1a shows a curve which reflects the distribution density of the value β_k under azimuthal isotropy, in dependence of the angles ϕ_i on n, and a large number of particles n. Large values of $\overline{\beta}_1$ indicate that the azimuthal isotropy and the independence of the departure angle of secondary particles are not observed, at least for the part of the showers under study.

As shown in [3], the law of conservation of momentum decreases the mathematical expectation and the variance of β_1 in comparison with their values in (2), and has little effect on the distribution of β_2. The aforementioned large values of $\overline{\beta}_1$ cannot be explained by the effects of the law of conservation momentum. They point out the azimuthal asymmetry of the shower particles and gray tracks because, for any symmetric distribution of azimuthal angles, the mathematical expectation of the value β_1 is equal to zero [1]. The values of $\overline{\beta}_1$ and $\overline{\beta}_2$ are in agreement with the assumption of a nonsymmetric distribution density /48

*Translator's Note: Commas represent decimal points.

$$P(\varphi) = \frac{1}{2\pi}(1 + a\cos\varphi), \quad 0 \leqslant a \leqslant 1, \tag{4}$$

and with the statistical independence of the departure angles of secondary particles. In this case,

$$\nu(\beta_1) > 0; \ \nu(\beta_2) = 0.$$

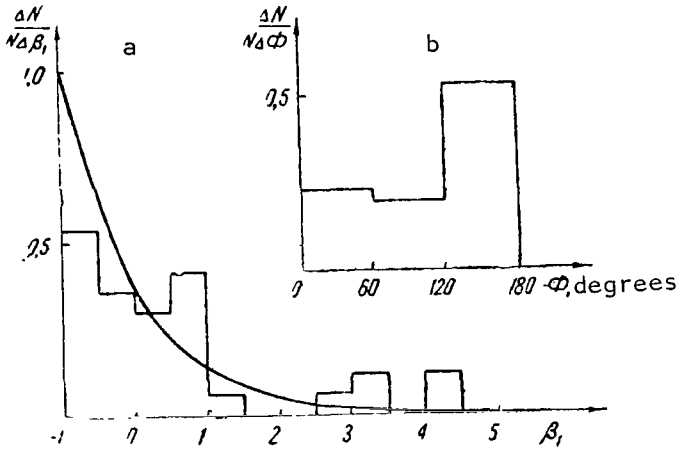

Figure 1. Distribution of Showers with respect to β_1 for Gray Tracks (a) and Distribution of the Angles Φ for 33 showers (b)

By utilizing the formula in [1], and assuming that the values of the parameter a are identical for all showers, we evaluated a from the experimental values of $\overline{\beta}_1$ (see the values of a above).

Under azimuthal asymmetry of gray tracks and shower particles, the question arises regarding the mutual orientation in the directions of predominant emission for these two groups of secondary particles. The direction of predominant emission of gray tracks (shower particles) in a separate shower is specified by the sum of single vectors which agree with the projections of the tracks on the plane perpendicular to the direction of the primary particle. The angle Φ between the directions of predominant emission of two groups of particles can be easily determined from the relation

/49

$$\cos\Phi = \frac{a_s a_g + b_s b_g}{\sqrt{a_s^2 + b_s^2} \cdot \sqrt{a_g^2 + b_g^2}}, \tag{5}$$

where

$$a_s = \sum_{i=1}^{n_s} \cos\varphi_i, \quad b_s = \sum_{i=1}^{n_s} \sin\varphi_i,$$

$$a_g = \sum_{j=1}^{n_g} \cos \varphi_j, \quad b_g = \sum_{j=1}^{n} \sin \varphi_j.$$

The distribution of the angles Φ for 33 showers (Figure 1b) is not in agreement with the isotropic distribution. The value of $\chi^2 = 6.7$, as calculated by us, exceeds the upper 5% limit equal to $\chi^2 = 6.0$ for two degrees of freedom. It follows from Figure 1b that, in at least part of the showers, there is a tendency to emit shower particles and gray tracks in opposite directions.

The effect observed can be qualitatively explained on the basis of a possible internuclear cascade generation process. The excess showers at large angles Φ are governed by the non-central collisions of primary particles with heavy nuclei in the emulsion because, for small impact parameters, an isotropic distribution of the angles Φ is expected. In a non-central collision (Figure 2), the flow of secondary high-energy particles is concentrated in region II of the nucleus-target near the extension of the trajectory of the primary particle, the form of which is unknown. Shower particles which move out into region I have a comparatively small energy; on this basis, we have here the absorption of shower particles and the formation of particles that leave gray tracks. However, the shower particles which move out into region III pass it without absorption. As a result, the shower particles of a wide cone fly predominantly downward in the laboratory system (Figure 2), if one looks in the direction of the primary particle, while the gray tracks fly predominantly upward. /50

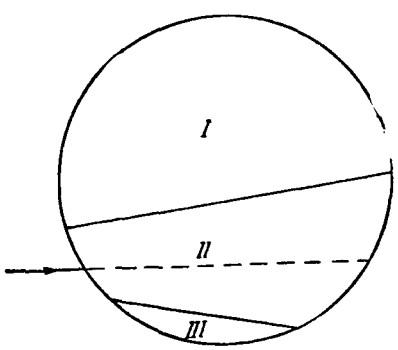

Figure 2. Non-central Collision of a Fast Particle with a Heavy Nucleus of an Emulsion (laboratory reference system).

For shower particles of a narrow cone ($\Theta < \Theta_{1/2}$), there is no azimuthal asymmetry according to the experimental data in [1].

The authors express their gratitude to I.M. Gramenitskiy for a discussion of the work and to Sh. Abduzhamilov, L. P. Chernova, and G. M. Chernov for the measurement of the departure angle of the shower particles.

REFERENCES

1. Abduzhamilov, Sh., S. A. Azimov, L. P. Chernova and G. M. Chudakov, *ZhETF*, Vol. 45, p. 407, 1963.
2. Abduzhamilov, Sh., V. M. Belen'kiy, L. P. Chernova and G. M. Chernov, *Izv. AN Uzbek SSR*, No. 1, p. 98, 1965.
3. Azimov, S. A., Sh. Abduzhamilov, L. P. Chernova and G. M. Chernov, *DAN Uzbek SSR*, No. 1, p. 11, 1965.

ON INELASTIC COHERENT INTERACTIONS OF HIGH-ENERGY PROTONS WITH COMPLEX NUCLEI

Sh. Abduzhamilov, S. A. Azimov, L. P. Chernova,
G. M. Chernov, and V. M. Chudakov

During recent years, the increasing attention of researchers has been drawn to inelastic processes in which the target nucleus receives from the primary high-energy ($E \gtrsim 10^{10}$ ev) particle a small momentum and participates in the interaction as a whole without being destroyed or excited, while conserving its charge. Due to the small magnitude of the process cross section, the number of experimental studies of such interactions so far accomplished is not large; moreover, all the experiments have considered the dissociation of pions in the field of the nucleus.

For example, coherent interactions of negative pions with complex nuclei of a photoemulsion at an energy of 14-17 BeV have been described in [1], where the authors studied reactions of the type

$$\pi^- + \text{nucleus} \rightarrow \text{nucleus} + n\pi \qquad (1)$$

in which the nucleus is not destroyed and is not excited upon receiving a small momentum q. At the same time, a study was made of the interactions in which the target nucleus is weakly excited and then passes into the basic state (it is difficult to distinguish "pseudocoherent" interactions from coherent). It should be noted that reactions (1) comprise approximately 30% of the total number of stars with the number of secondary shower particles $n_s = 3$ and the number of strongly ionizing particles $n_h = 0$.

Similar interactions with complex nuclei can be experienced by high-energy protons. At the same time, the longitudinal momentum $q_{\parallel}$ of the recoil nucleus is

$$q_1 \approx \frac{M + p_0}{2Mp_0} q_\perp^2 + \frac{M^{*2} - m^2}{2p_0} + T_{ex}, \qquad (2)$$

where M is the mass of the target nucleus; T_{ex} is the energy of excitation, which /52 is equal to zero for coherent interactions; $q_\perp$ is the transverse momentum of the recoil nucleus; m is the mass of the nucleon; P_0 is the momentum of the primary proton; and M* is the effective mass of all the secondary particles with the exception of the recoil nucleus, (the speed of light c = 1).

The conditions of validity of this formula are

$$q \text{ and } T_{ex} \ll p_0 \text{ and } M \text{ when } p_0 \approx \varepsilon_0 \qquad (3)$$

(ε_0 is the energy of the primary particle) and are satisfied for interactions (1). By utilizing Equation (2), it is easy to show that in reactions with fixed values of p_0, M, T_{ex}, and a fixed number n of pions formed during the dissociation of the proton, the minimum momentum of the recoil nucleus is equal to

$$q_{min} \approx \frac{n\mu(2m + n\mu)}{2p_0} + T_{ex} \qquad (4)$$

(μ is the mass of the pion). During its realization, all the secondary particles, including the recoil nucleus, fly at an angle of 0 with the direction of the primary proton in the laboratory system (l. s.). The values of (4) are greater than during the dissociation of the pions; however, even for a primary proton energy of the order of 10^{10} ev, the minimum momentum becomes sufficiently small and corresponds to recoil nuclei not observed in the emulsion. For this reason, it is natural to assume that the coherent interactions of the protons with the complex nuclei of the photoemulsion appear frequently as narrow showers without recoil nuclei and with a number of strongly ionizing particles $n_h = 0$ and an odd number n_s of secondary shower particles (the latter is related to the fact that the nucleus conserves its charge).

In studying inelastic proton-nucleon (pN) interactions with free and quasi-free nucleons of a photoemulsion, the coherent interactions with complex nuclei could be erroneously taken for proton-nucleon interactions (pn), but they should be absent among the showers which satisfy the necessary criteria of the selection of proton-proton (pp) collisions. Consequently, with a contribution of coherent interactions, the natural assumption of the difference therein, and pN-collisions of angular distributions in pn-interactions, then the angular distribution of secondary particles should possess an increased nonhomogeneity (the presence of two classes of collisions), in comparison with /53
pp-interactions. Below is described a method that we developed earlier [2] which makes it possible to register with a high effectiveness the degree of nonhomogeneity of the angular distributions in the laboratory system, as well as the differences between the angular distributions of the secondary particles discovered in showers which are taken for pp- and pn-collisions. These differences are easily explained by the contribution of the coherent interactions of the protons with complex nuclei.

Method of Study.

Let us examine m showers with the same energy of the primary particles and the same number n of secondary charged particles. Let $x = f(\Theta)$ be a random monotonic function of the departure angle of the secondary particles relative to the direction of the primary ones in the laboratory system, while $x_{ij} = f(\Theta_{ij})$ is the value of this function for the j-th particle of the i-th shower (i = 1,2..., m; j = 1,2..., n). Earlier [2], in a study of the angular non-homogeneity of showers, we utilized the value F given by

$$F = \frac{m(n-1)}{(m-1)\left(S^2/S_1^2 - 1\right)} > 0, \tag{5}$$

where

$$S^2 = \frac{1}{mn}\sum_{i=1}^{m}\sum_{j=1}^{n}\left(x_{ij}-\bar{x}\right)^2;\quad S_1^2 = \frac{1}{m}\sum_{i=1}^{m}\left(\bar{x}_i-\bar{x}\right)^2;$$

$$\bar{x}_i = \frac{1}{n}\sum_{j=1}^{n}x_{ij};\quad \bar{x} = \frac{1}{m}\sum_{i=1}^{m}\bar{x}_i = \frac{1}{mn}\sum_{i=1}^{m}\sum_{j=1}^{n}x_{ij}.$$

The values x_j are assumed to be equally distributed. For a large number m of showers (tests) and statistical independence of the angles Θ_j (j = 1,2..., n), the following approximate equations are satisfied:

$$S^2/S_1^2 \approx n;\ F \approx 1. \tag{6}$$

For a finite number m of showers and independence of the angles Θ_j (the assumption of the normal distribution of the values x_j is not required for the number of particles $n \geqslant 4$ [3], the values of F follow (in complex tests) a certain well-known distribution with m - 1 and m(n - 1) degrees of freedom. For this reason, it is easy to establish a reliable range within which the value of F should lie with a probability close to unity. If the resulting value of F will not fall within this range, it can be assumed that the independence of the departure angle of secondary particles essentially does not take place in showers of the given energy and multiplicity. /54

The law of the conservation of momentum disturbs the independence of the emission of particles and the results of (6). Due to its influence, the values of F for random stars which imitate pp-collisions at an energy of 11 BeV do not exceed 0.5 in accordance with the statistical theory (see [2]). An increase in the magnitude of F is facilitated by:

(a) the asymmetric emission of secondary particles in the center-of-mass system (c.m.s.) of NN-collisions (this phenomenon was discovered by N. A. Dobrotin, S. A. Slavatinskiy, et al, [4, 5] at energies of the order of $\sim 10^{11}$ev);

(b) the presence of two or more classes of showers with substantially different angular distributions in the laboratory system for the given values of the energy and multiplicity n.

These causes intensify the difference between the values of $\bar{x}_i$ for individual showers, decrease the ratio S^2/S_1^2, and thus cause an increase in the magnitude of F.

The influence of the asymmetric showers has been examined in [2]. For a quantitative evaluation of the influence of the second factor on the value of F, and a clarification of the effectiveness of the criteria, we assume the existence of two classes of showers which satisfy the specified selection criteria: (1) pn-collisions and (2) coherent interactions of primary protons with complex nuclei of an emulsion.

We shall define the function of x in accordance with [2]:

$$\left.\begin{aligned} x &= +1 \text{ when } \theta \leqslant \theta_{1/2};\ \gamma_c = \cot\theta_{1/2} \\ x &= -1 \text{ when } \theta > \theta_{1/2} \end{aligned}\right\}, \tag{7}$$

where $\theta_{1/2}$ is the theoretical half-angle of emission of particles in the laboratory system for NN-collisions; and γ_c is the Lorentz-factor of the center-of-mass system for NN-collisions. The fraction of coherent interactions among the showers with a number of secondary particles n is designated by α and the probability of obtaining the value of x = +1 for coherent interactions is designated by p. For the sake of simplicity, we shall assume that for pn-collisions this probability is equal to 0.5 (the method remains valid for any a-priori value of $\theta_{1/2}$, in particular when $\theta_{1/2} = (\theta_{1/2})_{exp}$). Taking into consideration Equation (7), we shall represent the variance S^2 in the form

$$S^2 = 1 - \bar{x}^2, \tag{8}$$

while the value of F is expressed in terms of the new variance S_2^2 as /55

$$F = m(m-1)^{-1}\left[1 + n\left(S^2/S_2^2 - 1\right)\right],$$

where

$$S_2^2 = \frac{1}{m}\sum_{i=1}^{m}\left[\frac{1}{n-1}\sum_{j=1}^{n}\left(x_{ij}-\bar{x}_i\right)^2\right]. \tag{9}$$

For a large total number of showers m and independence of the angles θ_j, the following approximate relations are valid for each class of showers separately:

$$\left.\begin{aligned}\bar{x} &\approx (1-\alpha)\nu_1 + \alpha\nu_2\\ S_2^2 &\approx (1-\alpha)\sigma_1^2 + \alpha\sigma_2^2\end{aligned}\right\}, \tag{10}$$

where $\nu_1 = 0$ and $\nu_2 = 2p-1$ are the mathematical expectations of a random value of x for pn-collisions and coherent interactions respectively; $\sigma_1^2 = 1$ and $\sigma_2^2 = 1 - \nu_2^2$ are the individual variances of such a value. By means of Equations (8) - (10), we get the final result:

$$F \approx 1 + n\frac{\alpha(1-\alpha)(2p-1)^2}{1-\alpha(2p-1)^2}. \tag{11}$$

For example, when $\alpha = 0.1$, $p = 1$ and $n = 5$, we have $F \approx 1.5$. Thus, the criterion for F is highly sensitive to the detection of a small fraction of narrow showers of the second class.

The value F is characterized by two basic properties:

(1) when there is independence of the angles θ_j, the relation $F \approx 1$ is satisfied regardless of the form of the angular distribution of secondary particles, the choice of the function x, and the number of particles n.

(2) the value F is a measure of the angular nonhomogeneity of showers for a fixed number n of particles.

The second property arises from the first and from the fact that the value F can be represented in the form

$$F = \frac{mnS_1^2}{(m-1)S_2^2}. \tag{12}$$

This formula shows that the value of F is directly proportional to the variance S_1^2, which reflects the spread of the values of $\bar{x}_i$ among showers, and is inversely proportional to the variance S_2^2 which characterizes the spread of the values of x within the showers (x is a random function of the angle). /56

It should be noted that the difference of the angular distributions of particles of different kinds (for example, protons and pions) in our method of numeration of secondary particles, where the magnitudes of x_j equally distributed, can lead to a breakdown in the independence of the values of x_j. This difference, on one hand, can intensify the spread of the x values within the showers due to the presence in the same shower of particles of a different kind and, on the other hand, can increase the spread of the $\bar{x}_i$ values among the showers due to the presence of showers with a different number of protons for a given total number n of particles. For this reason, the influence of the factor under consideration on the value of F is not clear in general. However, if the number n of particles is not large and the fraction of the protons is small, then this influence can hardly play a major role in the selection of the function x in the form (7).

Experimental Data

Let us discuss the results of the processing of showers that were formed in a photoemulsion by protons with an energy of 24 BeV and that satisfy the necessary selection criteria [2] of pN-collisions. Measurements were made earlier by us with the number of particles $n \geqslant 4$. Besides, we also used the results of measurements made in the high-energy laboratory of the United Institute of Nuclear Research during the course of a study of inelastic pN-interactions of protons with an energy of 10 BeV with free and quasi-free nucleons of the photoemulsion.

The values of F are shown in the table and in the figure (a). It is evident that large values of F occur when the number of secondary charged particles n = 3 and 5, in comparison with the values of F when n = 2, 4, and 6. As can be seen from the table, the value of F when ε_0 = 24 BeV and n = 5 exceeds the upper critical limit F_{crit}. This difference between the values of F for even and odd n cannot be explained by the internuclear motion of target nucleons, which leads to an increase in F by not more than several hundredths [2]. The non-monotonic dependence of F (of angular nonhomogeneity of showers) on n makes it possible to assume that essentially basic pp-collisions are selected for an even number n of particles, while for n = 3 and 5, there are showers of another nature besides pn-collisions, with a substantially different angular distribution in the laboratory system (narrower or wider in comparison with the angular distribution in pn-collisions). With such an assumption it is easy to explain the relatively larger angular nonhomogeneity of showers when n = 3 and n = 5. It should be noted that the experimental values of F for an even n are considerably larger /57

than the corresponding values for random stars which simulate head-on pp-collisions at an energy of 11 BeV in accordance with the statistical theory. This indicates the greater role of the peripheral pp-interactions and the higher share of asymmetric showers in the center-of-mass system relative to the case of head-on collisions.

ε_0	n	m	F	F^*_{crit}	β	α 'from (13)	α 'from (15)
10 BeV	2	213	0,64	—	0,239±0,034	—	—
	3	142	1,16	—	0,345±0,049	0.210±0,062	0,16
	4	197	0,72	1,31	0,102±0,023	—	—
	5	44	1,59	1,68	0,114±0,051	0,044±0,059	0,16
	6	44	0,82	1,67	0,045±0,032	—	—
	7	16	0,88	2,23	0	—	—
	8	8	0,83	2,98	0	—	—
24 BeV	4	171	1,03	1,34	0,117±0,026	—	—
	5	124	1,54	1,39	0,161±0,036	0,084±0,043	0,12
	6	135	0,86	1,36	0,052±0,020	—	—
	7	65	0,97	1,51	0,031±0,022	—	—
	8	49	1,12	1,58	0	—	—

Tr. Note: Commas represent decimal points.

*F_{crit} is the critical limit for the value of F such that the probability of obtaining a value of $F < F_{crit}$ is equal to 1%, (assuming independence of θ_j).

For every value of n, we determined the fraction β of the narrow showers, arbitrarily designating as narrow those showers for which all the secondary particles have departure angles $\theta < \theta_{1/2}$ with the direction of the primary proton in the laboratory system (see table and figure, b). When the numbers of particles are n = 3 and 5, the fraction β is greater than for neighboring odd values of n. Hence, it follows that showers with the numbers of particles n = 3 and 5 have on the average a narrower angular distribution in the laboratory system in comparison with pn-collisions of the same multiplicity. We assume that these showers are the coherent interactions of protons with complex nuclei of the emulsion, for which an odd number of secondary charged particles is always formed. /58

The comparatively narrow angular distribution of secondary particles when their numbers are n = 3 and 5 can, of course, be related to the asymmetric forward emission of protons in the center-of-mass system of pn-collisions. However, it is difficult to explain the large values of F for the same n from this point of view because the value of F does not depend on the form of the angular distribution (assuming independence of θ_j) but is a measure of the angular nonhomogeneity of the showers. If one excludes from the selection of showers the pN-interactions with a gray track of the recoil proton which flies

back in the center-of-mass system, and calculates the values of F for the remaining stars with $n_h = 0$ ("white" stars), then these values will not differ noticeably from the original values [2].

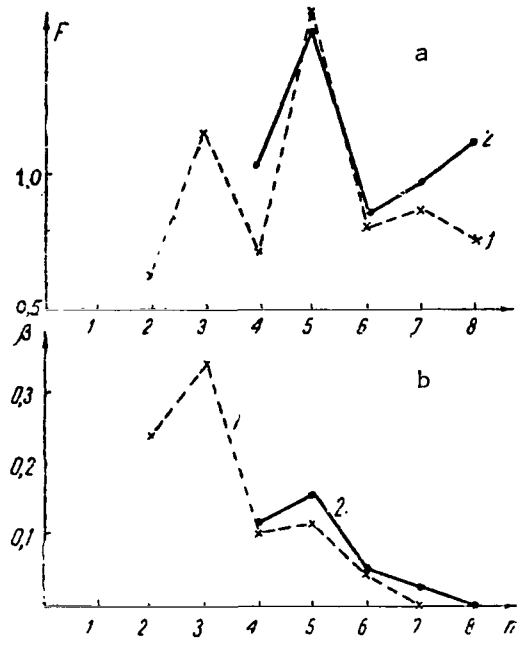

Values of F (a) and of the fractions of narrow showers β (b) as functions of the number n of particles at energies of 10 BeV (1) and 24 BeV (2).

For a rough estimation of the fraction α of the coherent interactions among showers with a given odd number n of particles, we shall apply the formula /59

$$\alpha = \frac{\beta - \beta_1}{\beta_2 - \beta_1} \geqslant \frac{\beta - \beta_1}{1 - \beta_1}, \qquad (13)$$

where β_1 is the fraction of narrow showers among the pn-collisions of multiplicity n and β_2 is the fraction of narrow showers among the coherent interactions of the same multiplicity:

$$\beta_1 \sim \frac{1}{2}(\beta_{n-1} + \beta_{n+1}). \qquad (14)$$

Another method of making a rough estimation of α is based on a comparison of the values of F for an even and odd number of particles. If, besides the assumptions utilized in the derivation of Equation (11), an assumption is made regarding the independence of the departure angles of the particles in pp-collisions, then Equation (11) can be rewritten in the form

$$\alpha \geqslant \frac{\alpha(1-\alpha)(2p-1)^2}{1-\alpha(2p-1)^2} \approx \frac{1}{n}\left[F - \frac{1}{2}(F_{n-1} + F_{n+1})\right] \qquad (15)$$

Here the value of F corresponds to an odd number n of particles. If all the coherent interactions are narrow, then the equality sign is always present in Equations (13) and (15) simultaneously. The values of the lower boundary α' of the fraction α of the coherent interactions, as calculated from Equations (13) and (15) are listed in the table (when use is made of (15), it is difficult to evaluate the error $\Delta\alpha'$).

Among the 124 showers measured with ε_0 = 24 BeV and n = 5, there are 43 showers with an explicit track of an electron that emanates from the apex of the star. A β-electron can originate in a pn-collision, while the track of the electron should be absent in coherent interaction. In case of nucleus excitation, the emission of an internal conversion electron is possible; however, such reactions (1) have not been observed so far. For this reason, it can be expected that the indicated 43 showers with an explicit electron track are essentially pn-collisions. In connection with this, we calculated the values of F and β for showers with an electron and also for the remaining 81 showers with ε_0 = 24 BeV and n = 5, which resulted in $F = 1.26$ $(F_{crit} = 1.70)$;

$\beta = 0.116 \pm 0.052$ in the presence of an electron; and $F = 1.71$ $(F_{crit} = 1.49)$; /60

$\beta = 0.185 \pm 0.048$ for the remaining showers. These values of F and β for the two groups of showers are in qualitative agreement with the expected dependence.

The authors are grateful to Academician V. I. Veksler for the permission to utilize the experimental data obtained in the Laboratory of High Energies in the United Institute of Nuclear Research, and to Professor M. I. Podgoretskiy for his consideration of the work.

REFERENCES

1. Caforio, A., and D. Ferraro, a.o., *Nuovo Cimento*, Vol. 32, p. 1471, 1964.
2. Abduzhamilov, Sh., S. A. Azimov, L. P. Chernova, G. M. Chernov, and V. M. Chudakov, *ZhETF*, Vol. 47, p. 24, 1964.
3. Van-der-Varden, B. L., *Matematicheskaya Statistika*, [Mathematical Statistics], Moscow, Foreign Literature Press, 1960.
4. Guseva, V. V., N. A. Dobrotin, N. G. Zelevinskaya, K. A. Kotel'nikov, A. M. Lebedev, and S. A. Slavatinskiy, *Izv. AN SSSR, seriya fizich*, Vol. 26, p. 549, 1962.
5. Dobrotin, N. A., V. V. Guseva, K. A. Kotel'nikov, A. M. Lebedev, S. V. Ryabikov, S. A. Slavatinskiy, and N. G. Zelevinskaya, *Nuclear Physics*, Vol. 35, p. 152, 1962.

STUDY OF INELASTIC π^-p-COLLISIONS WITH A SLOW RECOIL PROTON AT AN ENERGY OF 17 GeV

S. A. Azimov, B. K. Nikishin,
I. V. Rechiskiy, and V. M. Chudakov

In this paper, we study inelastic π^-p-interactions with free and quasi-free protons of a photoemulsion. Ilford G5 emulsions were irradiated in EURATOM /61
[European Atomic Energy Community] with π^--mesons with a momentum of 17.2 GeV/c. As a result of the inspection of 4 km of the track of the primary particles, 86 π^-p-interactions were found with the number of secondary charged particles being 4 and 6, and a slow recoil proton. These events satisfy the following selection criteria.

1. The star should contain one gray track (recoil proton) which has a lobe density greater than 1.4 g_0 (g_0 is the density of the lobes on the track of the primary π^--meson) and the range should be greater than 2.8 mm, which corresponds to a kinetic energy of the proton greater than 25 MeV.

2. The gray track should be projected into the forward hemisphere in the laboratory system.

3. There should be no recoil nucleus and lobe in the interaction point.

4. There is no electron track emanating from the apex of the star.

5. The invariant mass of all the secondary particles, except for the recoil proton (residual effective mass), exceeds the magnitude $n_s\mu$ (n_s is the number of secondary shower particles, μ is the pion mass) when calculated on the assumption of a π^-p-interaction.

6. The Birger-Smorodin criterion [1] is satisfied.

The enumerated criteria are necessary but not sufficient for the selection of the events of interest to us.

The identification of the recoil protons and their energy were made by the Fowler-Perkins method [2]. Only angular measurements were taken on the tracks of the shower particles.

One of the problems of this study was the search for hidden resonances /62
from the distribution of the residual effective masses for the events where definite angular correlations were manifested. These correlations can take place in the case of high-pion decompositions of polarized or aligned resonances, and thus the selection of events having correlations makes it possible to increase in the test material the proportion of the reactions which take place through the formation of resonances.

Method of Study. The invariant mass M of all the secondary particles, except the recoil proton (residual effective mass), is determined from the formula

$$M^2 = (\varepsilon_0 - T)^2 - (\vec{p}_0 - \vec{p})^2 = \mu^2 + 2pp_0\cos\theta_p - 2T(\varepsilon_0 + m), \quad (1)$$

where ε_0 and p_0 are the energy and momentum of the primary π^--meson in the laboratory system; m is the nucleon mass; T, p, and θ_p are the kinetic energy, momentum, and departure angle of the recoil proton with the direction of the primary particle in the laboratory system; and the speed of light c = 1.

The angular distributions are studied in the center-of-mass system XYZ of all the secondary particles, with the exception of the recoil proton. Its Lorentz factor γ^* in the laboratory system is

$$\gamma^* = \frac{\varepsilon_0 - T}{M}. \quad (2)$$

The Z axis (Figure 1) coincides with the direction of motion of the system XYZ, the X axis lies in the reference plane which contains the momenta $\vec{p}$ and $\vec{p}_0$, while the Y axis is directed along the vector product $\vec{p} \times \vec{p}_0$ of these momenta.

The departure angle of the secondary particle with the Z axis in the system XYZ is designated by θ, while the azimuthal angle in the XY plane with the X axis is designated by ϕ. The relative distribution of the projections of the tracks of secondary shower particles on the XY plane in an individual shower will be characterized by a parameter introduced earlier by us [3] and given by

$$\beta = \frac{\sum_{i \neq j} \cos(2\varepsilon_{ij})}{\sqrt{n_s(n_s-1)}} = \frac{\left[\sum_{i=1}^{n_s} \cos(2\varphi_i)\right]^2 + \left[\sum_{i=1}^{n_s} \sin(2\varphi_i)\right]^2 - n_s}{\sqrt{n_s(n_s-1)}}; \quad (3)$$

here $\varepsilon_{ij}\,(0 \leqslant \varepsilon_{ij} \leqslant \pi)$ is the azimuthal angle between the projections of the tracks of the i-th and j-th particles; n_s is the number of secondary shower particles (the recoil proton is not included in this number, so that the shower contains n_s + 1 secondary charged particles); and the number of terms in $\sum_{i \neq j} \cos(2\varepsilon_{ij})$ is equal to $n_s(n_s - 1)$. /63

The value of β depends only on the joint distribution of the track projections and does not depend on their orientation with respect to the X and Y axes. In case of azimuthal isotropy, i.e., in case of a uniform distribution of ϕ_i in the interval $(0, 2\pi)$, and when n_s is independent of angles ϕ_i $(i = 1, 2, \ldots, n_s)$, the mathematical expectation and the standard deviation of β are given respectively by

$$\nu(\beta) = 0; \ \sigma(\beta) = 1. \tag{4}$$

Hence, it follows that during the generation by the Monte-Carlo method of N showers with an arbitrary, but not necessarily equal n_s, the value of $\overline{\beta} = \frac{1}{N}\sum_{m=1}^{N}\beta_m$ should lie with a probability of about 95% within the interval

$$-\frac{2}{\sqrt{N}} < \overline{\beta} < \frac{2}{\sqrt{N}}, \tag{5}$$

if the azimuthal angular distribution is isotropic and the number N of showers is sufficiently large. If the experimental value of $\overline{\beta}$ does not lie within interval (5), it can be assumed that azimuthal correlations take place.

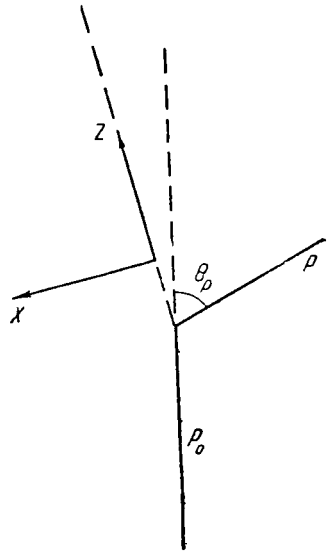

Figure 1. Selection of a Reference System in the Study of Angular Distributions.

The correlations shown in Figure 2a (predominance of angles ε close to 0 and π) and Figure 2b (predominance of angles $\varepsilon \sim 0$) lead to an increase in the value of β, which can reach its maximum value of $\sqrt{n_s(n_s-1)}$. The correlations in Figure 2a can originate in reactions

$$\pi^- + p \to p + 0^- \\ \qquad\qquad \downarrow \to n_s\pi^{\pm} + n\pi^0, \tag{6}$$

which proceed through the formation and high-pion decomposition of the resonance or of the "fireball" 0, which has a great spin and is polarized along the Y axis with a maximum (in absolute value) projection of the spin on this axis. We designated by Θ' the departure angles of the secondary pions with the Y axis in rest system 0, and we designate by ϕ' the corresponding azimuthal angles. It should be expected that the momenta of the pions formed during the decomposition of 0 will be

/64

concentrated near the XZ plane, perpendicular to the direction of the resultant orbital moment of the pions. For this reason, the distribution of the magnitude of cos Θ' will be nonisotropic with a predominance of the values of cos $\Theta' \sim 0$, while the distribution of ϕ' is isotropic.

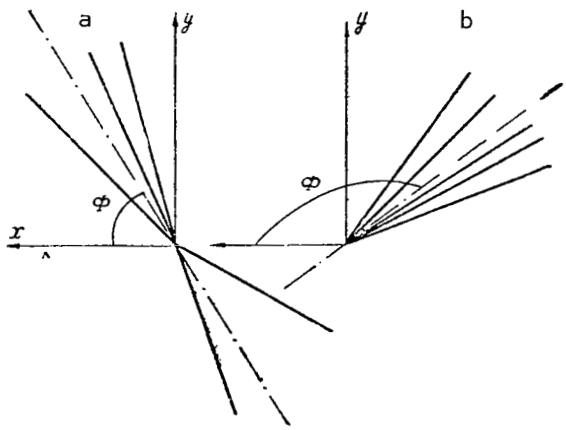

Figure 2. Possible Azimuthal Correlations when n = 5. The Solid lines are Track Projections of Secondary Shower Particles on the XY Plane; the dotted line Characterizes the Predominant Emission of Particles.

Calculation of the decomposition $0 \to 2\pi$ by means of spherical functions confirms such a form of angular distribution. In the case under consideration, the distribution of angles ϕ of interest is extended along the X axis, while the distribution of cos Θ (Θ is the angle with the Z axis in rest system 0 previously introduced), is nonuniform, with a predominance of values of cos Θ close to ± 1.

The polarization of the resonance or of the "fireball" should lead not only to large values of β in individual showers, but also to a predominant emission of particles along the X axis (see Figure 2a). In connection with this, we /65 determine in each shower the line of the predominant emission of particles in the XY plane, provided that the sum of the squares of the distances from n_s points of intersection of the track projections to the circumference of the unit radius up to the line under consideration is minimum (Figure 2). The angle Φ which is formed by this line with the X axis is found from the conditions

$$\left.\begin{aligned} \tan(2\Phi) &= \frac{\sum_{i=1}^{n_s} \sin(2\varphi_i)}{\sum_{i=1}^{n_s} \cos(2\varphi_i)}; \\ \frac{\sin(2\Phi)}{\sum_{i=1}^{n_s} \sin(2\varphi_i)} &> 0 \\ 0 < \Phi &< \pi \end{aligned}\right\} \qquad (7)$$

It should be expected that in reactions (6), at the indicated polarization of the resonance with a large spin, the angles Φ will as a rule assume values close to 0 and π, while the average value $\bar{\beta}$ of β will be essentially positive.

On the other hand, it can be assumed that for phonon events the distribution of angles Φ is isotropic for all values of β, while the azimuthal correlations are absent ($\bar{\beta} \approx 0$) for all angles Φ. This assumption seems natural because the value of β, in accordance with expression (3), depends only on the mutual orientation of the track projections and does not depend explicitly on angle Φ.

If the experimental material has reactions (6), besides phonon events, the anisotropy of the distribution of angles Φ should increase with an increase in β, while the average value of $\bar{\beta}$ increases with an increase in the absolute value of the difference $\Phi - \frac{\pi}{2}$. If this independence actually takes place, it is necessary to select showers with large values of β and of $\left|\Phi - \frac{\pi}{2}\right|$, plot for them the distribution of the residual effective masses, and compare it with the phonon distribution for small values of $\left|\Phi - \frac{\pi}{2}\right|$. The phonon curve of the distribution of the effective masses is easily normalized on the assumption of isotropic distribution of Φ for phonon events. /66

In order to evaluate the nonuniformity in the distribution of angles Φ, we shall utilize the value γ given by

$$\gamma = \left(\Phi - \frac{\pi}{2}\right)^2. \tag{8}$$

Under isotropic distribution of Φ, its mathematical expectation and standard deviation are, respectively,

$$\left.\begin{aligned} \nu(\gamma) &= \frac{\pi^2}{12} \approx 0{,}82 \\ \sigma(\gamma) &= \frac{\pi^2}{\sqrt{180}} \end{aligned}\right\}. \tag{9}$$

For this reason, the value of $\bar{\gamma} = \frac{1}{N}\sum_{m=1}^{N} \gamma_m$, the average with respect to N showers, should lie within the interval

$$\frac{\pi^2}{12} - \frac{2\pi^2}{\sqrt{180N}} < \bar{\gamma} < \frac{\pi^2}{12} + \frac{2\pi^2}{\sqrt{180N}} \tag{10}$$

with a probability of ≈ 95%. If the experimental value of $\overline{\gamma}$ exceeds the upper bound of interval (10), this indicates an excess of angles Φ close to 0 or π.

The azimuthal angular distribution of secondary shower particles (in the total shower) will be characterized by

$$\left.\begin{aligned}\delta_1 &= \frac{n_1 - n_2}{n_1 + n_2}\\ \delta_2 &= \frac{n_1' - n_2'}{n_1' + n_2'}\end{aligned}\right\}, \tag{11}$$

where n_1 is the number of particles within the interval $0° < \phi < 180°$; n_2 is the number within the interval $180° < \phi < 360°$; n_1' is the number within the intervals $45° < \phi < 135°$ and $225° < \phi < 315°$; and n_2' is the number with angles ϕ that do not lie within the last two intervals.

For any symmetric distribution, $\delta_1 = 0$; and under azimuthal isotropy both δ_1 and δ_2 are equal to zero.

In order to describe the distribution of secondary shower particles with respect to angles Θ with the Z axis of reference system XYZ, which moves in the laboratory system with Lorentz factor (2), we shall utilize the values /67

$$\left.\begin{aligned}\alpha_1 &= \frac{m_1 - m_2}{m_1 + m_2}\\ \alpha_2 &= \frac{m_1' - m_2'}{m_1' + m_2'}\end{aligned}\right\}, \tag{12}$$

where m_1 is the number of particles with $\cos\Theta > 0$; m_2 are those with $\cos\Theta < 0$; m_1', those with $|\cos\Theta| > 0.5$; and m_2' those with $|\cos\Theta| < 0.5$. Under symmetric angular distribution, $\alpha_1 = 0$; and under isotropic conditions $\alpha_1 = \alpha_2 = 0$. In order to convert the latitude angles from the laboratory system to the XYZ system, it is necessary to know the velocities of the secondary shower particles. Inasmuch as these were not measured, we utilized the ultrarelativistic approximation as done in work on cosmic rays, i.e., the assumption of equality of the velocities of the secondary shower particles in the XYZ system with the velocity of this system in the laboratory system. For this reason, our results on the distribution of angles Θ should be treated with certain caution; they should be regarded as auxiliary data.

Angular distributions of secondary shower particles. Due to the insufficiency of statistics, we will reduce the experimental data for the π^-p-

interactions with the numbers 4 and 6 (n_s = 3 and 5) of secondary charged particles taken together. Such an approach can be justified by the possibility of decomposition of the resonance in accordance with different systems with emission of a different number n_s of secondary charged particles. The effects described below are observed separately for showers with n_s = 3 and showers with n_s = 5, but here they are not always statistically reliable.

Following the aforesaid program, we selected 41 showers with $\beta > 0$ and we calculated for them the average value $\overline{\gamma}$ of γ (column 1 in the table). Inasmuch as the experimental value is less than the lower bound of confidence range (10), the distribution of angles Φ can be considered nonisotropic with an excess of angles Φ close to $\pi/2$. In accordance with this, the azimuthal angular distribution of secondary shower particles in the XYZ system is anisotropic ($\delta_2 > 0$, the difference from zero exceeds 2 standard deviations), but symmetric ($\delta_1 \approx 0$, the difference from zero is less than 1 standard deviation). The positive value of δ_2 indicates that the azimuthal angular distribution is /69
extended along the Y axis, i.e., there is a predominance of angles ϕ close[1] to $\pi/2$ and $\frac{3}{2}\pi$. On the other hand, it should be expected that for phonon events the distribution of angles Φ, and consequently also the azimuthal angular distribution of the secondary particles (in the total shower), is isotropic for all values of β. This isotropy is actually observed for 45 showers which have $\beta < 0$ (row 2 in table). We wish to observe that in case of the selection of showers with respect to β, the calculation of the values α_1 and α_2 is meaningless because the distribution of secondary particles with respect to angles Θ for phonon events can depend on β.

Row 3 of the table shows the average value $\overline{\beta}$ of β for 34 showers in which angles Φ lie within the interval $60° < \Phi < 120°$. The positive value of $\overline{\beta}$, which exceeds the upper bound of confidence range (5), is explained by the correlations shown in Figure 2. Nevertheless, for phonon events, it seems that the correlations should be absent ($\overline{\beta} \approx 0$) for all angles Φ, as was observed (row 4 in the table) in the selection of 52 showers with angles Φ that do not lie within the interval (60°, 120°). Rows 3 and 4 in the table do not show the values of δ_1 and δ_2 because the azimuthal angular distribution of secondary particles in phonon events should depend on Φ.

[1] Our experimental data do not correspond to the case of resonance polarization examined above, viz., the plane of the predominant emission of particles is oriented otherwise.

Group No.	Selection criterion	N	$\overline{\beta}$	$\frac{2}{\sqrt{N}}$	$\overline{\tau}$	Interval	b_1	b_2	a_1	a_2
1	$\beta>0$	41	—	—	0,58	0,59—1,05	−0,02±0,08	0,22±0,08	—	—
2	$\beta<0$	45	—	—	0,92	0,60—1,04	0,02±0,08	−0,01±0,08	—	—
3	$60°<\Phi<120°$	34	0,43	0,34	—	—	—	—	0,16±0,09	0,19±0,09
4	$\Phi<60°$ & $\Phi>120°$	52	0,11	0,28	—	—	—	—	0,16±0,07	0,01±0,07
5	$60°<\Phi<120°$									
	2,9 GeV$<M<$3,5 GeV	17	0,76	0,48	—	—	—	—	−0,02±0,13	0,36±0,12
6	$60°<\Phi<120°$									
	$M<$2,9 GeV & $M>$3,5 GeV	17	0,11	0,48	—	—	—	—	0,33±0,12	0,02±0,13
7	$\beta>0$									
	2,9 GeV$<M<$3,5 GeV	16	—	—	0,30	0,45—1,19	−0,06±0,13	0,45±0,11	—	—
8	$\beta>0$									
	$M<$2,9 GeV	25	—	—	0,76	0,53—1,12	0,01±0,11	0,06±0,11	—	—
	$M>$3,5 GeV									

Translator's Note: Commas represent decimals.

The effects observed can be understood by assuming the presence in the experimental material of reactions (6), besides phonon events, in which there is the formation of resonance of "fireball" 0, aligned with large (in absolute value) projections of the spin on the X axis (polarization along the X axis is prohibited by the P-invariance of strong interactions). In such an alignment, an angular distribution of secondary shower particles extended along the Y axis is expected (see the corresponding discussion for the case of resonance polarization previously mentioned). For this reason, it can be assumed that each of reactions (6) has $\beta > 0$ and angle Φ lying within the interval $60° < \Phi < 120°$, and thereby they explain the experimental results described above. Also, the assumption of alignment makes it possible to interpret the /70
experimental data on the distribution of angles Θ, as shown in rows 3 and 4 of the table. For the phonon events considered (row 4) we observe forward asymmetry, ($\alpha_1 > 0$), and isotropic distribution of $|\cos \Theta|$, ($\alpha_2 \approx 0$). The showers in row 3 [phonon events and reactions (6)] have anisotropic distribution of $|\cos \Theta|$, ($\alpha_2 > 0$); moreover, there is observed an excess of particles with $|\cos \Theta| > 0.5$, which is explained by the alignment assumption.

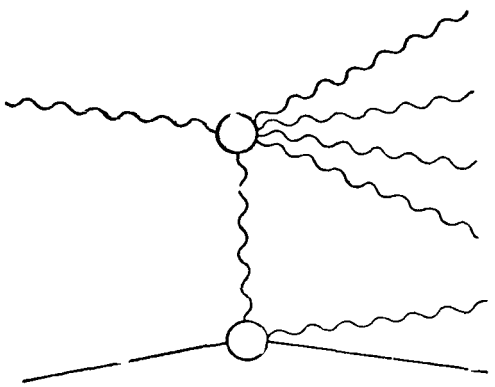

Figure 3. Single-meson Diagram Corresponding to the Formation of a Large Number of Pions in the Upper Star Point and of a Small Number of them in the Lower Star Point.

The predominance of the values $\cos \Theta > 0$ (forward asymmetry) for phonon events can be related to the large role of single-meson diagrams of the type shown in Figure 3. The group of pions formed in the upper star point moves in the laboratory system more rapidly than the group of pions formed in the lower star point. For this reason, the pions formed in the upper star point can be projected forward into system XYZ, while those formed in the lower star point go backward. If many pions originate in the upper star point and few in the lower, one can then understand the cause of forward angular asymmetry in system XYZ.

Study of angular correlations and distribution of effective masses. In order to determine the distribution of phonon events with respect to M within the interval $60° < \Phi < 120°$, shown by the dotted line in Figure 4a, the ordinates of the histograms plotted for stars with angles $\Phi < 60°$ and $\Phi > 120°$ were reduced by a factor of one-half on the assumption that the distribution of /71
M for phonon events does not depend on Φ, while the distribution of angles Φ is isotropic. Figure 4a shows a peak in the region of masses 2.9 GeV < M <

3.5 GeV. The number n_0 of cases in this region above the phonon curve can be evaluated from the formula

$$n_0 = n_1 - \frac{1}{2} n_2, \tag{13}$$

where n_1 is the number of π^-p-interactions with angle Φ within the interval $60° < \Phi < 120°$ and mass M in the range of 2.9 GeV < M < 3.5 GeV; and n_2 is the number of events with angle Φ outside the interval (60°, 120°) and mass M in the same range of 2.9 GeV < M < 3.5 GeV.

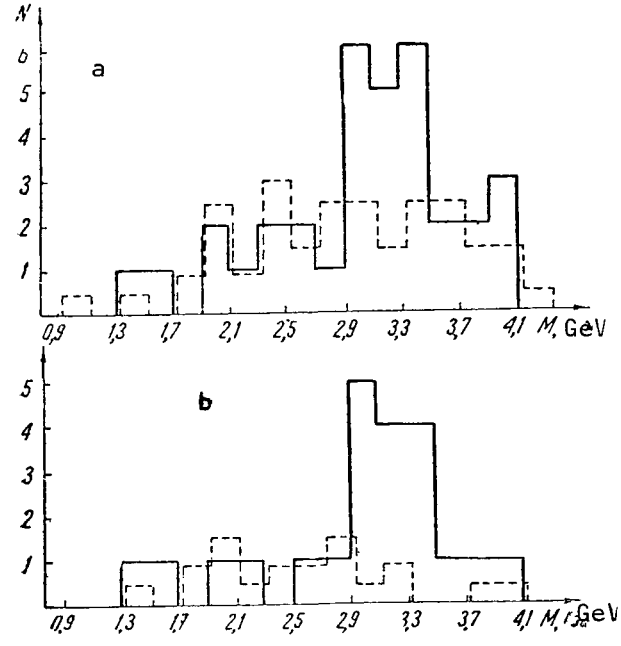

Figure 4. Distributions of Residual Effective Masses: (a) π^-p-interactions with angles Φ lying within the interval 60° < Φ<120°;--- π^-p-interactions with angles Φ lying outside the interval 60-120°; (b) π^-p-interactions having $\beta > 0$ and an angle within the interval 60°< Φ < 120°;--- π^-p-interactions having $\beta > 0$ and angle Φ outside the interval 60-120°. The number of cases in each interval of the broken-line histogram has been reduced to half.

Although $n_0 = 10.5 \pm 4.5$ differs from zero by more than two standard deviations, we do not consider the effect statistically reliable because the range of masses of 2.9 GeV < M < 3.5 GeV was marked after the histogram was plotted. /72

A strong argument in favor of the possible existence of resonance with a mass of 3.2 GeV is the fact that the azimuthal correlations observed for stars with angles Φ within the interval $60° < \Phi < 120°$ (row 3 in the table) are concentrated precisely in the mass range 2.9 GeV < M < 3.5 GeV (see rows 5 and 6 in the table). Actually, the value of $\overline{\beta}$ in row 5 differs from zero by more than 3 standard deviations, whereas in row 6 the value $\overline{\beta}$ is considerably less and differs from zero by 0.5 standard deviation. Also, for the stars of row 5, among which reactions (6) are assumed to predominate, the distribution of the cos Θ is symmetric ($\alpha_1 \approx 0$), but of an anisotropic nature ($\alpha_2 > 0$, while for the proposed phonon events of row 6 we observe forward asymmetry ($\alpha_1 > 0$) and isotropic distribution of $|\cos \Theta|$ ($\alpha_2 \approx 0$). Such was the distribution of Θ for the other group of phonon events (row 4) with angles Φ which lie within the interval (60°, 120°).

If one selects 16 events with $\beta > 0$ and a mass within the range 2.9 GeV < M < 3.5 GeV (row 7), among which reactions (6) are assumed to comprise a majority, the distribution of angles Φ is anisotropic, while the azimuthal angular distribution of secondary particles is symmetric ($\delta_1 \approx 0$), but anisotropic (δ_2 differs from zero by 4 standard deviations). On the other hand, for the phonon events considered in row 8, which have $\beta > 0$ but a mass M less than 2.9 GeV or more than 3.5 GeV, the distribution of Φ and the azimuthal angular distribution of the secondary shower particles are isotropic.

Figure 4b shows a notable decrease in the background in comparison with Figure 4a; however, the number of cases in the mass region 2.9 GeV < M < 3.5 GeV before deduction of the background is equal to $n_0 = 11.5 \pm 3.7$ and does not differ from the number of events in the peak of Figure 4a. This equality of the two values of n_0 is in agreement with the earlier assumption that all reactions (6) have $\beta > 0$ and angle Φ which lies within the interval $60° < \Phi < 120°$.

The value of n_0 obtained by us corresponds to a reaction (6) cross section equal to ~ 0.9 mb. Consideration of the possible collisions with quasi-free protons can reduce this cross section. We wish to note that the error in in the determination of M, which is related to errors in the measurements and the spread with respect to the momenta of the primary π^--mesons, amounts on /73
the average to 120 MeV for the mass range 2.9 GeV < M < 3.5 GeV. The great width of the peak in Figure 4b can be attributed to the true width of the resonance or to the influence of the internuclear motion of the quasi-free protons.

The proposed resonance should have an isotropic spin T equal to 1 or 2. When T = 1, the reaction

$$\pi^- + n \to p + 0 \qquad (14)$$

is prohibited, while when T = 2, its cross section exceeds 4 times the reaction (6) cross section. In order to determine T, we studied 41 $\pi^- n$-interactions with a slow recoil proton and a number of secondary shower particles $n_s = 4$ and 6. For the selection of $\pi^- n$-interactions, we used the criteria described at the start of the paper, with the exception of criterion (4). On the assumption that the proportion of reactions (14) among $\pi^- n$-reactions in the four times the corresponding fraction for $\pi^- p$-events, the expected number of reactions (14) is equal to 20. The observed number of $\pi^- n$-reactions in the mass range 2.9 GeV < M < 3.5 GeV before reduction of the background, which is $n_0 = 0 \pm 2.1$, contradicts the value T = 2 and is consistent with the assumption that T = 1. It is necessary to note, however, that consideration of the Fermi moments in the case of target neutrons can lead to an increase in n_0.

The conclusion of the existence of resonance with a mass of ~ 3.2 GeV can be made only on the basis of much experimental evidence which we do not possess. Our task is to point out its possible existence and to illustrate a procedure which can be useful in a study of high-pion resonances.

REFERENCES

1. Gramenitskiy, I. M., Preprint Joint Institute on Nuclear Research, Vol. 553, p. 15, 1960.
2. Fowler, P. H. and D. H. Perkins, *Phil. Mag.*, Vol. 46, p. 587, 1955.
3. Abduzhamilov, Sh., S. A. Azimov, L. P. Chernova, G. M. Chernov, and V. M. Chudakov, *ZhETF*, Vol. 45, p. 407, 1963.

STUDY OF COHERENT INELASTIC INTERACTIONS OF PIONS WITH AN ENERGY OF 17.2 BeV WITH HEAVY NUCLEI OF A PHOTOEMULSION

S. A. Azimov, Ye. B. Beter, U. G. Gulyamov,
N. B. Yeroshkina, and A. Ya. Levin

Among the inelastic interactions of high-energy particles with complex /74
atomic nuclei of matter, a special place is occupied by coherent inelastic processes in which the target nucleus receives a small momentum transfer and remains in the basic state. Some processes of such a type have been known for a long time: the elastic (diffraction) scattering, suppressed radiation, and direct generation of an electron pair in the Coulomb field of the nucleus.

The study of coherent inelastic interactions with the generation of pions started rather recently. The possibility of such reactions was pointed out for the first time by E. L. Feinberg and I. Ya. Pomeranchuk [1], and then by Good and Walker [2]. They proposed "diffraction" and "Coulomb" mechanisms for the process and they discussed the general characteristics and the different variations of the reactions. Afterwards, the problem was examined theoretically by other authors [3 - 10].

The diffraction and the Coulomb dissociation of the primary particle are described in a general form by the diagram shown in Figure 1. The composition of the cited secondary particles is explained by the fact that in the future we shall be interested in the coherent reaction

$$\pi^- + A \to \pi^- + \pi^+ + \pi^- + A'. \qquad (1)$$

The diffraction mechanism of the process should be characterized by the following:

(a) the characteristic quantum numbers of the primary particle should coincide with the quantum numbers that describe the group of secondary particles involved in the dissociation.

(b) the resultant momentum vector $\vec{p} = \sum_i \vec{p}_i$ of the group of secondary /75
particles into which the primary is dissociated should have the angular distribution of the primary particle, elastically scattered on the given nucleus. This circumstance leads to certain restrictions for the three-dimensional transfer components of the momentum $\vec{q}$; its distribution in the elastic diffraction scattering is given by the distribution of the perpendicular component $q_\perp$, while the longitudinal component is determined from the formula

$$q_{\parallel} = \frac{M_A + p_0}{2M_A \cdot p_0} \cdot q_{\perp}^2 + \frac{M^{*2} - \mu^2}{2p_0} + T', \tag{2}$$

which is easily obtained from kinematic considerations. Here, M_A and T' are the mass of the nucleus and the energy used to excite it slightly; p_0 and μ are the momentum and the mass of the primary π-meson; and M* is the invariant mass of all the secondary particles, with the exception of the recoil nucleus.

The distribution of $q_{\perp}$ for the coherent inelastic process on a nucleus radius R is given by the Belen'kiy formula

$$p(q_{\perp})\,dq_{\perp} = \frac{R^2}{2} \cdot q_{\perp} \cdot \exp\left[-\left(\frac{q_{\perp} \cdot R}{2}\right)^2\right] \cdot dq_{\perp}. \tag{3}$$

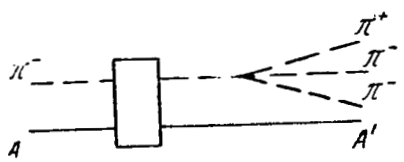

Figure 1.

In Equation (2), the main contribution (for a primary energy of $E_0 \approx 10$ BeV) is the term containing M^{*2}. The dependence of $q_{\parallel}$ on $q_{\perp}$ is very weak, and the distribution with respect to M* is closely related to the distribution with respect to $q_{\parallel}$.

The minimum value of $q_{\parallel}$ is given by the expression

$$q_{\parallel \min} = \frac{\left(\sum_i m_i\right)^2 - \mu^2}{2p_0}. \tag{4}$$

For a primary momentum p_0 = 17.2 BeV/c and three pions in the final state, $q_{\parallel\ \min}$ = 4.5 MeV/c.

A rough estimate of how small the transferred momentum must be in order for the interaction to remain coherent can be made on the basis of the principle of indeterminancy. In the case of a Coulomb dissociation, which comprises the exchange involving a virtual photon and the electromagnetic field of the

target nucleus, the transferred momentum should be localized beyond the limits /76
of the nucleus; and on this basis,

$$q \lesssim \mu \cdot A^{-1/3}. \tag{5}$$

Less rigid requirements are usually applied to the diffraction mechanism with a wide characteristic distribution of $q_\perp$; condition (5) for the longitudinal component is left in the form

$$q_\parallel \lesssim \mu \cdot A^{-1/3} \tag{6}$$

and the condition of the absence of nuclear breakdown is introduced as

$$q_\perp \lesssim \mu. \tag{7}$$

The bounds in (6) and (7), which comprise both mechanisms of the process, can (in lieu of better ones) be applied to the accurate selection of the coherent reaction cases.

In the system of secondary pions, resonance interactions are possible. Condition (6), together with Equation (2), gives an energy threshold $p_{0\ min}$ for the coherent process $\pi + A \to B + A'$ with the production of the boson particle or reson B:

$$p_{0\ min} = \frac{1}{2\mu} \cdot m_B^2 \cdot A^{1/3}. \tag{8}$$

In modern accelerators, the generation of bosons is kinematically possible only with a mass $m_B \lesssim 1.7$ BeV. At present, it has apparently been established reliably that reaction (1) involving ρ^0-resonance in the $\pi^+ \pi^-$ system (m = 763 MeV), which is of interest to us, does exist. With reference to the resonance in the $\pi^+ \pi^- \pi^-$ system, which was observed by some authors for M* = 1.08 BeV (see, for example, [11]), this issue remains open. It is quite possible that the presence of a peak in the distribution of M* in (1) can be explained from purely kinematic considerations.

The resonance ρ^0 also appears in the Ademollo-Chiuderi scheme [7], which is illustrated in Figure 2. The exchange π^--meson is now scattered elastically on the nucleus, and the authors establish the scattering cross section from the experiment. The cross section of the entire process on a carbon nucleus for a primary momentum of 18.1 BeV/c is found to be equal to 2.2 millibarns.

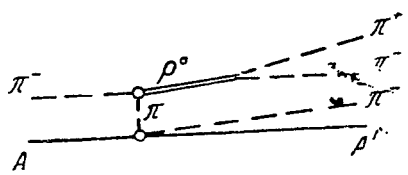

Figure 2.

Reference [12] was the beginning of the experimental study of coherent reaction (1). The authors examined 168 m of primary track in the pile of a nuclear photoemulsion irradiated by π^--mesons with a momentum of 14 BeV/c. Five cases of reaction (1) which satisfy conditions (6) and (7) were discovered. One of these cases satisfied the more strict condition (5). The bounds were established from the average nucleus of the emulsion. The value of $q_\perp$ was determined from direct momentum measurements, while $q_\parallel$ was evaluated from Equation (2). With reference to corrections, the lower bound for the free range of the interactions, which behaves in accordance with the Coulomb mechanism, amounted to 120 m. The authors could not, of course, make reliable conclusions regarding the dynamics of the process on the basis of such limited statistics, and the study was continued for this reason. Preliminary results (based on more complete statistics) were reported by the authors at the conference in Aix-en-Provence (1961), and final results were published in a recent paper [13]. /77

In three piles of an emulsion irradiated with π^--mesons having momenta of 14, 16.2, and 17 BeV/c, the study covered 972 m of the primary track. The authors showed that there is a considerable fraction of coherent interactions among the cases of the 0 + 3 type with the absence of explicit signs of breakdown or radioactive decomposition of the target nucleus. This conclusion can also be obtained without performing direct momentum measurements: the authors utilized the selection criteria proposed in [14] and based only on information derived from angular measurements. The bounds of the momentum transfer components were established from the carbon nucleus, and all nuclei of the emulsion were considered. The average free range for the selected cases was found to be about 51 m. An analysis of the distributions with respect to $q_\perp$ plus evaluations of the process of the cross section leads the authors to the conclusion that the increase of the cross section with atomic weight behaves in accordance to a law of the type $A^{2/3}$. The heavy nuclei of the emulsion should thus be responsible for the main contribution. The Coulomb mechanism of the process does not play an important role. For the 20 cases selected, the distribution of $q_\perp$ is in evident agreement with the assumption of the diffraction mechanism.

The study of the process by the method of nuclear photoemulsion is thoroughly considered by the two publications. Three other papers [11, 15, 16] deal with the study of the phenomenon in bubble chambers. In these papers, the existence of the process (its characteristics differ sharply from the characteristics of an ordinary inelastic process studied earlier by the same method) has been confirmed on the basis of extensive statistical data. A process cross section

has been obtained on light nuclei (strictly speaking, the upper cross section), /78
as well as an indication of the existence of A_1-resonance in the system of three pions. An attempt was made to determine the spin and parity of A_1-resonance (in the opinion of the authors of [11], most likely 1^+ or 2^-).

Here, it is necessary to point out the great difference in the procedures of the bubble chamber and the nuclear photoemulsion with respect to the important method of selection of coherent reaction cases. The bubble chamber, with its capability of automating the data processing and with its magnetic field for the identification and measurement of the secondary particle momenta, ensures the rapid accumulation of statistical data and a satisfactory classification. The bubble chambers presently in use also have a high efficiency of registration of secondary π^0-mesons ($\sim$ 75%). On the other hand, the bubble chamber is somewhat inferior in comparison with the photoemulsion. In the visual selection of coherent cases, it is necessary to establish the absence of the explicit excitation of the nucleus. A photoemulsion reliably registers short (down to 2 microns) particle vaporization and Auger electrons tracks, whereas the particles which have a range of less than 500 microns in the photoemulsion are not registered in the chamber. With reference to π^0-mesons, their fraction is very small in the "coherent" cases (i.e., in cases selected from angular criteria and which yield, within the limits of measurement errors, a small balance of momentum energy). Thus, the choice of the photoemulsion procedure for the study of coherent interactions is fully justified, despite its comparatively poor statistical data. The pile of the Ilford G = 5 nuclear photoemulsion (thickness - 600 microns) had 16 plates and was irradiated in CERN on October 17, 1961 by π^--mesons with a momentum of 17.2 $\pm$ 0.2 BeV/c. The investigation was conducted in accordance with an accelerated procedure proposed by M. I. Podgoretskiy (Joint Institute of Nuclear Research, Dubna). On the basis of the proposal to use the test material for several projects, and also for an effective control of the study, all interactions were recorded regardless of the number of black, gray, and relativistic rays. All relativistic tracks which agreed in angular spread ($\sim$ 5 Mrad) with the direction of a primary beam were examined. The examination was conducted with a magnification of 60 $\times$ 1 $\times$ 15; the entire plate length was divided into three observation strips according to the limited motion (7 cm) along the axis of the MBI-9 microscope.

In our project, 1760 m of primary track were used, and this length exceeds almost twice the observation length in [13]. The average free run of the in- /79
elastic interactions was found to be equal to 42.6 cm. The purpose of the project was to study reactions (1) on heavy nuclei of the photoemulsion, and the first problem facing us was that of the preliminary selection of the statistical data that could be supplemented with our cases of interest. The bounds of Equations (6) and (7) were established by us from the Br nucleus, and found to be

$$\left.\begin{aligned} q_{\parallel\,\max} &\cong 32\ M\ \text{eV/c} \\ q_{\perp\,\max} &\cong 140\ M\,\text{eV/c} \end{aligned}\right\}. \tag{9}$$

In 194 cases of the 0 + 3 type, the solid angles of the secondary particles were measured. The polar angle θ of the secondary particle with respect to the direction of the primary particle and its azimuthal angle ϕ with respect to the plane which passes through the primary track were determined from the expressions

$$\left.\begin{aligned} \tan\,\Theta &= \frac{\sqrt{a^2+b^2}}{c} \\ \tan\,\varphi &= \frac{a}{b} \end{aligned}\right\}, \tag{10}$$

where the projections a, b, c of the segment of the secondary track are obtained from measurements after correcting for the immersion angle of the primary track and the shrinkage coefficient of the plate. The information obtained only from the angular measurements can be utilized in the selection of "triplets" with a small momentum transfer. In principle, such a selection at the preliminary stage is more advantageous than the laborious selection on the basis of direct momentum measurements [14]. Also, the unavoidable coarseness in the momentum measurements (the typical error in the track chamber is of the order of 20%) only ensures a satisfactory evaluation of $q_\perp$ while the evaluation of the longitudinal component $q_\parallel$ is somewhat worse. The selection of "coherent triplets" should, in our opinion, be made in the order now described [17].

From the aggregate of cases of the 0 + 3 type, we discard the reactions in which the secondary relativistic ray is directed into the back hemisphere. We discard reactions in which there are explicit indications of nuclear excitation - slow electron, vaporization particle or lobe which occupies an area greater than 3-4 grains (1 ~ 2 microns) and not explained by the random imposition of background grains as well as of the primary and secondary tracks. The cases in which two secondary rays undergo a strong (visual) repeated Coulomb scattering, while remaining relativistic are discarded; such cases have a characteristic form and are easily referenced to the class of direct /80
generation by the pion of an electron pair in the field of the nucleus, after momentum and ionization measurements.

Further, in each case of interaction, there is the evaluation of the minimum $q_\parallel$, which is independent of the momenta of secondary charged particles and of the number of secondary neutral particles:

$$q_\parallel > \mu \cdot \sum_i^{\pm} \sin\Theta_i - \frac{m_0^2}{2p_0}, \tag{11}$$

where the summation is carried out with respect to charged secondary pions. The case in which the experimental evaluation $q_{\parallel\ min}$ is greater than the given $q_{\parallel\ max}$ should be discarded. Condition (11) reduces in our case to the requirement

$$\sum_i^{\pm} \sin\Theta_i < 0{,}24. \tag{12}$$

One can also derive an additional criterion similar to that proposed in [14], but more suitable for practical purposes.

The kinematics of reaction (1) are described by the system of equations

$$\left.\begin{aligned} A_1p_1 + A_2p_2 + A_3p_3 &= -x \\ B_1p_1 + B_2p_2 + B_3p_3 &= -y \\ p_1\cos\Theta_1 + p_2\cos\Theta_2 + p_3\cos\Theta_3 &= p_0 - q_1 \\ E_1 + E_2 + E_3 &= E_0 - T \end{aligned}\right\}, \tag{13}$$

where $A_i = \sin\Theta_i \cdot \sin\varphi_i$; $B_i = \sin\Theta_i \cos\varphi_i$; x and y represent the components of $q_\perp$; and T is the energy transferred to the target nucleus. By subtracting the third equation from the fourth and introducing the definitions

$$z = q_1 - T + \frac{m_0^2}{2p_0} - \sum_i t_i ,$$
$$t_i = E_i - p_i ,$$

we get the system

$$\left.\begin{aligned} \sum_i A_i p_i &= -x \\ \sum_i B_i p_i &= -y \\ \sum_i C_i p_i &= +z \end{aligned}\right\}. \tag{14}$$

In the limited cases that remained after the application of criterion (12), we have $C_i = 1 - \cos\Theta_i \approx \frac{1}{2}\sin^2\Theta_i$ with a greater accuracy. The values $\frac{m_0^2}{2p_0}$ and T in the equation for z can be disregarded. In our case, $E_0 - p_0$ = 0.6 MeV and when $q_{max}^2 \approx \mu^2$, we have $T < \frac{q_{max}^2}{2M_A}$ = 4.5 MeV for the average nucleus of the emulsion. If $\sum_i t_i \leqslant q_{\parallel max}$, the value of $q_{\parallel\ max}$ can be taken as

/81

the evaluation of the upper bound of $|z|$. The values of t_i rapidly decay to zero with increasing p_i; $t_{i\,max} = m_i$. All three secondary particles are relativistic: $p_i \geqslant m_i$. On the other hand, the approximate relation $\sum_i p_i \approx p_0$. should be satisfied. On this basis, if among the secondary particles there are two of low energy, then

$$\left(\sum_i t_i\right)_{cr} \approx 2\left[\left(p_{cr1}^2 + \mu^2\right)^{1/2} - p_{cr1}\right].$$

If there is only one such particle, then

$$\left(\sum_i t_i\right)_{cr} \approx \left(p_{cr2}^2 + \mu^2\right)^{1/2} - p_{cr2}.$$

Hence

$$p_{cr1} = \left(\mu^2 - \frac{1}{4} q_{\parallel\,max}^2\right) / q_{i\,max},$$
$$p_{cr2} = \left(\mu^2 - q_{i\,max}^2\right) / 2q_{i\,max} \qquad (15)$$

The criterion derived below is known to be inapplicable to those triplets where the momenta of two secondary particles lie in the region $(\mu \ldots p_{cr1})$ or the momentum of one is in the region $(\mu \ldots p_{cr2})$. These regions are small. For the value of $q_{\parallel\,max}$ used we have $p_{cr1} \approx 0.59$ BeV/c and $p_{cr2} \approx 0.28$ BeV/c. A consideration of the minimum value of $q_\parallel$, which exists in each interaction, makes these values even more limited; and when $q_{\parallel\,max} \geqslant 2(\sqrt{2}-1)\mu \approx 116$ MeV/c (≈ 58 MeV/c) in the second case, these are generally not present.

It is clear from phase considerations that the number of cases where the criterion is inapplicable is very small; in the special case of process selection in accordance with the Ademollo-Chiuderi scheme, where the pion which is quasi-scattering on the target nucleus, has a small energy, the aforesaid circumstance should have been examined in detail.

The solution of system (14) with respect to p_i leads to linear forms with respect to x, y, z: /82

$$\sum_i p_i \cos\Theta_i = \alpha x + \beta y + \gamma z; \tag{16}$$

where

$$\begin{aligned}
\alpha &= D^{-1} \cdot [(B_3C_2 - B_2C_3)\cos\Theta_1 + (B_1C_3 - B_3C_1)\cos\Theta_2 + \\
&\quad + (B_2C_1 - B_1C_2)\cos\Theta_3]; \\
\beta &= D^{-1} \cdot [(A_2C_3 - A_3C_2)\cos\Theta_1 + (A_3C_1 - A_1C_3) \times \\
&\quad \times \cos\Theta_2 + (A_1C_2 - A_2C_1)\cos\Theta_3]; \\
\gamma &= D^{-1} \cdot [(A_2B_3 - A_3B_2)\cos\Theta_1 + (A_3B_1 - A_1B_3) \times \\
&\quad \times \cos\Theta_2 + (A_1B_2 - A_2B_1)\cos\Theta_3]; \\
D &= C_1 \cdot (A_2B_3 - A_3B_2) + C_2(A_3B_1 - A_1B_3) + C_3(A_1B_2 - A_2B_1).
\end{aligned}$$

If it is taken into account that $x^2 + y^2 \leqslant q^2_{\perp\ \max}$ and $|z| \leqslant q_{\parallel\ \max}$, it is easy to evaluate the maximum modulus of Equation (16) on the basis of the Cauchy-Bunyakovskiy inequality

$$|\alpha x + \beta y + \gamma z| \leqslant (\alpha^2 + \beta^2)^{1/2} \cdot q_{\perp\,\max} + |\gamma| \cdot q_{\parallel\,\max}.$$

The case of an interaction in which

$$(\alpha^2 + \beta^2)^{1/2} \cdot q_{\perp\,\max} + |\gamma|\, q_{\parallel\,\max} < p_0 - q_{\parallel\,\max} \tag{17}$$

should be discarded. The criterion reduces to a calculation if the measured values of a_i, b_i, c_i are substituted according to the relations

$$\left.\begin{aligned}
A_i &= \frac{a_i}{\sqrt{a_i^2 + b_i^2 + c_i^2}} = \frac{a_i}{k_i}, \quad B_i = \frac{b_i}{k_i} \\
C_i &= \frac{1}{2} \cdot \frac{a_i^2 + b_i^2}{k_i^2}, \quad \cos\Theta_i = \frac{c_i}{k_i}
\end{aligned}\right\}. \tag{18}$$

Finally, in solving system (14) where $z = p_0 - q_{\parallel}$ and $C_i = \cos \theta_i$, it is not difficult to obtain the momentum ranges of the secondary particles evaluated by their measured departure angles:

$$\left.\begin{aligned} p_1 &= \frac{p_0 - q_{\parallel}}{D}(A_2B_3 - A_3B_2) \pm \frac{q_{\perp \max}}{|D|} \times \\ &\times \sqrt{(B_3C_2 - B_2C_3)^2 + (A_2C_3 - A_3C_2)^2}, \\ p_2 &= \frac{p_0 - q_{\parallel}}{D}(A_3B_1 - A_1B_3) \pm \frac{q_{\perp \max}}{|D|} \times \\ &\times \sqrt{(B_1C_3 - B_3C_1)^2 + (A_3C_1 - A_1C_3)^2}, \\ p_3 &= \frac{p_0 - q_{\parallel}}{D}(A_1B_2 - A_2B_1) \pm \frac{q_{\perp \max}}{|D|} \times \\ &\times \sqrt{(B_2C_1 - B_1C_2)^2 + (A_1C_2 - A_2C_1)^2}. \end{aligned}\right\} \quad (19)$$

The case in which the entire momentum range of any secondary particle is contained in the range of negative values should also be discarded because of the obvious presence therein of neutral particles. /83

By using visual criteria and condition (11), we selected 48 cases. Two successive applications reduced this number to 40. The errors in angular measurements were accounted for by applying the criteria to 2 or 3 independent measurements. The effective range for the selected cases is ~ 44 mm, which yields a value of 11.2 millibarns for the upper bound of the process cross section on heavy nuclei of the emulsion.

Ionization and momentum measurements were made on secondary tracks of the 40 cases. In order to measure the relative ionization on relativistic rays with an accuracy of ~2.5%, we employed the following procedure. In each plate, three depth zones in which 15 primary tracks were scattered uniformly were considered. On each of these, up to 3000 lobes were counted. From the lobe densitites indicated on the plot, the straight line of the gradient development of the plate was drawn by means of the least-squares method. The slope of this straight line was then used for "reducing" the densitites of the primary tracks to the average depth of the secondary track in the given zone of the plate. The secondary track (with the 3000 lobes counted thereon) was divided into segments by zones and plates. In each zone, three primary tracks were measured directly near the segment of the secondary track, from which $(B/B_0)_s$ was found. "Cross-correlation" of $(B/B_0)_s$ for all zones and plates was conducted with the proper statistical weights.

For momentum measurements, we selected a calibration procedure. As is well known, the measured second difference consists of the Coulomb error D_c, /84
table noise D_γ, counting noise, noise of the grains D_ε and that due to false scattering D_{ss}:

$$\overline{D}_{\mathrm{m}}^2 = \overline{D}_c^2 + \overline{D}_\gamma^2 + \overline{D}_\varepsilon^2 + \overline{D}_{ss}^2 = \overline{D}_c^2 + \overline{D}_n^2. \tag{20}$$

We made careful measurements on 1.2 m of the primary tracks on different cells (40 tracks of 3 cm each). The results of the measurements are given below:

t	100 μ	500 μ	1 mm	2 mm	4 mm
D_{m} (μ)	0.16040	0.19068	0.23331	0.36536	0.82256

In the calibration procedure, the total noise $\overline{D}_n$ was computed from the second difference for the secondary track $\overline{D}_{meas}$ determined for a given cell, and $\overline{D}_n$ was established from extensive statistical data for the same cell on the primary track:

$$\overline{D}_c^2 = \overline{D}^2_{\mathrm{m}} - \overline{D}_n^2. \tag{21}$$

The typical error of our momentum measurements amounted to 20%: on this track, it was calculated from the formula

$$\frac{\Delta D_c}{D_c} = \frac{0{,}756}{\sqrt{N}} \cdot \left(\frac{\overline{D}_{\mathrm{m}}}{\overline{D}_c}\right)^2. \tag{22}$$

The systematic momentum measurements conducted by us makes it possible to state certain conclusions about false scattering. Its dependence on the length t of the cell has yet to be established: it is either exponential with a small exponent, or linear. By disregarding D_γ (it is very small on good microscopes) and assuming that D_ε = const and D_{ss} = mt + c, then, as is quite obvious, by making measurements on four cells of multiplicity 1 : n_2 : n_3 : n_4, we may determine the momentum

$$p\beta = \left(\frac{Kt^{3/2}}{573}\right)_1 \cdot \left(\frac{m'}{u_1\overline{D}_4^2 + u_2\overline{D}_3^2 + u_3\overline{D}_2^2 + u_4\overline{D}_1^2}\right)^{1/2}, \tag{23}$$

where

$$u_1 = (n_3 - 1)(n_3 - n_2);$$
$$u_2 = -(n_3 - 1)(n_4 - n_2);$$
$$u_3 = \frac{n_3 \cdot n_4 (n_4 - n_3) + (n_3 - 1) n_3 - (n_4 - 1) \cdot n_4}{n_2 - 1};$$

$$u_4 = -\frac{(n_4 - n_3)(n_4 - n_2)(n_3 - n_2)}{n_2 - 1};$$
$$m' = u_1 \cdot n_4^3 + u_2 \cdot n_3^3 + u_3 \cdot n_2^3 + u_4.$$

Equation (23) should be applied for large statistical data (for example, a single-energy beam of unknown energy). In our case ($p\beta \approx 17.2$ BeV/c), Equation (23) gives values of 16.5 and 17.1 BeV/c for two different sets of cells. On the basis of data by other authors, we also became convinced of the good agreement when using the theoretical values of the beam momenta as determined from Equation (23). We believe that all this indicates the linearity of $D_{ss}(t)$.

Let us return to the results of a study of coherent reaction (1). It is seen from Equation (11) that the distribution of the cases in some classes of interactions with respect to $\sum_i \sin\Theta_i$ reflects the distribution of the momentum being transferred to the nucleus. Figure 3 shows the histograms:

(a) 76 "pure" interactions of the 0 + 3 type;

(b) 84 "dirty" interactions, i.e., those which have in the center a slow electron or a brief (2 microns $< l \lesssim$ 15 microns) track of the recoil particle; the dotted lines designate cases whose phonon conditions did not permit us to conduct a definite classification. The histogram does not include cases of direct generation of an electron pair by the pion in the field of the nucleus. The 1a and 1b distributions differ sharply from one another (the probability of agreement in accordance with the x^2-criterion is $p < 1\%$), whereas similar classes of interactions of the 0 + 2, 0 + 4, 0 + 5 type [13] are not in bad agreement with each other. This indicates the presence in the "pure triplets" class of a considerable individual group of cases with a small parallel momentum transfer.

In 24 of the 40 cases selected, $\sum_i p_{\perp i}^2$ exceeded 13 BeV/c; these cases yielded a balance of energy which is characteristic of coherent interactions, /86

within the limits of the measurement errors. Ionization data of their secondary tracks are shown in Figure 4. The theoretical curves were calculated based on Sternheimer [18] for I = 270 eV; T_0 = 10 KeV; B_{min}/B_0 = 0.905.

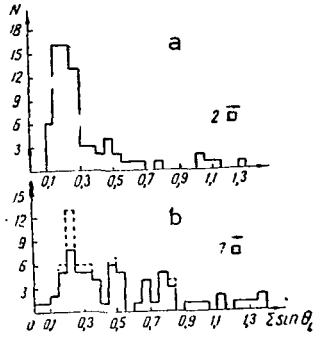

Figure 3.

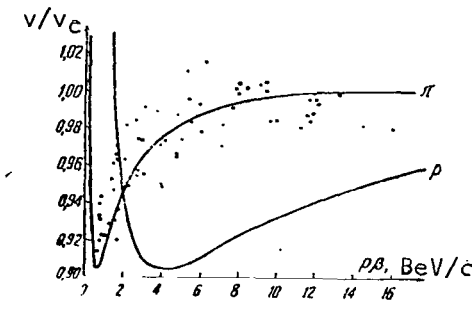

Figure 4.

Translator's Note: Commas represent decimal points.

The contamination of the 24 cases selected by reactions with formation of π^0-mesons should be very small. The fraction of "pure triplets" with $\sum_i E_i > 0.75 \cdot E_0$, $q_{\parallel} < 40$ MeV/c and with joined γ-quanta in the bubble chamber when the momentum of the primary pions is 18.1 BeV/c amounts only to 10% of the total number of such cases [16]. We have previously mentioned the non-equivalence of the registration of nuclear excitation by a bubble chamber and by a nuclear photoemulsion. In view of this discussion, the indicated fraction will only decrease in our case.

Figure 5 shows the results of a comparison of the magnitude of the parallel momentum transfer $\frac{q_{\parallel} - T}{\mu}$ with the minimum evaluation (11) (the straight line with the slope $\tan \alpha = 1.0$ corresponds to equality). These results indicate that the true value of $q_{\parallel}$ in most cases is much higher than the minimum value obtained from angular data alone. The distribution of the cases with respect to M* is shown in Figure 6.

Figure 7 shows the distribution of the 24 cases with respect to the transverse momentum transfer $q_{\perp}$ determined directly from momentum measurements. The average error in the determination of $q_{\perp}$ (corresponding to the standard deviation) amounted to 60 MeV/c. In the case of the diffraction mechanism of the coherent inelastic process, the experimental histogram should be compared with the distributions (3) corrected for the measurement error. For the Br nucleus:

$$p(q_{\perp})\, dq_{\perp} \sim q_{\perp} \cdot \exp\left[-(q_{\perp}/90)^2\right] dq_{\perp};$$

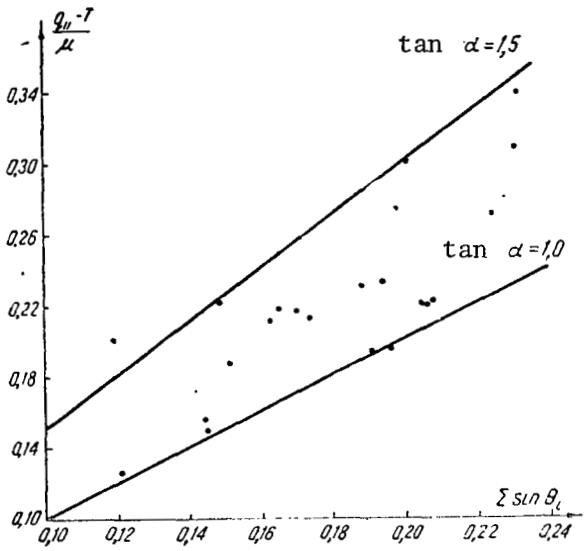

Figure 5

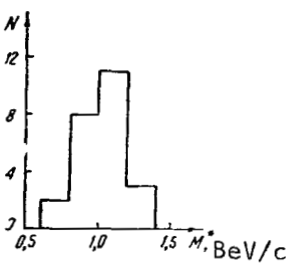

Figure 6

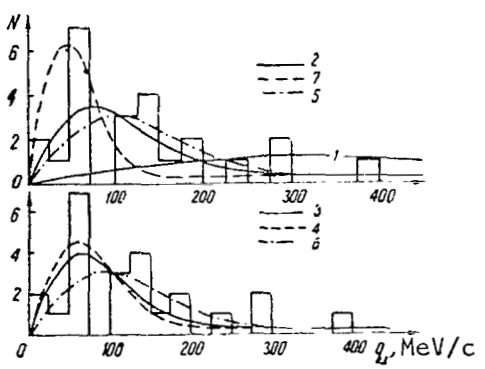

Figure 7

Translator's Note: Commas represent decimal points.

and there remains less than 1% of the cases of interest beyond the limits of 200 MeV/c. On this basis, four cases with $q_\perp$ > 200 MeV/c, shown in the histogram in Figure 7, can be considered noncoherent; and the distribution of $q_\perp$ /87 for these can be considered similar to the distribution of the transverse momenta of the recoil proton, which has been studied in a hydrogen bubble chamber for a primary π^--meson momentum of 16 BeV/c [19]. The background of the noncoherent cases among the remaining 20 can be evaluated from the ratio of 4 : 9 for the "dirty" triplets with $q_\perp$ < 200 MeV/c and $q_\perp$ > 200 MeV/c, which is given in [13]. Thus, the average number of cases which satisfy the requirements imposed for coherent reactions on heavy nuclei is found to be equal to (18.2 ± 4.7). This value, after correction for the 5% μ-meson impurity in the primary beam with which our pile was irradiated, leads to a free range of 92^{+32}_{-19} m, which gives a good evaluation for σ (Ag, Br) = (5.4 ± 1.4) millibarns.

The assumption of the dominant role of processes on heavy nuclei is confirmed by an analysis of the distribution with respect to $q_\perp$. The form of the resultant theoretical distributions depends on the diffraction characteristics of the nuclei which participate in the process, the law of the increase in the cross section with an increase in the atomic weight and the background of noncoherent interactions. Figure 7 shows the theoretical curves of the /88 following cases:

(1) where all 24 cases are incoherent, and then 6 of the 24 are incoherent and the other 18 are coherent on the nuclei:

(2) Ag, Br, C, N, O in equal parts;

(3) Ag, Br, C, N. O in accordance with the law of $A^{2/3}$;

(4) Ag and Br in accordance with the law of $A^{2/3}$;

(5) C only;

(6) C, N, O in accordance with the law of $A^{2/3}$.

Curve 7, which was drawn on the assumption that the true values of $q_\perp$ of 18 cases are much smaller than the experimental error of 60 MeV/c, corresponds to a certain degree to the Coulomb mechanism of the coherent process.

The theoretical distributions were compared with the histogram for the χ^2 -criterion in three intervals: (0 to 75 MeV/c), (75 to 150 MeV/c), (150 MeV/c and higher). Curve 1 (see Figure 7) notably contradicts the experiment ($p < 0.1\%$), while curves 2, 3, and 4 are in good agreement (40, 80 and 90%, respectively) and the available statistical data of these cases do not make it

possible to separate them. Curve 7 gives poor agreement (15%). The distributions of 5 and 6 also diverge from the histogram (3 and 6%). All this leads to the conclusion that the predominant contribution to the selected set of cases is made by the diffraction processes on heavy nuclei; besides, the Coulomb mechanism hardly plays a substantial role here.

A comparison of our evaluation of σ (Ag, Br) = (5.4 ± 1.4) millibarns with the evaluation of the carbon cross section ($1.7^{+0.6}_{-1.3}$) millibarns, which can be obtained from the data of a bubble chamber study [16], suggests that /89 the dependence of the cross section of the coherent inelastic diffraction process on the atomic weight of the target nucleus is of the $A^{1/3}$ or $A^{2/3}$ type. In any case, a dependence of the A^2 type is discarded with confidence [20]. The assumption of the dominant role of the nuclei, which was advanced earlier [2], is not confirmed by experiment either. The fact that the Coulomb mechanism of the process does not give a noticeable contribution also arises from our earlier evaluation of the cross section of this mechanism [21].

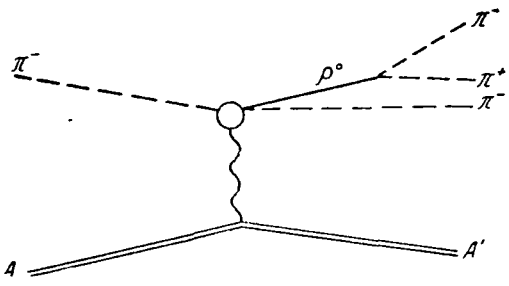

Figure 8.

The reaction model proposed by us takes into consideration the strong interaction in the final state. The diagram in Figure 8 contains a ρ^0-meson which is produced after exchange with a virtual photon and then decomposes into two oppositely charge pions. The reaction cross section can be related to the photoprocess cross section

$$\gamma + \pi^- \to \rho^0 + \pi^-. \qquad (24)$$

We evaluate the latter on the basis of the matrix element of the radiation-induced decomposition of the ρ^0-meson:

$$\rho^0 \to \pi^+ + \pi^- + \gamma. \qquad (25)$$

It is quite obvious that decomposition (25) includes strong interaction channels and its correct calculation with the available modern theory is impossible. We give the calculation according to the perturbation theory on the basis of the three diagrams in Figure 9 with a virtual nucleonic "loop", having assumed in this instance that the momenta of "external" particles are substantially less than the momenta and masses of the virtual particles; for this reason, we only take the first non-zero terms in the expansion of the

corresponding integrals with respect to external momenta. Since the mass of the ρ^0-meson is not small, such an approximation is rather rough; however, /90 these can be satisfied [22] for order approximation.

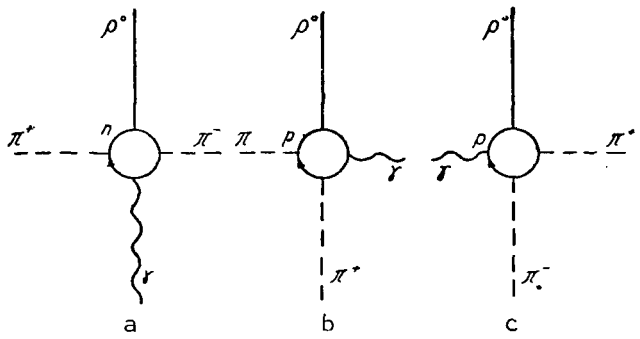

Figure 9.

The matrix element which corresponds, for example, to diagram a is equal to

$$m_a = (4\pi)^2 2g^2 G \sqrt{\alpha} \int Sp\, \gamma_5 \frac{1}{\hat{p}+\hat{k}_1-M} \gamma_3 \frac{1}{\hat{p}+\hat{k}_1+\hat{k}_2-M} \times$$
$$\times \gamma_5 \frac{1}{\hat{p}+\hat{k}_1+\hat{k}_2+\hat{k}_3-M} \gamma_\alpha \frac{1}{\hat{p}-M} \cdot \frac{d^4p}{(2\pi)^4} \varphi_{\pi^+} \varphi_{\pi^-} \varphi^\rho_\alpha \varphi^\gamma_\beta ,$$

where k_1, k_2, k_3 are four-momentum π^+, γ, and π^-, respectively; $\alpha = 1/137$; g and G are coupling constants of the pion and ρ-meson with the nucleon; and M is the nucleon mass.

In making the expansion and utilizing in four-dimensional integration the formula

$$\int \frac{f(p^2)\, d^4p}{(p^2-M^2)^{n+1}} = (-1)^n \pi^2 i \int_0^\infty \frac{x f(-x)}{(x+M^2)^n} dx,$$

we obtain, after several laborious calculations, the expression for the matrix element corresponding to the sum of the three diagrams:

$$m = -\frac{4\sqrt{\alpha}\, g^2 Gi}{3M^2}\left[3M^2(\varepsilon^\rho \varepsilon^\gamma) + 2(k_2 k^\rho)(\varepsilon^\rho \varepsilon^\gamma) - 2(k_2 \varepsilon^\rho)(k^\rho \varepsilon^\gamma)\right], \quad (26)$$

/91

since in the case of a real photon, $k_2^2 = 0$. Here, the four momentum of the ρ-meson is

$$k^\rho = k_1 + k_2 + k_3;$$

ε^ρ and ε^γ are the polarization vectors of the ρ-meson and photon. The probability of the decomposition is

$$w = \int \frac{1}{2m}\overline{|m|^2}\,(2\pi)^4\,\delta^4(k^\rho - k_1 - k_2 - k_3) \times \times \frac{d\vec{k}_1}{(2\pi)^3 \cdot 2E_1} \cdot \frac{d\vec{k}_2}{(2\pi)^3 \cdot 2E_2} \cdot \frac{d\vec{k}_3}{(2\pi)^3 \cdot 2E_3}.$$

Substituting (26), we get

$$w = \frac{\alpha g^4 G^2}{4(2\pi)^3}\, m\left[1 + 4\left(\frac{m}{3M}\right)^2 + 3\left(\frac{m}{3M}\right)^4\right] f, \quad (27)$$

where the coefficient $f \approx 0.51$ is determined by consideration of the masses of the π-mesons ($f \to 1$, when the pion mass $\mu \to 0$). When $g^2 = 14.5$ and $G^2 = 1.27$ [23] we have $w \approx 1.0$ MeV.

The photoprocess cross section (24), obtained by means of matrix element (26), (where $k^\rho = k_1 + k_2 - k_3$), can be written in the form

$$d\sigma_\rho(M^*) = \frac{\alpha g^4 G^2}{\pi} \cdot \frac{k_\rho}{M^* \cdot (M^{*2} - \mu^2)}\left\{3 + \frac{(M^{*2} - \mu^2)(M^{*2} + m^2 - \mu^2)}{M^2 M^{*2}} + \right.$$
$$\left. + \frac{(M^{*2} - \mu^2)^2 (M^{*2} + m^2 - \mu^2)^2}{18 M^4 M^{*4}} + \frac{(M^{*2} - \mu^2)^2 [M^{*2} - (m-\mu)^2]\,[M^{*2} - (m+\mu)^2]}{54 M^4 M^{*4}}\right\}, \quad (28)$$

where

$$k_\rho = \frac{[M^{*2} - (m-\mu)^2]^{1/2}[M^{*2} - (m+\mu)^2]^{1/2}}{2M^*}.$$

The differential reaction cross section of interest to us can be determined by the Weizsekker-Williams method in its covariant form [24]:

$$d\sigma_c = \frac{z^2\alpha}{\pi} \cdot \frac{dq^2}{(q^2)^2} \cdot \frac{dM^{*2}}{M^{*2}-\mu^2}\left[q^2 - \frac{(M^{*2}-\mu^2)^2}{4E_0^2} \right] \times \\ \times |F(q^2)|^2 d\sigma_p(M^*), \tag{29}$$

where q^2 is the invariant square of the momentum being transferred to the nucleus and E_0 is the energy of the primary π^--meson in the laboratory system. /92

The electrical nucleus factor F is taken by us in the functional form [25]:

$$F(q^2) = \frac{1}{1+q^2R^2/6}, \tag{30}$$

where R is the radius of the nucleus. In this case, the effective values of the transferred momentum satisfy $q \lesssim \frac{\sqrt{6}}{R}$, which for the lead nucleus (z = 82, A = 207) amounts to about 60 MeV/c and for the bromine nucleus (z = 35, A = 80), to about 80 MeV/c. These conditions are less strict than those which we should have taken in accordance with (5); for this reason, one should expect a certain increase in the reaction cross section.

Within the range of M* values 0.903 BeV $\leqslant$ M* $\leqslant$ 1.2 BeV, which will be effective in the integration, the expression in the braces in (28) is a weak function of M*:

$$d\sigma_p(M^*) \approx \frac{5\alpha g^4 G^2}{\pi} \cdot \frac{k_\rho}{M^* \cdot (M^{*2}-\mu^2)}. \tag{31}$$

Let us carry out the integration of (29), with consideration of (30) and (31), within the limits

$$\left(\frac{M^{*2}-\mu^2}{2E_0}\right)^2 \leqslant q^2 \leqslant 6/R^2,$$

$$(m+\mu)^2 \leqslant M^{*2} \leqslant \mu^2 + 2E_0\frac{\sqrt{6}}{R}.$$

Then, for the cross section of the coherent reaction

$$\pi^- + A \to \pi^- + \pi^+ + \pi^- + A'$$

on lead and bromine nuclei, we get the values

$$\sigma_c(\mathrm{Pb}) \approx 0.4 \text{ mbarn},$$
$$\sigma_c(\mathrm{Br}) \approx 0.2 \text{ mbarn},$$

which indicate insignificant role of the Coulomb mechanism of the process.

REFERENCES

1. Feinberg, E. L. and I. Ia. Pomeranchuck, *Suppl. Nuovo Cim.*, Vol. 3, p. 652, 1956.
2. Good, M. L. and W. D. Walker, *Phys. Rev.*, Vol. 120, pp. 1855, 1857, 1960.
3. Ferretti, B., *Nuovo Cim.*, Vol. 19, p. 193, 1961.
4. Drell, S. D., *Rev. Mod. Phys.*, Vol. 33, p. 458, 1961. /93
5. Matthews, P. T. and A. Salam, *Nuovo Cim.*, Vol. 21, p. 126, 1961.
6. Drell, S. D. and K. Hiida, *Phys. Rev. letters*, Vol. 7, p. 199, 1961.
7. Ademollo, M. and C. Chiuderi, *Nuovo Cim.*, Vol. 25, p. 1113, 1962.
8. Zhizhin, Ye. D. and Yu. P. Nikitin, *ZhEFT*, Vol. 43, p. 1731, 1962.
9. Berman, S. M. and S. D. Drell, *Phys. Rev. letters*, Vol. 11, p. 220, 1963.
10. Feinberg Ye. L. and D. S. Chernavskiy, *Uspekhi Fizicheskikh Nauk*, Vol. 82, No. 1, 1964.
11. Allard, J. F., et al., *Physics letters*, Vol. 12, p. 143, 1964.
12. Baldassare, F., et al., *Nuovo Cim.*, Vol. 21, p. 459, 1961.
13. Caforio, A., et al., *Nuovo Cim.*, Vol. 32, p. 1471, 1964.
14. Fisher, C. M., W. M. Gibson, A. Mason, W. A. Venus and D. Evans, *Nuovo Cim.*, Vol. 27, p. 761, 1963.
15. Huson, F. R. and W. B. Fretter, *Nuovo Cim.*, Vol. 33, p. 1, 1964.
16. Bellini, G., E. Fiorini, A. J. Herz, P. Negri and S. Ratti, *Nuovo Cim.*, Vol. 29, p. 896, 1963.
17. Azimov, S. A., Ye. V. Beter and U. G. Gulyamov, *Yadernaya fizika*, No. 1, p. 72, 1965.
18. Sternheimer, R. M., *Phys. Rev.*, Vol. 103, p. 511, 1956.
19. Goldsack, S. J., et al., *Nuovo Cim.*, Vol. 23, p. 941, 1962.
20. Castoldi, P. C., *Nuovo Cim.*, Vol. 34, p. 501, 1964.
21. Beter, Ye. V. and U. G. Gulyamov, *Izv. AN Uzbek SSR, seriya fiz.-mat.naum*, No. 1, p. 90, 1964.
22. Kobzarev, I. Yu and L. B. Okun', *ZhEFT*, Vol. 43, p. 1288, 1962.
23. Jackson, J. D. and H. Pilkuhn, *Nuovo Cim.*, Vol. 33, p. 906, 1964.
24. Pomeranchuck, I. Ia. and J. M. Shmushkevich, *Nucl. Phys.*, Vol. 23, p. 452, 1961.
25. Barmin, V. V., et al., *ZhEFT*, Vol. 43, p. 1223, 1962.

STUDY OF ANGULAR CORRELATIONS OF PARTICLES IN NUCLEAR DISINTEGRATIONS WITH FRAGMENTS

S. A. Azimov and R. Karimova

A study of the characteristics of nuclear disintegrations with fragments /94
($z \geqslant 3$) has led to the appearance of a number of fundamentally different hypotheses about the emission mechanism of fragments and of the disintegration of nuclei accompanied by the emission of fragments during the interaction of a fast particle with the target nucleus.

However, most researchers in recent years have only considered the more specific problem of the nature of the emission process of fragments in the observed disintegrations of nuclei. At the same time, studies are being made only of those characteristics (angular and energy distribution of fragments) which have a direct relationship to this process. This limited approach is apparently caused either by the complexity of the wider scope covered by a study of the various characteristics of all the products of the nuclear disintegrations and their correlations, or by an underestimation of the significance of the results of such a study, which are very useful for establishing the nature of the emission process of fragments and the other particles in these same disintegrations as well as of the interrelationship of these processes.

In order to solve the problem of the time relationship of the indicated processes, i.e., of the genetic relationship among the products of the nuclear disintegrations under study, the most promising, due to the effect of the law of conservation of momentum during the disintegration process, are the results of a study of the angular correlations among the disintegration products.

In the past, the following angular correlations have been observed:

(a) the predominance of an angle of divergence greater than 90° between the fragment and the residual nucleus [1, 2];

(b) a certain excess of protons and α-particles at angles of 90° with the fragments [3];

(c) the predominance of angles of divergence greater than 90° between /95
two fragments in one disintegration [3, 4];

(d) an excess of light particles at angles greater than 90° with the residual nuclei [3].

The effects (a) and (d) are natural and caused by the recoil of the residual nucleus during the emission of particles from the nucleus. On the basis of the angular correlation (b) of protons and α-particles with the fragments, as observed in [3], the hypothesis of the simultaneous irradiation of the test fragment and a certain part of light particles has been advanced. In order to coordinate the existence of angular correlation between two fragments in one disintegration with the hypothesis of the independent emission of these fragments, as advanced in [4], the authors of this paper assume that the fragments are emitted from opposite regions of the nucleus.

We present a study of the indicated angular correlations and their possible dependence on the energy and number of fragments in the disintegration.

Experimental Results

In this study, we used a nuclear emulsion of the P9-ch type which has an average sensitivity of 30-40 MeV with respect to protons, and which was irradiated with protons of 660 MeV on the synchrocyclotron at the Laboratory of Nuclear Processes, JINR[1]. An emulsion of this type satisfactorily discriminates among one-charge particles, two-charge particles and particles with $z \geqslant 4$ (fragments), which made it possible to perform a visual selection in the analysis of the disintegrations of nuclei. The accuracy of the visual determination of the nature of the particles was controlled by measurements of the density of Ag grains in the tracks using the scale method [5], and by photometric measurements of the width of the fragment tracks. The selection in the nuclear disintegrations of Ag and Br was made in accordance to the following criteria:

(a) a resultant charge of the particles greater than or equal to eight;

(b) the presence of a residual nucleus track;

(c) the absence of "sub-threshold" light particles in low-beam disintegrations without a visible residual nucleus track.

For the analysis, we selected cases of nuclear disintegration of Ag and Br with fragments, the run of which is $R_f \geqslant 15$ microns. For each track in the disintegrations under study, measurements were made of the angle in the plane of the emulsion between the projection of the particle track and the direction of the primary protons, the immersion angle of the track (with the exception of the residual nucleus track) and the run.

Table 1 contains some general characteristics of the disintegration of Ag and Br nuclei with respect to four disintegration groups under study in this work; for comparison, some data on disintegration without fragments are also presented.

We now quote some data on the anisotropy of the angular distribution of the fragments:

[1] JINR = Joint Institute for Nuclear Research (Dubna) -- Tr.

Type of disintegrations		N (0—90°)/N (90—180°)
$N_f=1$	R_f <80 microns	2.83±0.33
	R_f ≥80 microns	5.82±1.24
$N_f=2$	Both fragments with R_f < 80 microns	2.10±0.43
	One fragment with R_f < 80 microns	2.60±1.33
	The other fragment with $R_f \geqslant 80$ microns	6.20±3.88

/96

The experimental angular correlations of the light particles with the fragments were compared with the corresponding correlations calculated by the Monte Carlo method on the assumption of independent random emission of fragments and light particles which have nonisotropic angular distributions (Figure 1) in the laboratory system. As can be seem from Table 2, the degree of divergence of D_{max} for each pair of comparable distributions is always less than the corresponding critical value D_q of this magnitude for a significance level q = 5%, which indicates a sufficiently good agreement of the distributions. Hence, the observed angular correlation between the light particles and the fragment is a secondary effect relative to the correlation of all these particles with the direction of the primary protons in the laboratory system of coordinates.

In order to study the angular correlations of the light particles and fragments with residual nuclei, 437 and 109 disintegrations of Ag and Br nuclei were analyzed; they contained a visible track of the residual nucleus with a range $R \geqslant 1$ micron and one or two fragments with $z \geqslant 3$. This minimum range of the residual nucleus corresponds to a momentum of ~ 500 MeV/c. Such a value leads to the exclusion of about 32% of the disintegrations with a range of the residual nucleus R < 1 micron.

The range of the residual nucleus in the disintegrations under study is determined by the sum of the momentum acquired by the nucleus after the completion of the cascade stage of the disintegration ($\vec{P}_{cas}$), the recoil momentum from the fragment ($\vec{P}_f$), and the momentum acquired by the nucleus in the evaporation stage of the disintegration ($\vec{P}_{evap}$), if it is assumed that the disintegration of the nucleus takes place in accordance with the cascade evaporation scheme. In connection with this, it is of interest to study the influence of the recoil momentum of the fragment on the kinematic characteristics of the residual nuclei.

/97

Table 1

Type of disintegration		$\bar{n}_p$	$\bar{n}_\alpha$	$\bar{n}_p$ with $R_p \leq 100\ \mu$
$N_f = 1$	$R_f < 80\ \mu$	2,93±0,22	1,47±0,12	0,17±0,03
	$R_f \geqslant 80\ \mu$	2,80±0,26	1,19±0,13	0,15±0,04
$N_f = 2$	both fragments with $R_f < 80\ \mu$	3,34±0,47	2,05±0,32	0,20±0,06
	at least one fragment with $R_f \geqslant 80\ \mu$	3,20±0,68	1,53±0,37	0,09±0,05
$N_f = 3$		3,82±1,47	1,76±0,82	0,82±0,47
$N_f = 0$ (data by Ostroumov)		2,4	0,98	

Type of disintegration		$\bar{n}_\alpha$ with $R_\alpha < 50\ \mu$	$\bar{n}_p + \bar{n}_\alpha$	n_α / n_p
$N_f = 1$	$R_f < 80\ \mu$	0,25±0,03	4,40±0,34	0,50±0,03
	$R_f \geqslant 80\ \mu$	0,15±0,03	3,99±0,39	0,42±0,04
$N_f = 2$	both fragments with $R_f < 80\ \mu$	0,52±0,11	5,39±0,79	0,61±0,06
	at least one fragment with $R_f \geqslant 80\ \mu$	0,33±0,12	4,73±1,05	0,48±0,08
$N_f = 3$		0,67±0,36	5,60±2,20	0,46±0,15
$N_f = 0$ (data by Ostroumov)			3,38	0,4

Translator's Note: Commas represent decimal points.

Table 2

Type of disintegration	Protons		α-particles	
	D_{max}	$D_{5\%}$	D_{max}	$D_{5\%}$
$N_f = 1$, $R_f < 80\ \mu$	0,032	0,054	0,032	0,075
$N_f = 1$, $R_f \geqslant 80\ \mu$	0,020	0,068	0,031	0,102

From a comparison of the range distribution of the residual nuclei in disintegrations with and without a fragment (Figure 2), it is seen that the appearance of a fragment in the disintegration has a noticeable influence on the visible length of the residual nucleus track.,

/98

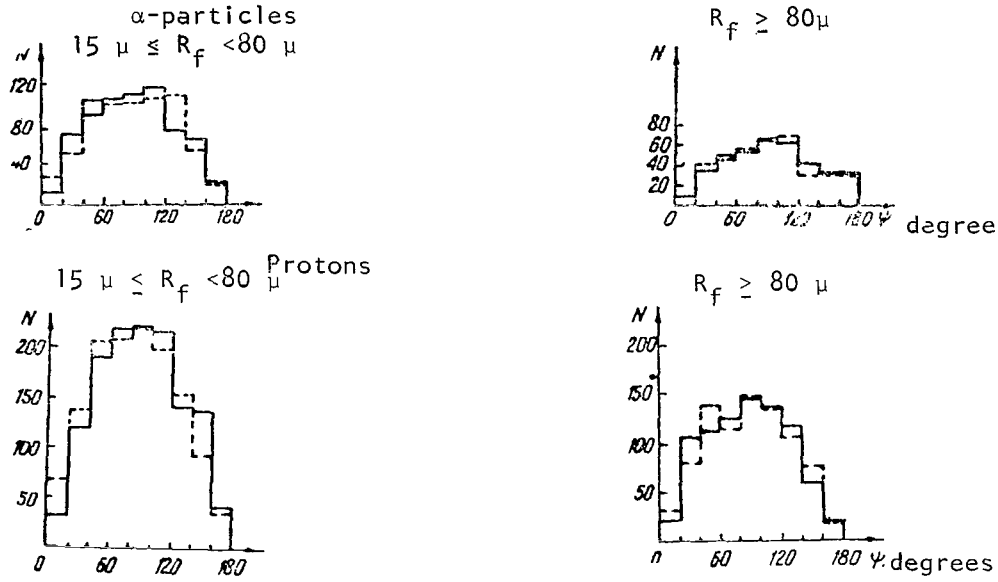

Figure 1. Angular Correlations of Light Particles with Fragments; Solid line - experimental; Broken line - theoretical.

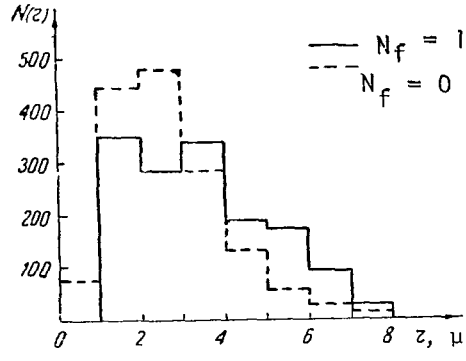

Figure 2. Range Distribution of Residual Nuclei.

/99

The range of the residual nucleus depends on the direction of the fragment emission; the average range of the residual nucleus is equal to (2.90 ± 0.20) microns and (3.40 ± 0.30) microns in the cases where the fragment is emitted at angles of 0-45° and 45-90°, respectively.

If one takes into consideration the aforesaid anisotropy of the angular distribution of the fragments and the angular correlation of the fragments with the residual nuclei (Figure 3), one should expect a distribution of the residual

nuclei (Figure 4). The anistropy of the angular distribution decreases approximately by a factor of two in passing from disintegrations with $N_f = 0$ to disintegrations containing one fragment, and it disappears in disintegrations with a fragment whose range is $R_f \geqslant 80$ microns (Figure 4a). The magnitude of the influence of the fragment departure angle on the angular distribution of the residual nuclei is illustrated in Figure 4c, which compares the angular distributions of the residual nuclei in disintegrations with fragments emitted at angles of 0-45 and 45-90°. The anisotropy of the angular distribution of the residual nuclei amounts to 0.98 ± 0.15 and 5.26 70 for disintegrations with fragments that fly into the forward and back hemispheres, respectively. /100

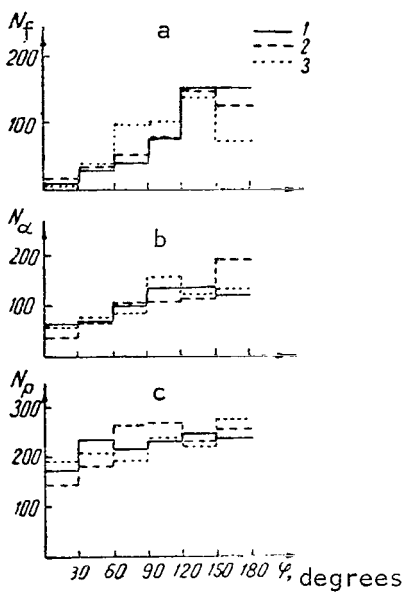

Figure 3. Angular Correlations of Fragments (a), α-particles (b), protons (c) with residual nuclei: 1 - disintegrations with $N_f = 1$, $R_f <$ 80 microns; 2 - $N_f = 1$, $R_f \geqslant 80$ microns; 3 - $N_f = 2$, $R_f < 80$ microns.

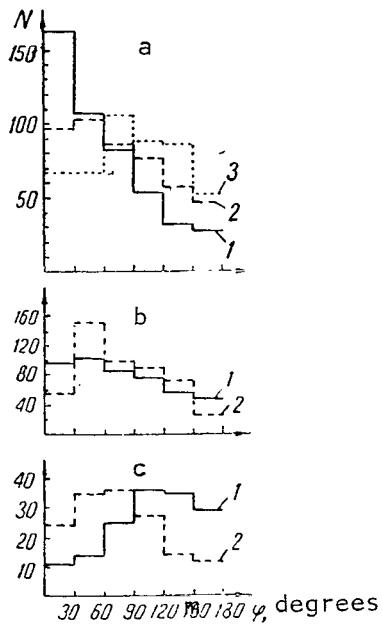

Figure 4. Angular Distributions of Residual Nuclei: a): 1 - $N_f = 0$; 2 - $N_f = 1$, $R_f < 80$ microns; 3 - $N_f = 1$, $R_f \geqslant 80$; b): 1 - $N_f = 1$; 2 - $N_f = 2$; c): 1 - fragments at angles of (0-45)°; 2 - at angles of (45-90)°.

The observed angular correlation of light particles with residual nuclei (see Figure 3), i.e., predominance of angles with residual nuclei greater than 90°, does not depend on the energy or the number of fragments emitted in one disintegration. The trend in the angular correlation does not depend on the forward or backward direction of motion of the residual nucleus with respect to the direction of the primary protons. The angular correlation becomes most

distinct for low-energy particles ($R_p \leqslant 100$ microns and $R_\alpha \leqslant 50$ microns). For comparison purposes, the backward/forward ratios are given for low-energy particles and for all particles relative to the residual nuclei:

Type of Particles	Low-energy Particles	All Particles
Protons	2.57 ± 0.08	1.20 ± 0.08
α- Particles	2.64 ± 0.12	1.80 ± 0.11

In order to study the angular correlations between the fragments, all the disintegrations with $N_f = 2$ were divided into two groups: (1) 125 disintegrations with two slow fragments ($E < 4$ MeV/nucleon) and (2) 55 disintegrations with one slow fragment and one fast fragment. The obvious angular correlation observed between the two slow fragments and the absence of such correlation between the slow and fast fragments (Figure 5) suggest that the two slow fragments are emitted simultaneously in one disintegration, while the fast and slow fragments are emitted at different times. The agreement of the angular correlations between fragments observed in this work with the corresponding correlations observed by A. P. Gorichev for a primary proton energy of 2-9 GeV (degree of divergence of the compared distributions $D_{max} = 0.060$ and $D_{max} = 0.224$ is less than the corresponding critical values for a 5% significance level of the values $D_{5\%} = 0.140$ and $D_{5\%} = 0.244$) indicates the absence of a dependence of these correlations on the energy of the falling protons. /101

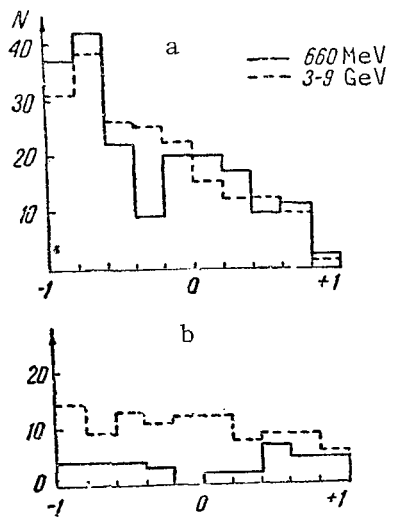

Figure 5. Angular Correlations Between Two Fragments in One Disintegration: (a) both slow ($R_f < 80$ microns); (b) at least one fast ($R_f \geqslant 80$ microns)

Discussion of Results

The absence of angular correlation between the light particles and the fragment in the center-of-mass system indicates that the emission processes of light particles and of fragments are not simultaneous in most cases. Hence, it seems that the models based on the assumption of a simultaneous occurrence of these processes (the model of an instantaneous nuclear breakdown, the model of the decomposition of a larger excited fragment, etc.) are not valid.

Taking into account the absence of the indicated correlation, its independence of the energy of the fragment, and the fact that among the fragments with z = 4-- 9 only 10% are not resistant to α-decomposition [6], it can be concluded that the fragments with z = 4-- 9 formed during disintegrations of Ag and Br nuclei have in most cases an almost constant p/d ratio and do not have an excitation energy during emission from the nucleus. It is possible, however, that some fraction of light particles is emitted in one process with the fragments [3].

The study has shown that the emission of fragments in a disintegration, (their number, energy, and direction of emission) strongly influences the characteristics (mainly the angular distribution) of the residual nuclei. The obvious angular correlation (of the type backward/forward > 1) of the light particles with the observed residual nuclei does not depend, however, on the indicated factors and is similar to that observed in disintegrations without fragments [7]. The general trend in the angular correlation is preserved in passing from disintegrations with a residual nucleus in the front hemisphere /102
to disintegrations with a residual nucleus in the back hemisphere.

On the basis of the previous comments, it can be concluded that the light particles correlate specifically with the observed track of the residual nucleus formed after the emission of the fragment, i.e., the emission of the fragment precedes the emission of the light particles. Otherwise, the angular correlation between the light particles and the residual nucleus, which is expected on the basis of the data in [7], would be disturbed as a result of the strong influence of the fragment momentum on the angular distribution of the residual nuclei.

In connection with this, it was of interest to study the energy spectra of light particles in disintegrations with fragments, and to compare these with the energy spectra of the same particles in disintegrations without fragments. If it is assumed that the average excitation energy in the test disintegrations is equal to 150 MeV [3], and also that the evaporation of light particles precedes the emission of the fragment, then the energy spectrum, in particular that of α-particles, should agree with the spectrum of α-particles from ordinary disintegrations ($N_f = 0$) in which the nuclei have the same excitation energy.

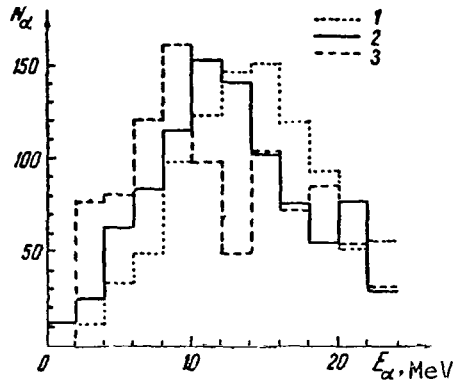

Figure 6. Energy Spectra of α-particles: 1 - disintegration with $N_f = 0$; 2 - with $N_f = 1$; 3 - with $N_f = 2$.

Figure 6 shows for comparison the energy spectra of α-particles for disintegrations with $N_f = 1$ and $N_f = 2$, and the energy spectrum (taken from [8]) for disintegrations without fragments - with the number of evaporated particles greater than or equal to eight, which corresponds to an excitation energy of the nucleus of 150-200 MeV. There is a noticeable tendency to a gradual smoothing of the spectrum with an increasing number of fragments emitted in one disintegration. The observed increase in the fraction of the low-energy α-particles can be established from a decrease of the potential barrier of the evaporating nucleus or from an increase in the velocity of motion of the residual nucleus. It is difficult to indicate the extent of the influence of each of these two factors; however, it can be assumed that both are caused by the preceding emission of fragments. /103

Thus, on the basis of a qualitative analysis of the experimental data, it can be concluded that the emission of fragments from the nucleus precedes the evaporation of light particles.

In order to verify this assumption, we considered the evaluation of the angular correlations of the particles with the residual nucleus in disintegrations of the Ag and Br nuclei for an energy of the primary protons of 660 MeV, in accordance with the model obtained from an analysis of the experimental data: the disintegration of the nucleus is accomplished in accordance with the cascade evaporation scheme and the fragment emission takes place prior to the evaporation of the light particles.

We calculated approximately 1,000 cases for both the disintegrations of Ag and Br nuclei by the Monte Carlo method on a computer.

The initial values of the parameters (charge, mass number, velocity, angle with direction of primary protons) used in the calculation of the evaporation stage of the disintegration of the nucleus were determined by a selection with respect to the number of cascade protons, velocities, and angles of residual nuclei from the distributions obtained after calculation of the cascade stage of disintegration of the Ag and Br nuclei for an energy of the primary protons of 660 MeV, which was contributed by O. V. Lozhin. The initial excitation energy was developed in accordance with the experimental distribution of events

with respect to the number of rays, recalculated as the distribution with respect to the excitation energies by means of the curve of the number of rays in the star as a function of the excitation energy for the Ag nucleus [9]. This made it possible to assume a probability of fragment emission equal to unity and thus save computer time. It was assumed in each disintegration calculated that a fragment is emitted with average parameters $\bar{z} = 4.5$ and $\bar{A} = 10$. The density level parameter in the case of fragment emission was set equal to $a = A/20$ in the calculation [9]; in the case of emission of light particles we used $a = A/10$. It was assumed that $r_0 = 1.5 \times 10^{-13}$ cm. The /104
Coulomb barrier is determined from the formula [10]

$$V_{\text{eff}} = k \frac{V_0}{1 + \frac{U_{\text{pos}}}{1000}},$$

where the permeability coefficient k was set equal to 0.7 for the protons, 0.6 for α-particles and 0.5 for fragments on the basis of the possibility of the existence of an intensified permeability for complex particles [11] and the experimental fact of a low potential barrier ($V_{\text{eff}} = 0.3\ V_0$) for α-particles and Li [12].

The energy of the evaporating particle in the center-of-mass system was determined in accordance to the well-known distribution function

$$\int_V^E \frac{E - V}{T^2} \exp - \frac{E - V}{T} dE = n f_{\max},$$

where n is a pseudorandom number uniformly distributed in the segment {0,1} and the magnitude $f_{\max}$ is obtained as a result of the integration of the integral in the left-hand side where the upper bound of the integral set is $E = \infty$ in the general case. The particle emission angle was determined on the assumption of an isotropic emission in the center-of-mass system. It was assumed that after evaporation of the fragment there exists successive evaporation of the light particles (z = 1 and z = 2). At each stage of the evaporation cascade, for the corresponding set of parameters of the residual nucleus (z, A, cos α and v), the concurrence of the particles n, p, d, t, He^3, and He^4 was calculated in accordance with [9]. The values of the bond energy of these particles in the nucleus were taken from the Gizeng tables [13]. The calculation of disintegration of the nucleus was made up to an excitation energy of about 10 MeV. The resulting values of the energies and angles of all the particles in the center-of-mass system were converted to the laboratory system of coordinates. The velocity and direction of motion of the residual nucleus

at each evaporation stage were recalculated with consideration of the recoil momentum from the particle being evaporated. The block diagram of the calculation is shown below.

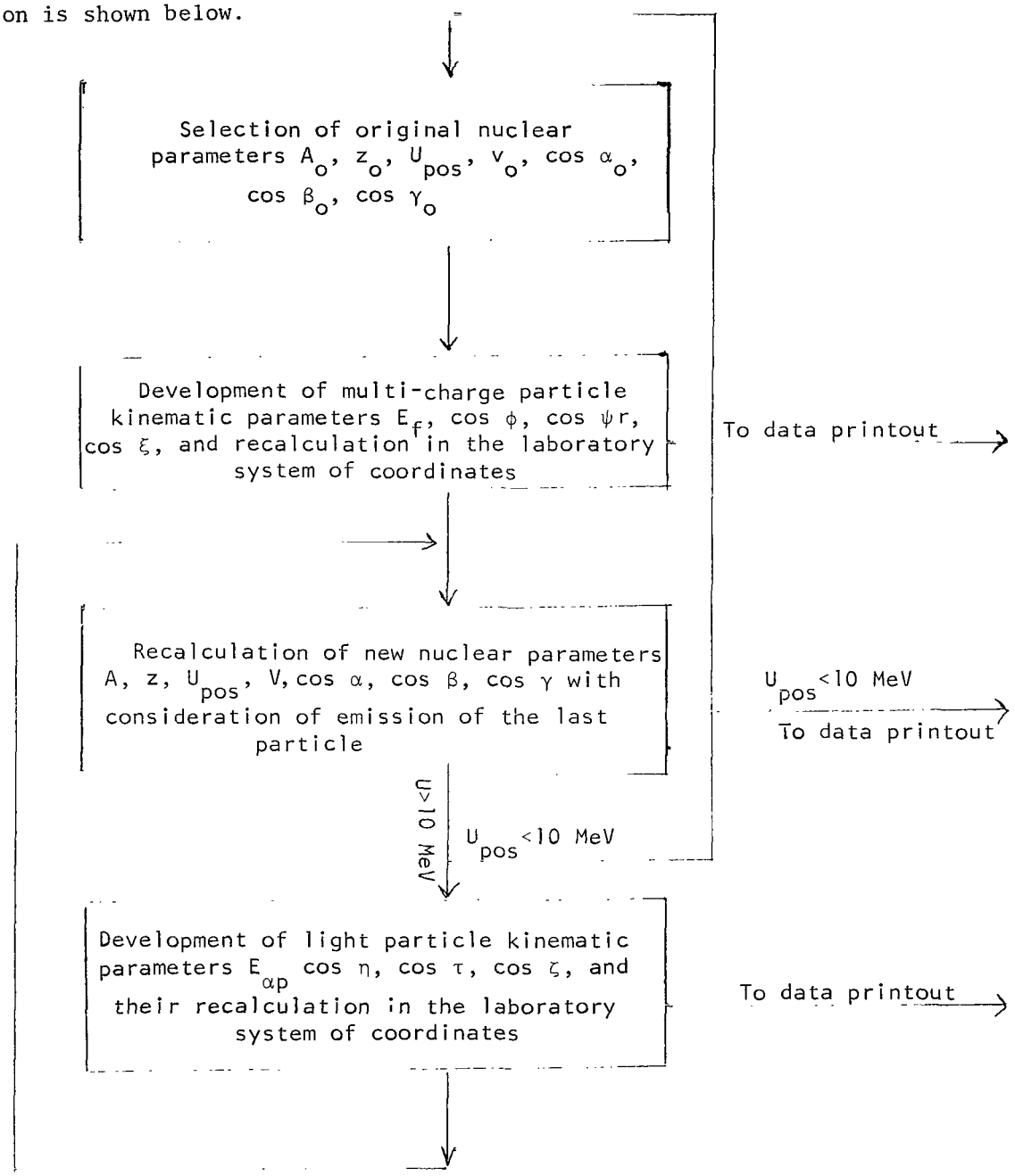
Selection of original nuclear parameters A_o, z_o, U_{pos}, v_o, cos α_o, cos β_o, cos γ_o
Development of multi-charge particle kinematic parameters E_f, cos ϕ, cos ψr, cos ζ, and recalculation in the laboratory system of coordinates
To data printout
Recalculation of new nuclear parameters A, z, U_{pos}, V, cos α, cos β, cos γ with consideration of emission of the last particle
U_{pos}<10 MeV
To data printout
U>10 MeV
U_{pos}<10 MeV
Development of light particle kinematic parameters $E_{\alpha p}$ cos η, cos τ, cos ζ, and their recalculation in the laboratory system of coordinates
To data printout

Block diagram of the calculation of the evaporation stage in the disintergration of Ag and Br nuclei by the Monte Carlo method carried out by computer.

As a result of the calculation, the following results were obtained:

(1) angular distributions of fragments and particles with z = 1 and z = 2, and of residual nuclei;

(2) angular correlations of fragments and particles with z = 1 and z = 2 with residual nuclei;

(3) energy spectra of the disintegration products in the laboratory system of coordinates.

From the point of view of the time relationship of the fragment emission and the emission process of the remaining light particles, and consequently of the validity of the model used in the calculation, it is obvious that the results of the calculation of the angular correlations of the light particles with the residual nuclei are of considerable importance. The sufficiently good agreement of the experimental and calculated angular correlations of the fragments and light particles with residual nuclei (Figure 7), which can be seen from the values of the experimental and calculated backward/forward ratios given below, suggests that the model used in the calculation is valid: /106

Type of Particle	Experiment	Calculation
Multi-charge particle	4.66 ± 0.16	3.77 ± 0.10
α-particle	1.64 ± 0.11	1.72 ± 0.09
Protons	1.17 ± 0.08	1.26 ± 0.06

A comparison of the experimental and calculated values of the anisotropy of the angular distributions (forward/backward ratio) of the protons and α-particles with respect to the primary protons shown below, and of the energy spectra, in particular that of α-particles (Figure 8), suggests that the average values of the velocities of the initial nuclei used in the calculation are reduced: /107

Type of Particle	Experiment	Calculation
Multi-charge	2.43 ± 0.13	1.10 ± 0.08
α-particles	1.24 ± 0.10	1.06 ± 0.06
Protons	1.34 ± 0.07	1.15 ± 0.05
Residual nuclei	1.59 ± 0.03	1.82 ± 0.08

An additional study of the angular correlations between two slow fragments (E < 4 MeV/nucleon) and between two fragments with a different energy, from the point of view of the sequence of emission of fragments with a different energy from the nucleus has shown:

(1) a sufficiently good agreement of the distributions with respect to ranges ($D_{max} = 0.032 < D_{5\%} = 0.081$) and of the angular distributions ($D_{max} = 0.098 < D_{5\%} = 0.231$) of fast fragments from the disintegrations with $N_f = 1$ and with $N_f = 2$.

(2) a disagreement of these characteristics for slow fragments from the same groups of disintegrations.

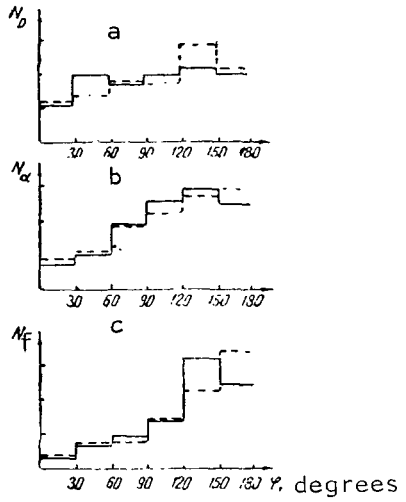

Figure 7. Angular Correlations of Protons (a) α-particles (b) and fragments (c) with residual nuclei; solid line -- experiment, broken line -- calculation.

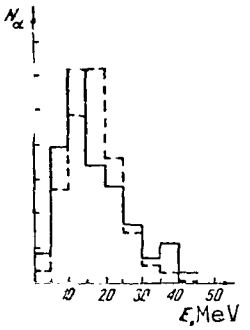

Figure 8. Energy Spectra of α-particles; solid line -- experiment, broken line -- calculation.

The latter points out the independence of the kinematic characteristics of a fast fragment and the dependence of the same characteristics for a slow fragment on the emission of a second fragment in the same disintegration, which makes it possible to conclude that a fast fragment ($E \geqslant 4$ MeV/nucleon) is emitted at an earlier stage in the nucleus disintegration than a slow fragment ($E <$ MeV/nucleon).

Conclusions

1. The process of fragment emission and the process of emission of the remaining (light) particles are not related by one common time instant.

2. Fragment emission precedes the evaporation of light particles.

3. Two slow fragments (E < 4 MeV per nucleon) are more frequently emitted simultaneously.

4. Fast fragments (E $\geqslant$ 4 MeV/nucleon) are emitted at an earlier stage of nucleus disintegration than slow fragments (E < 4 MeV/nucleon).

REFERENCES

1. Lozhkin, V. and N. A. Perfilov, *ZhETF*, Vol. 31, p. 913, 1956.
2. Gorichev, P. A., O. V. Lozhkin and N. A. Perfilov, *ZhETF*, Vol. 45, p. 1784, 1963.
3. Lozhkin, O. V. Author's abstract of Candidate Dissertation, *GPB Press, Leningrad*, 1957.
4. Goritchev, P. A. and W. F. Darovskikh, et al, *Phys. Rev.*, Vol. 126, p. 2196, 1962.
5. Rimskiy-Korsakov, A. A. and O. V. Lozhkin, *PTE*, Vol. 5, No. 20, 1960.
6. Perfilov, N. A. and N. S. Ivanova, et al, *ZhETF*, Vol. 38, p. 345, 1960.
7. Baker, E. W., S. Katcoff and C. P. Baker, *Phys. Rev.*, Vol. 117, p. 1352, 1960.
8. Vaganov, P. A. and V. I. Ostroumov, *ZhETF*, Vol. 33, p. 1133, 1957.
9. Dostrovsky, J., R. Bivins and P. Rabinowitz, *Phys. Rev.*, Vol. 111, p. 1659, 1958.
10. Katcoff, S., *Phys. Rev.*, Vol. 114, p. 905, 1959.
11. Zakher'ev, B. N. and S. N. Sokolov, *Preprint P-1473 LTF, Dubna*, 1963.
12. Burte, E. G. and Gangulim, et al., *Nuovo Cimento*, Vol. 36, No. 3, 1965.
13. Hoyzington, D. B., *Osnovy Yadernoy Tekhniki*, [Fundamentals of Nuclear Engineering], Gosatomizdat, Moscow, 1961.

GAS-DISCHARGE TUBES WITH A LARGE EFFECTIVE AREA

S. A. Azimov, E. S. Bakhromi, Yu. D. Bogachkin,
Kh. Zainutdinov, and R. Karimov

During recent years, some new type of detectors of charged particles /109
have come into use in experiments with high-energy particles in cosmic rays. These include gas-discharge tubes (flash tubes) or, as they are still called, Conversi tubes [1, 2].

Gas-discharge tubes are relatively inexpensive detectors of ionizing particles with a sufficently high efficiency of registration and a large effective area. It is sufficient to say that their length can be reduced to 200 cm with a diameter of 2 cm. This last fact plays a decisive role in the selection of gas-discharge tubes as detectors in the experimental study of cosmic rays on large areas, since by arranging them in several intersecting layers, it is possible to record the tracks of ionizing particles on large areas with a sufficiently good spatial resolution.

This paper describes the methods of synthesizing gas-discharge tubes and their characteristics.

Principle of Operation of Gas-Discharge Tubes and Factors That Influence the Effectiveness of Registration of Ionizing Particles.

A gas-discharge tube is made of vacuum glass. After exhaustion of the air, it is filled with neon and placed between two parallel metallic electrode plates. The tube gives a flash if a high-voltage pulse is applied to the electrodes directly after the passage of an ionizing particle through the gas.

A characteristic of gas-discharge tubes is the fact that during the /110
registration of a particle, the entire volume of the tube glows and not just the region where the particle has passed, but also where an electron avalanche is formed under the action of the applied electric field. This phenomenon can be explained by photon ionization and excitation of the atoms of the whole gas in the tube by those photons, which were formed during the electron avalanche in the place where the particle passed.

The magnitude of the pulse potential applied to the plates is selected to be much smaller than that which can cause breakdown in the gas and flash, independent of the passage of the ionizing particle. Thus, false discharges of the tubes are excluded.

Usually, gas-discharge tubes have several crossing layers and the ends of the flashed tubes photograph, which makes it possible to determine the track of a particle.

Let us analyze from a qualitative viewpoint the factors that influence the efficiency of registration of gas-discharge tubes.

During the passage of a charged particle, the gas in the tube ionizes. It is natural that the high-voltage pulse is applied to the electrodes with a certain delay with respect to the instance of passage of the particle. Let us examine how this delay will affect the efficiency of registration by the tubes. During the delay of the high-voltage pulse, there is diffusion of the electrons from the region of passage of the particle over the volume of the tube with the simultaneous recombination of ion-electron pairs. The number of ion-electron pairs remaining after the recombination will be [3]:

$$n_1 = n_0 (1 - \rho_e \tau_d), \tag{1}$$

where ρ_e is the recombination coefficient and τ_d is the delay time of the pulse.

If N particles begin motion when t = 0, then their density (n in 1 cm^{-3}) at a distance r and time t for spherical diffusion is [4]:

$$n = \frac{N}{(4\pi D t)^{3/2}} \cdot e^{r^2/4Dt}, \tag{2}$$

where D is the diffusion coefficient for ions, given by

$$D^+ = \frac{1}{3} \lambda_i v_r^+ \tag{3}$$

and for electrons, /111

$$D = \frac{1}{3} \lambda_e \cdot v_r, \tag{4}$$

where λ and v_r are the length of the free path and the avalanche speed, respectively. In our case, $t = \tau_d$.

It is seen from Equation (2) that the delay time should be decreased in order to obtain the best conditions for the formation of an electron avalanche in the gas in the region of passage of the particle.

The recombination coefficient ρ_e in Equation (1) increases in inert gases with increasing gas density $\rho_e \sim \sqrt{P}$ (P is gas pressure) when $T < 300^0$K [3].

Since the cross section of a gas-discharge tube is circular, the number of ion-electron pairs which were formed and moved during the pulse delay-time on the walls, will vary depending on the place of passage of the particle, i.e., the effective registration will be a function of the coordinates of the place of passage of the ionizing particle. It is obvious that the best conditions orginate during the passage of a particle in the center of the gas-discharge tube.

After the passage of the particle, not only diffusion and recombination of the ion-electron pairs is observed but also (in some gases) the electrons adhere to the atoms and molecules of the gas with the formation of heavy negative ions. This effect is particularly distinct in oxygen and hydrogen and is absent in inert gases. In connection with this, it is necessary to ensure as high a vacuum as possible prior to filling the tubes with neon.

Let us examine the ionization of a gas in a uniform electric field. If primary electrons and ions originate in the gas placed in an electric field due to an external ionization source, then these primary charges form new ions and electrons while moving under the action of the electric field to the corresponding electrodes and colliding on their way with gas molecules. Thus, there can be a repeated multiplication of the primary electrons.

The number of dn ion pairs formed by a cloud of n electrons moving with avalanche speed and passing through the distance dx in the direction of the uniform electric field X can be described by the Townsend coefficent α [4]:

$$dn = n\alpha\, dx.$$

The value of α depends on the potential of the field X, the gas pressure P, and the type of gas. It is convenient to utilize the normalized magnitudes /112 of the Townsend coefficient and of the potential of the electric field α/P and X/P. Ionization in an electric field can be described by means of the coefficient η, which is equal to the number of ion pairs created by an electron passing through a potential difference of 1 v. Then,

$$\eta = \frac{\alpha}{X}, \qquad (6)$$

and $1/\eta$ is the average energy (in volts) spent by the electron in the formation of one pair of ions.

The dependence of the ionization coefficient on the normalized field X/P for different gases is given in Figure 1 [4]. For gas-discharge tubes the parameter X/P is usually of the order of 10 v $\cdot$ $cm^{-1}\cdot(mm\ Hg)^{-1}$. For small values of X/P, the ionization coefficient in neon has a greater magnitude in comparison with the other inert gases and particularly with air, (excluding helium, for which the characteristics are not given completely).

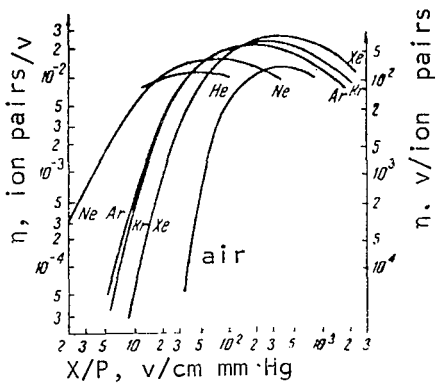

Figure 1. Dependence of the Ionization Coefficient η on the Normalized Field X/P.

The ionization of the gas molecules by positive ions plays a substantial role only at very low pressure (free paths occur at high pressures) and large values of the electric fields. It is also necessary to take into account the secondary processes which are of great significance in the ionization of a gas. Such is the emission of electrons from the cathode under bombardment with ions, photons, or fast neutral atoms which form during recharging. For small values of X/P and for small average energies of the electrons, the photoelectric effect predominates because there are more excitation events than ionizing collisions.

Photo-ionization may or may not lead to breakdown. If the photons are /113
strongly absorbed in the gas, then they create almost the same number of ion pairs as in the initial ionization and this effect shows up only as an increase in the coefficient α. But if the absorption is small, then the photons will depart from this space or they will get onto the cathode. Thus, photo-ionization is only an important secondary process in certain gases or mixtures, and for certain values of the electric field and pressure (particularly at high pressures).

The influence of the parameters of a high-voltage pulse on the efficiency of tubes shows up in the following manner.

The drift of the electrons starts from the moment the high-voltage pulse is applied. If the field increases slowly with time, then the electrons will reach the walls before their speed becomes sufficiently high for the ionization of the gas and the formation of an avalanche. Consequently, the efficiency of the tubes falls with decreasing curvature of the forward front of the pulse [5].

From simple physical considerations, it is clear how the magnitude of the electric field should change, depending on the different factors, with references to a gas breakdown in the place of passage of the ionizing particle. The larger the distance between the electrodes (i.e., the larger the diameter of the tube), the smaller the field needed for the formation of a discharge because in this case there is a great probability that the electron will cause ionization until it strikes the walls.

The gas pressure in the tube exerts the following influence. At a high pressure, the electrons receive a small amount of energy along the length of the free run and lose it in elastic collisions. With rising pressure, there is a decrease in the energy acquired along the length of each average free run. Consequently, in order to maintain the speed of ionization, the field intensity should increase approximately proportional to $1/\lambda_e$, i.e., to the pressure.

With decreasing pressure, the ignition potential will decrease to a certain value that depends on the distance between the electrodes. It can happen that, with decreasing pressure, the electron will undergo very few ionizing collisions prior to departure onto the walls. A further decrease in pressure will require a larger field for the formation of a discharge.

On the other hand, a decrease in pressure and in magnitude of the electric field will reduce the light output, which is also very important. /114

It was assumed earlier that the rate of increase of ionization in the gas is equal to about zero. However, when the potential is applied in the form of short pulses, the breakdown can take place only if the density of the ions and of the electrons increases so rapidly that the discharge is formed during the action of the applied pulse.

One usually speaks about the statistical delay time of a discharge τ_s and about the development (formation) time of a discharge τ_f [3, 4]. The magnitude of the statistical delay time depends on the initial ionization and on the magnitude of the field. The larger the initial ionization and the potential, the smaller τ_s. The development time of a discharge also decreases with an increase in the applied potential. Thus, the sum of the statistical delay and the formation delay of a discharge should be less than the duration of a pulse.

Procedure.

Production of tubes. We used molybdenum glass of the ZS-5 type, prewashed with water and aviation gasoline, as the tube material. One side of the tube, intended for photographing, was made into a blank plane, while the other end of the tube was soldered to a vacuum unit for exhaustion and filling; the unit was provided with a forevacuum pump of the VN-461 type and an oil-vapor pump. During the exhaustion, the tube was degassed three times (uniform heating of the tubes with a gas burner). The residual air pressure in the tubes was reduced to 2×10^{-4} mm Hg, and then the tubes were filled with neon to the necessary pressure and sealed.

Our purpose was to develop a tube of low cost and of good registration efficiency so that it would be sufficiently simple for mass production. For this reason, technical neon, which is much less expensive than spectrally pure neon, was used as the filler.

The literature [2] indicates that the addition of 10^{-2}% argon to spectrally pure neon raises the efficiency of the tubes only slightly while a large addition even decreases it. Since we used technical neon which has small impurities of argon and other gases, we did not use a special argon additive. The tubes were filled to a pressure that did not exceed atmospheric, /115 because the sealing of the tubes presents serious technical difficulties for a greater pressure.

Experimental unit. The block diagram of the experimental unit is shown in Figure 2. Cosmic rays were used as the source of ionizing radiations. The intensity of the cosmic radiation depends on the solid angle with the vertical axis and is determined by the relationship

$$I = I_0 \cos^2 \varphi.$$

Therefore in order to increase the speed of selection of statistical data, the gas discharge tubes were installed in a vertical plane with Geiger counters. The pulses from the Geiger counter were fed to the twofold coincidence circuit. A standard "Yablonya"-type unit was used as a coincidence circuit. The separated coincidence pulses were fed to the generator of high-voltage pulses, which developed the required high-voltage pulse to be fed to the electrodes.

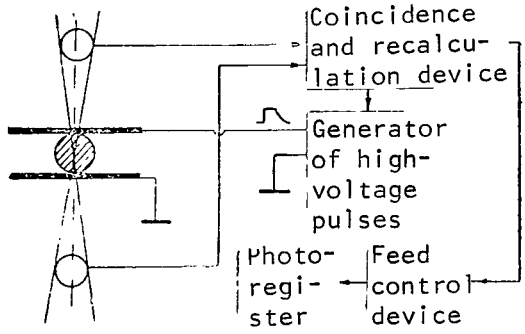

Figure 2. Block Diagram of the Experimental Unit.

The flash in the tube was photographed by a photo register with a normally open lens. Control of the photo register was accomplished by a standard control device of the photo register feed. The control pulse was fed from the coincidence circuit to this device.

From knowledge of the total number of separated coincidences and the number of ignitions of the tube, it is possible to calculate its efficiency. The correction for random coincidences was not taken into account and on this basis the resulting efficiency was somewhat lower. The resolution time of the coincidence circuit was 10^{-6} sec.

In order to develop a pulsed electric field on the electrodes, it was /116 necessary to design a generator circuit that produces a rectangular pulse with controlled duration and amplitude.

High-voltage pulse generator. A high-voltage rectangular pulse is formed by a generator stage in the following manner [6]. Two thyratrons are connected in the circuit shown in Figure 3. The first starting pulse triggers thyratron V_1 and its cathode potential sharply increases to the magnitude E_a. The second pulse triggers thyratron V_2 after a time interval equal to the required duration of the pulse at the output of the generator; the capacitance C is rapidly discharged through the active thyratrons, after which they are cut off.

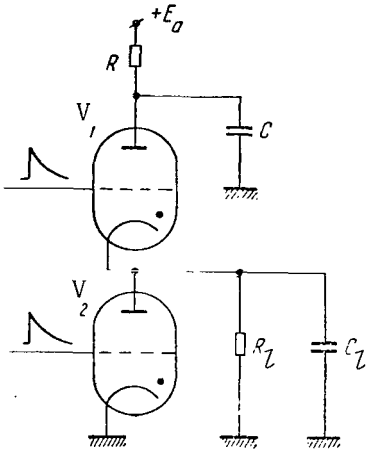

Figure 3.

The basic circuit of the generator is shown in Figure 4. The first circuit stage (tube V_1) is a pulse distributor from which pulses are fed to the ignition channels of the main (V_4) and the cutoff (V_7) thyratrons. In the channel of the cutoff thyratron, the pulse should be delayed for a time equal to the required duration of the pulse at the output of the generator. The delay is accomplished in the following manner. The pulse from V_5 moves to the integrating ladder network R_{25} + C_{10}, the time constant of which is regulated by the potentiometer R_{25}. The amplitude and duration of the forward wavefront moving onto the integrating ladder network can be regulated by the potentiometer R_{24}. The pulse with a moderate-slope wavefront, which results after integration, is fed to the grid of the thyratron V_6. The pulse delay will be determined by how fast the potential on the network of the thyratron V_6 reaches the trigger potential. Thus, by regulating the pulse at the generator output by means of potentiometers R_{24} and R_{25}, it is possible to obtain pulses with a duration that varies from fractions to 30 microsec.

Upon triggering of thyratron V_4, a positive voltage step takes place on the anode of the thyratron V_7; it appears on the grid through the interelectrode capacitance and can cause premature triggering of thyratron V_7. If this is not /117 to occur, the thyratron grid should be shunted by large capacitance C_{12} and

small resistance R_{29}. The resistance R_{14} of the type PE-75-500 ohms limits the step of the grid current of the thyratron V_4 during its triggering.

The generator develops single rectangular pulses (a maximum repetition frequency of 0.5 Hz) with an amplitude of 5-25 kv. The forward wavefront of the pulse is of the order of 0.1 μsec and the back wavefront is about ~0.4 μsec. The oscillogram of the pulse at the generator output is shown in Figure 5. The delay time of the high-voltage pulse with respect to the pulse fed to the generator input is about ~0.8 μsec.

Experimental results and discussion. Gas-discharge tubes 80-cm long with an external diameter of 1.8 cm and a wall thickness of the order of 1.2 mm were made from type ZS-5 glass and tested. The tubes are light-sensitive. They are also ignited by being excited by a flash caused by the passage of a particle in a nearby tube. Consequently, in using Conversi tubes, it is necessary to mutually insulate them lengthwise. Good results are obtained even by one layer of black wrapping paper (for low field intensities of the order of 6 kv/cm). In [7], the tubes are optically insulated by nitrocellulose lacquer. /118

The dependence of the registration efficiency of the tubes as a function of the applied field is shown in Figure 6 with the residual air pressure as a curve parameter. For tubes whose characteristics correspond to curves 1 and 2, degassing was not performed. It is seen that the residual air pressure in the tubes should be decreased in order to get a high registration efficiency, and also to insure that the beginning of the plateau of the curve is shifted toward higher field intensities when the residual pressures are high. These correlations are in good qualitative agreement with the studies of other authors [2].

Figure 7 shows the dependence of the registration efficiency on the high-voltage pulse τ_{pulse} (curve 2), which we recorded, as well as the analogous correlation taken from [7], for smaller values of τ_{pulse} (curve 1). It can be concluded that for a pulse duration greater than 3 μsec the efficiency of the tubes essentially does not depend on the pulse duration. For pulse durations smaller than 3 μsec the registration efficiency decreases, in accordance with the theoretical prerequisites examined at the start of the paper. /119

The curves of efficiency as a function of the applied field (Figure 8, curves 3, 4) were compared with analogous curves obtained in [5] (curve 1) and [2] (curve 2). The filling and delay times were used as parameters. Curve 2 corresponds to the degree of efficiency of a layer in the tubes [2]. According to our data, a decrease in the neon pressure in the tubes and a decrease in the delay time shifts the curve toward smaller values of field intensity and increases somewhat the efficiency. For the given parameters of the pulse and a delay time τ_d = 1.5 μsec, the optimum value of the neon pressure in the tubes is 63 mm Hg, which is in agreement with the results in [7].

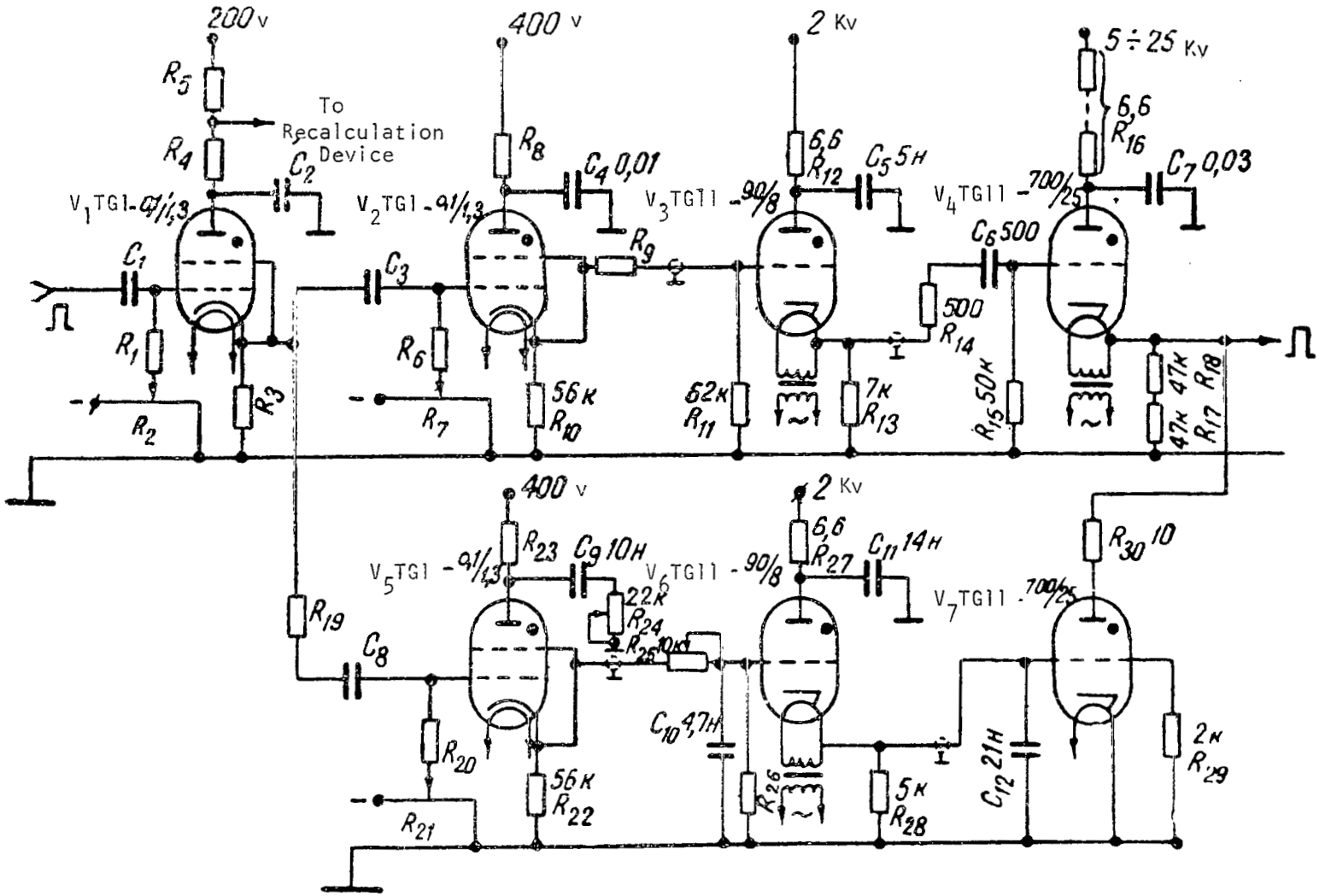

Figure 4. Basic Circuit of High-Voltage Pulse Generator.

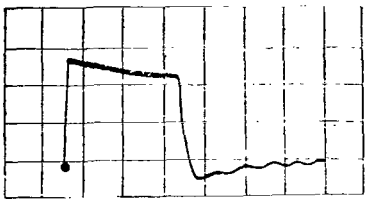

Figure 5. Oscillogram of a High-Voltage Pulse at the Generator Output. The Pulse Amplitude of 18 kv. Each Large Division is 2.5 μsec.

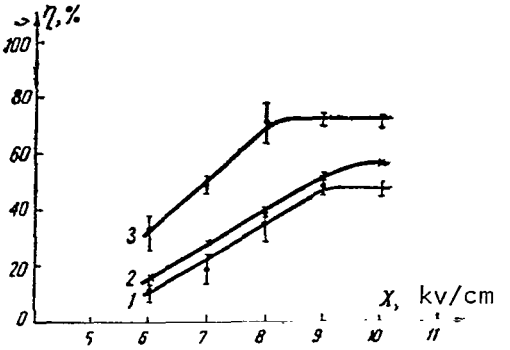

Figure 6. Dependence of Registration Efficiency of Tubes on the Residual Air Pressure: 1: 1.3×10^{-2} mm Hg; 2: 10^{-3}; 3: $2 \cdot 10^{-4}$ mm Hg; Filling - 730 mm Hg, Pulse Duration τ_{pulse} = 5 μsec, Pulse Delay Time τ_D = 2.5 μsec.

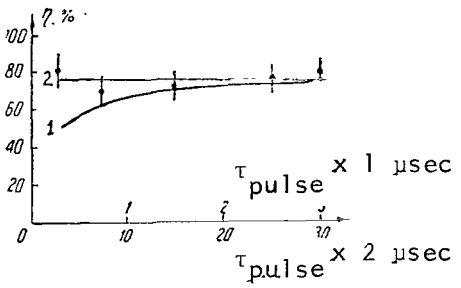

Figure 7. Dependence of Registration Efficiency on Pulse Duration: 1 - filling 630 mm Hg [7]; 2 - filling 630 mm Hg, field 4.5 kv/cm, pulse delay 1.5 μsec, residual air pressure 2×10^{-4} mm Hg.

In certain tubes with a neon pressure of 73 cm Hg, and under a relatively large residual air pressure and considerable field intensities (8-9 kv/cm), false ignitions were observed. With increasing pulse duration, the percentage of false ignitions increased somewhat. In tubes whose efficiency corresponds to curve 4, false ignitions were not observed within the cited range of field intensities.

In conclusion, it should be pointed out that we prepared tubes with the same diameter and glass thickness, but 160 cm in length. Preliminary data make it possible to state that for the aforesaid pressure and pulse parameters, the efficiency of the tubes does not depend on their length.

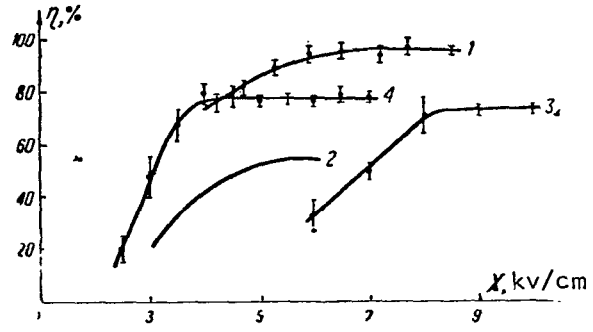

Figure 8. Dependence of Registration Efficiency of the Tubes on the Applied Field: 1 - filling - 2.3 atm, pulse delay τ_d = 3.4 μsec, pulse duration τ_{pulse} = 3.5 μsec 2 - filling = 66.5 mm Neon with addition of 0.17 mm Ar; τ_D = 3 - 6 μsec, τ_{pulse} = 3 μsec [2]; 3 - filling 730 mm Hg, τpulse = 5 μsec, τ_d = 2.5 μsec; 4 - filling 630 mm Hg, τ_{pulse} = 3 μsec, τ_d = 1.5 μsec.

REFERENCES

1. Conversi, M. and A. Gozzini, *Nuo. Cim.*, Vol. 2, p. 189, 1955.
2. Gardener, M., S. Kisdnasamy, E. Rossle, and A. W. Wolfendale, *Proc. Phys. Soc.*, Vol. 70, No. 7, p. 687, 1957.
3. Engel', A., *Ionizovannyye Gazy*, [Ionized Gases], Fizmatgiz Press, Moscow, 1959.
4. Frensis, A., *Ionizatsionnyye Yavleniya V Gazakh*, [Ionization Phenomena in Gases], Atomizdat Press, Moscow, 1964.
5. Rochester, Dzh., *Turdy Mezhdunaroonoy Konferentsii Po Kozmicheskim Lucham*, [Trans. International Conference on Cosmic Rays], Vol. 2, p. 331, 1960.
6. Finogenov, K. G., *PTE*, No. 4, p. 184, 1963.
7. Bonchak, B., R. Firkovski, Ye. Yatchak and A. Zavadski, *Nukleonika*, No. 9, p. 417, 1964.

ENERGY TRANSFER TO AN ELECTRON-PHOTON COMPONENT DURING THE INTERACTION OF PARTICLES WITH GRAPHITE NUCLEI

S. A. Azimov and Yu. V. Polyak

In order to determine the fraction of energy transferred to secondary particles of different types, it is first necessary to identify these particles and this is rather difficult when operating at energies of more than 10^{11} ev. /121

The method proposed by N. L. Grigorov and his coworkers [1] for measuring the energy of a primary particle from the resultant energy liberation in a thick layer of matter (the ionization calorimetric method) has made it possible to determine the energy of a primary particle with good accuracy (about 30% for an individual case). However, the identification of all secondary particles and the measurement of their energies is not possible in all cases. Unlike charged π-mesons, which contribute to the development of nuclear avalanches, π°-mesons transfer their energy to the electron-photon component in decomposing into γ-quanta.

At the present time, we do not know of any processes (except the decomposition of π°-mesons) which could make a substantial contribution to the formation of an electron-photon component during the nuclear interaction, or immediately after it. For this reason, one evaluates the energy of π°-mesons by the energy of the electromagnetic avalanches, and the average energy transferred to all π-mesons by the principle of charge independence.

In order to separate an electron-photon component, lead filters are commonly used and the development of the electromagnetic shower therein is tracked. Such selection is governed by the fact that the magnitude of the radiation per unit length (in g/cm^2) decreases with increasing atomic number, while the range for the interaction of nuclear active λ_{63} particles increases. At the same time. there is a decrease in the probability of secondary nuclear interactions and, consequently, of distortion of the electromagnetic avalanche.

The energy of the electron-photon component is measured by the number of particles at the maximum development of the avalanche [2, 3] or in the entire avalanche [4]. At the same time, it is necessary to take into account the absolute values of such parameters as the proportionality coefficient between the number of particles in the maximum avalanche and the energy of the electron-photon avalanche, the correction for the transient detector -- substance effect of ionization, the total ionization caused by the electron-nuclear shower, etc. For this reason, it is of interest to determine $\overline{K}_{\gamma}^{C}$ in the experiments, where these factors do not have any effect on the measurements. /122

Let us examine the liberation of energy to the electron-photon component in a layer of matter of thickness X_0 and resulting from primary nuclear-active particles with an average energy of E_0 and from second generation nuclear-active particles which originated as a result of the interaction of primary particles in the layer located above X_0. The average energy of these particles per interaction of a primary particle will be $(1-\bar{K}_\gamma^C)E_0$, since $\bar{K}_\gamma^C E_0$ is the energy transferred to the electron-photon component and, consequently, does not participate in the development of the nuclear avalanche.

If it is assumed in both cases that the energy liberated to the electron-photon component is proportional to the energy of the nuclear-active particles

$$\bar{E}_\gamma = \alpha \bar{E}_{na} \tag{1}$$

then, for primary particles,

$$(\bar{E}_\gamma)' = \alpha \bar{E}_0, \tag{2}$$

and for second generation particles,

$$(\bar{E}_\gamma)'' = \alpha(1-\bar{K}_\gamma^C)\bar{E}_0. \tag{3}$$

If in (3), however, α is larger for second generation particles than for primary particles, then the value of $\bar{K}_\gamma^C$ found by us will be reduced.

The measurement of the energy transferred to the electron-photon component in the two cases under consideration was based on the magnitude of the maximum avalanche which developed in the lead. If the average numbers $(\bar{n})_{max}$ of particles in the maximum avalanche is equal in both cases, then the transition effects will be identical, and therefore the ratio $(\bar{n}'')_{max}/(\bar{n}')_{max}$ will not depend on their magnitudes. The energy of the electron-photon avalanche and the average number of particles in the maximum avalanche are correlated as follows:

$$\bar{E}_\gamma = A\bar{n}_{max}, \tag{4}$$

where the coefficient A depends weakly on the energy of the avalanche [5]. /123
From (2), (3), and (4), we get the expression to be used in the determination of $\overline{K}_{\gamma}^{C}$:

$$\frac{(\bar{n}'')\max}{(\bar{n}')\max} = \frac{A'}{A''}(1 - \bar{K}_{\gamma}^{C}). \qquad (5)$$

Thus, having measured the ratio of the average numbers of particles in the maximum avalanche for the two types of interactions, we have eliminated the effect on $\overline{K}_{\gamma}^{C}$ of all the factors which contribute to the absolute values of the numbers of particles in question, namely the transient effect and the absolute value of coefficient A in Equation (4).

Measurements were conducted on the system shown in Figure 1. The selection of single particles was accomplished by means of a double row of hodoscopic counters located above the system. The energy of the primary radioactive particle was measured by the calorimetric method employing 13 rows of pulse ionization chambers located under the layers of lead, graphite, and iron. Each ionization chamber had a separate registration channel. The pulses, which originated in the individual chambers from the separate row, were added a second time with a weight corresponding to the energy liberation of a relativistic particle during passage through the given layer of matter.

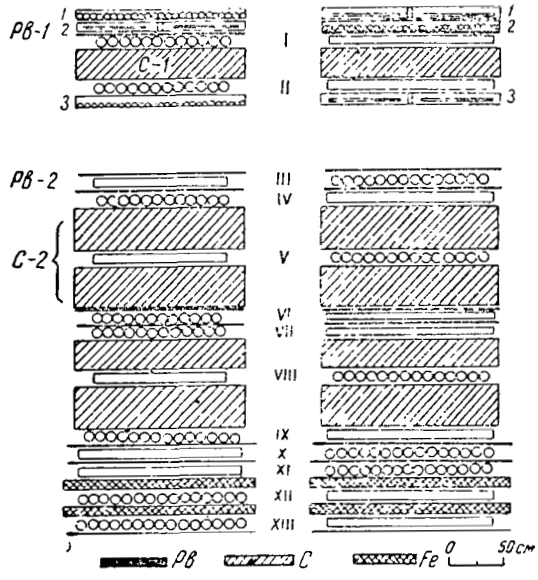

Figure 1.

The pulse, which is proportional to the energy liberation in the matter of the system, formed a control pulse when the ionization in the chambers corresponded to a liberation of energy greater than 100 GeV.

The block diagram of the electronic components of the systems is shown. The first row of ionization chambers, located under a 2-cm layer of lead, was used for the liberation of nuclear-active particles that move without an electron-photon accompaniment.

If a photon or electron from the air fell on the system, the ionization chambers of this row registered the particles of the electromagnetic avalanche which develops in the lead and such an event was thereafter excluded from the

analysis. In a similar manner, cases where the nuclear-active particles moved with the accompaniment of photons or electrons were discarded. For analysis, interaction cases were selected where a clear beam of the electron-nuclear shower was observed in the system and the axis of this shower did not exceed the limits of the system. In the first row of chambers, ionization was not observed when the number of operating hodoscopic counters was less than or equal to unit.

/124

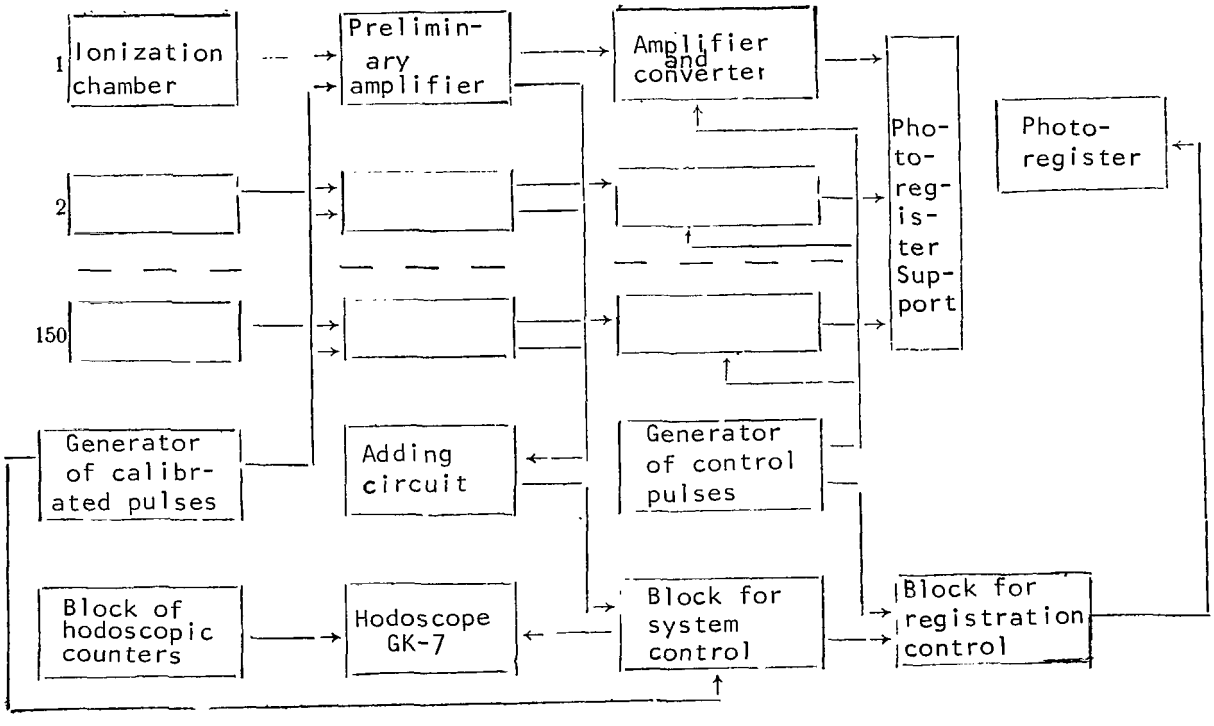

Block Diagram

Studies were made of the interactions in the second (graphite C-1) as well as in the fifth and sixth layers (graphite C-2). The nuclear-active /125
particles, which caused an interaction in the layer C-2, transferred a part of their energy to the electron-photon component which developed in the Pb-3 layer and was registered by the ionization chambers of the 6th and 7th rows in the region of the maximum.

The electron-photon component, which originated as a result of the interactions in the C-1 layer developed in the Pb-2 layers, while secondary nuclear-active particles interacted in the C-2 graphite block. The electron-photon component, which was formed during the interaction of these secondary particles, was measured also by the chambers of the 6th and 7th rows.

The combination of lead and graphite filters has made it possible to cut off almost completely the electron-photon component. In order to check this, the system was operated for some time without the Pb-1 and C-1 layers, registering the electron-photon component of wide atmospheric showers. At the same time, events were observed in which powerful electromagnetic avalanches developed in the Pb-2 layers, which were then completely extinguished in the C-2 graphite, and the chambers of the 6th and 7th rows did not register /126
ionization.

In view of the fact that secondary nuclear-active particles interact in the Pb-2 and C-1 layers, the electron-photon component which develops in Pb-2 will get additional energy; for this reason Equation (5) is written in the form

$$\frac{(\overline{n''})_{max}}{(\overline{n'})_{max}} = \frac{A'}{A''}(1 - \overline{K}_\gamma'), \qquad (6)$$

where

$$\overline{K}_\gamma' > \overline{K}_\gamma^C.$$

The value $\overline{K}_\gamma' = f(\overline{K}_\gamma^C)$ can be determined by calculating the energy transfer to the electron-photon component by secondary particles. The calculation was conducted on the following assumptions:

the run for the interaction of secondary nuclear-active particles is $\lambda^{Pb}_{interact.} = 180$ g/cm^2 in lead and $\lambda^{Pb}_{interact.} = 85$ g/cm^2 in graphite;

the energy fraction transferred to the electron-photon component by secondary particles is (1) $\overline{K}_\gamma^{second.} = \overline{K}_\gamma$ and (2) $\overline{K}_\gamma^{second.} = \frac{1}{3}$.

For each case of interaction which satisfies the selection conditions, the ionization distribution in the matter of the system was plotted and the energy of the primary particle was determined. The individual distributions were normalized to one energy value and averaged. During 620 hrs of operation of the system, 103 interactions were registered in the C-1 layer and 70, in the C-2 layer.

Considering that the interaction probability of secondary nuclear-active particles in the C-2 block is 0.8, while the interaction probability of primary particles in the same block is equal to unity for these selected cases, we get

$$\frac{(\bar{n}')_{max}}{(\bar{n}'')_{max}} = 0.56 \begin{matrix} +0.05 \\ -0.06 \end{matrix}. \qquad (7)$$

Figure 2 shows the dependence of this relationship on $\bar{K}_{\gamma}^{C}$, calculated for both cases, and also the experimental results (7). Corresponding to this experimental value, we have $\bar{K}_{\gamma}^{C} = 0.26^{+0.05}_{-0.04}$ for the first case and $\bar{K}_{\gamma}^{C} = 0.29^{+0.05}_{-0.03}$ for the second.

Thus, in the interaction of nuclear-active particles, a considerable fraction of the energy of the primary particle is transferred to the electron-photon component. If it is assumed that the main contribution to the energy of this component is made by the γ-quanta which originate from the decomposition of π^0-mesons, then this result indicates a large amount of inelasticity in the interaction of particles with the nuclei of light matter. /127

In the determination of $\bar{K}_{\gamma}^{C}$ by the described method, the influence of strongly ionizing particles shows up weakly on the results because in both cases they yield an increase in ionization registered by the 6th and 7th rows of ionization chambers. If this contribution increases with the development of the electron nuclear shower, then the value of $\bar{K}_{\gamma}^{C}$ determined from Figure 2 will be reduced in comparison with the true value.

The contribution of nuclear-active particles (relativistic and strongly ionizing) can also be determined from the readings of the 2nd row of ionization chambers under the layer of graphite of 48 g/cm^2. The ionization registered by these chambers is caused by strongly ionizing as well as by relativistic particles. Assuming that the entire ionization process is governed by nuclear-active particles, it is possible to introduce a correction in the value of $\bar{K}_{\gamma}^{C}$ determined in [2-5]. It amounts to 10% of the value of $\bar{K}_{\gamma}^{C}$, which corresponds to the results obtained above.

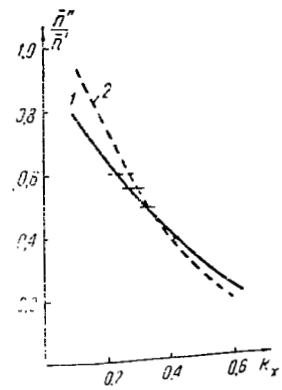

Figure 2

REFERENCES

1. Grigorov, N. L., V. S. Murzin and I. D. Rapoport, *ZhETF*, Vol. 34, p. 506, 1958.
2. Azimov, S. A., R. S. Abdullayev and Yu. V. Polyak, *Izv. AN SSSR, ser. fizich.*, Vol. 28, p. 1776, 1964.
3. Azimov, S. A., R. S. Abdullayev and Yu. V. Polyak, *DAN Uzbek SSR*, No. 3, p. 12, 1965.
4. Azimov, S. A., R. S. Abdullayev, G. A. Kochetkov, Yu. P. Kratenko, Yu. V. polyak and Ye. A. Pryakhin, *DAN Uzbek SSR*, No. 1, p. 9, 1962.
5. Azimov, S. A., R. S. Abdullayev and Yu. V. Polyak, *Izv. AN Uzbek SSR, ser. fiz.-mat. nauk*, No. 138, 1965.

Translated for the National Aeronautics and Space Administration under contract No. NASw-1695 by Techtran Corporation, P. O. Box 729, Glen Burnie, Maryland 21061

NASA-Langley, 1969 —— 29 F-535

NATIONAL AERONAUTICS AND SPACE ADMINISTRATION
WASHINGTON, D. C. 20546

OFFICIAL BUSINESS

FIRST CLASS MAIL

POSTAGE AND FEES PAID
NATIONAL AERONAUTICS AN
SPACE ADMINISTRATION

010 001 54 51 305 69100 00903
AIR FORCE WEAPONS LABORATORY/AFWL/
KIRTLAND AIR FORCE BASE, NEW MEXICO 8711

ATT E. LOU BOWMAN, ACTING CHIEF TECH. LI

POSTMASTER: If Undeliverable (Section 158 Postal Manual) Do Not Return

"The aeronautical and space activities of the United States shall be conducted so as to contribute . . . to the expansion of human knowledge of phenomena in the atmosphere and space. The Administration shall provide for the widest practicable and appropriate dissemination of information concerning its activities and the results thereof."

—NATIONAL AERONAUTICS AND SPACE ACT OF 1958

NASA SCIENTIFIC AND TECHNICAL PUBLICATIONS

TECHNICAL REPORTS: Scientific and technical information considered important, complete, and a lasting contribution to existing knowledge.

TECHNICAL NOTES: Information less broad in scope but nevertheless of importance as a contribution to existing knowledge.

TECHNICAL MEMORANDUMS: Information receiving limited distribution because of preliminary data, security classification, or other reasons.

CONTRACTOR REPORTS: Scientific and technical information generated under a NASA contract or grant and considered an important contribution to existing knowledge.

TECHNICAL TRANSLATIONS: Information published in a foreign language considered to merit NASA distribution in English.

SPECIAL PUBLICATIONS: Information derived from or of value to NASA activities. Publications include conference proceedings, monographs, data compilations, handbooks, sourcebooks, and special bibliographies.

TECHNOLOGY UTILIZATION PUBLICATIONS: Information on technology used by NASA that may be of particular interest in commercial and other non-aerospace applications. Publications include Tech Briefs, Technology Utilization Reports and Notes, and Technology Surveys.

Details on the availability of these publications may be obtained from:

SCIENTIFIC AND TECHNICAL INFORMATION DIVISION

NATIONAL AERONAUTICS AND SPACE ADMINISTRATION

Washington, D.C. 20546